Alma Mater Studiorum - Università di Bologna

Second cycle degree in

Science of Climate

Developing an analytical technique to study the critical zone through lignin phenols in speleothem samples:

paleoenvironmental reconstructions during the Early Holocene in the Apuan Alps Region

SUPERVISOR

Prof. Alessandro Amorosi

CANDIDATE

Letizia Roscelli

(Matriculation Number: 0001145441)

CO-SUPERVISOR

Dr. Tommaso Tesi

Graduation day: 27/03/2025

Accademic Year 2023 - 2024

Table of Contents

Abstract

Speleothems, which are secondary mineral deposits that form in caves, provide valuable archives of past climatic and environmental conditions. Among the variety of proxies contained within speleothems, lignin oxidation products (LOPs) have emerged as a promising marker for paleo-vegetation studies (Blyth et al., 2016). Lignin, a biopolymer found in terrestrial vascular plants, provides information about not only the abundance, but also the type of the source vegetation (Hedges & Mann, 1979). However, compared to other terrestrial climate archives, speleothems contain only a small fraction of organic matter and, therefore, only a few studies are available on organic biomarkers in speleothems, so far.

A new sensitive method that allows to analyse LOPs as vegetation biomarkers in speleothems was proposed by Heidke et al., (2018). The new method consists of the following main steps: acid digestion of the speleothem sample; solid-phase extraction (SPE) of the matter; degradation organic extracted polymeric lignin in a microwave-assisted alkaline CuO oxidation, producing monomeric LOPs; LOPs extraction via SPE; LOPs analysis. This method represents a powerful analytical tool for paleo-vegetation studies (Heidke et al., 2018).

The primary aim of this thesis was to assess the potential of LOPs in speleothems as a proxy for paleo-vegetation, while also improving the methodological approach for their analysis in speleothem samples. We also present the first quantitative record of lignin oxidation products obtained with such method from the Holocene speleothem RL18 sampled in the Renella Cave, central Italy.

The study begins with an evaluation of methodological improvements using blank and test samples. We found that sample contamination is largely due to airborne particles rather than specific steps in the analysis, still our results indicate that their signal-to-noise ratio and reproducibility are fully satisfactory. The LOP analysis reveals little variability in the C/V and S/V ratios -proxies for the plant type that originated the lignin (Hedges & Mann, 1979)- implying relatively stable vegetational conditions during the formation of the flowstone, with a general dominance of angiosperm-derived plant material over gymnosperm material.

The Σ8 signal, which is an estimate of the total content of lignin in a sample (Hedges & Mann, 1979), shows a remarkable peak at a depth between ca. 80 and 100 mm. We also investigated how the lignin signal in the RL18 flowstone correlates with other geochemical and climatic proxies. The comparison of the LOP data with trace element concentrations, stable isotopes ($\delta^{18}O$ and $\delta^{13}C$), and fluorescence emissions suggests that the increase in total lignin content occurred during a period of enhanced rainfalls, reduced water residence time, and increased water infiltration into the cave, possibly linked to less degradation of the surrounding soil. The lignin content is influenced by shifts in the hydrological cycle and the good coherence and correlation among different proxies indicates a trend of progressively drier climate in more recent times, starting from about half of the speleothem.

These results highlight the potential of the method developed by Heidke et al. (2018) for the quantification of LOPs in speleothems even with samples of limited mass (such as less than 2 g). Our outcomes demonstrate the great potential of LOP analysis to speleothems in paleo-vegetation studies. Nevertheless, the complexity of these signals calls for a multiproxy approach, to achieve a complete understanding of past climate, hydrological changes and vegetation dynamics. In addition, further refinement of the age model is needed to further improve the reliability of these interpretations.

1. Introduction

Speleothems are calcareous mineral deposits that form within caves in karstified carbonate rock. The most common types of speleothems are stalagmites, stalactites, and flowstones. Stalagmites are formed by water dripping on the cave ground, stalactites are formed by water dripping from the cave ceiling, and flowstones are formed by water films flowing on the cave walls and floor.

Speleothems can be used as paleoclimate archives, since they preserve information about climatic and hydrological conditions and the vegetation development above the cave (McDermott, 2004; Fairchild & Baker, 2012).

The use of speleothems for paleoclimatology studies has several advantages. First, speleothems are not limited to certain climatic regions. In addition, speleothems can grow continuously for 10^3-10^5 years, their growth layers are not mechanically disturbed, and the time resolution remains constant with age (Fairchild et al., 2006; Gałuszka et al., 2017). Moreover, using the 230Th–U method, it is possible to date speleothems up to 500.000 years back in time accurately (Richards & Dorale, 2003; Scholz & Hoffmann, 2008).

The main focus of most studies on speleothems is the analysis of stable isotope ratios like $\delta^{13}C$ and $\delta^{18}O$ (McDermott, 2004), inorganic trace elements (Fairchild & Treble, 2009), and, when the organic content of speleothems was considered, the total organic carbon content or fluorescent organic matter (Quiers et al., 2015). However, the interest in molecular organic proxies in climate archives has increased (e.g.: Blyth et al., 2008; 2016; Blyth & Watson, 2009; Giorio et al., 2018) in recent years. Among these molecular organic proxies, there is lignin. Lignin occurs almost exclusively in terrestrial vascular plants and is one of the main constituents of wood and woody plants (Jex et al., 2014). It is a biopolymer that mainly consists of multiple monomers, the three main ones being sinapyl alcohol, coniferyl alcohol, and p-coumaryl alcohol. The relative abundance of these three monomers varies with the type of plant, such as gymnosperm or angiosperm and woody or nonwoody material. Therefore, the composition of lignin permits the determination of the source and type of plant material giving enlightening insights into the paleoenvironment (Hedges & Mann, 1979).

To analyse the molecular composition of lignin phenolic components, it has to be converted into monomers by breaking C-O bonds. This makes lignin monomers volatile, which means that they can be quantified via gas chromatography. The most common method for the fractionation of lignin into phenolic monomers was developed by Hedges and Parker in 1976 and relies on alkaline oxidation with cupric oxide, CuO.

The product of the oxidation is a number of phenolic acids, aldehydes, and ketones that can be divided into four groups:

- the vanillyl group (V): vanillic acid, vanillin, and acetovanillone;
- the syringyl group (S): syringic acid, syringaldehyde, and acetosyringone;
- the cinnamyl group (C): trans-ferulic acid and p-coumaric acid;
- the p-hydroxyl group (P): p-hydroxybenzoic acid, p-hydroxybenzaldehyde, and p-hydroxyacetophenone.

In 1979, by analysing fresh plant tissues, Hedges and Mann showed that the phenols of the syringyl group are released by the oxidation of angiosperm plant tissues, but not of gymnosperm plant tissues.

In contrast, the phenols of the cinnamyl group are released by the oxidation of nonwoody plant tissues, but not of woody plant tissues. On the other hand, the phenols of the vanillyl group are products of the oxidation of all kinds of vascular plant tissues (Hedges & Mann, 1979).

Hedges and Mann then defined the lignin oxidation product (LOP) parameters C/V and S/V. C/V is given by the ratio of the sum of all LOPs of the C group over the sum of all LOPs of the V group, while S/V is given by the ratio of the sum of all LOPs of the S group over the sum of all LOPs of the V group. C/V and S/V help estimate the type of vegetation that is the source of the lignin under analysis. Because syringyl phenols are absent in gymnosperm plants but abundant in angiosperm plants, the S/V ratio provides information on the relative presence of these two types of vascular plant tissues. Similarly, the C/V ratios can provide information about the presence of woody tissues vs soft tissues (e.g. leaves and needles). Moreover, the sum parameter Σ8=C+S+V gives the sum of the eight products belonging to the C, S, and V groups and is used to estimate the total amount of LOPs in a sample (Hedges & Mann, 1979).

The sum of all lignin oxidation products of the P group, P, is usually not used when studying the origin of lignin because the source of such phenols can be protein-rich organisms, as well (Jex et al., 2014).

Lignin has been widely used as a paleo-vegetation proxy in lake sediment and peat cores (Tareq et al., 2004, 2011), which contain much larger amounts of organic matter than speleothems. Furthermore, it has been used to determine the source of dissolved organic matter in marine sediments (e.g.: Zhang et al., 2013) and natural waters (Standley & Kaplan, 1998; Hernes & Benner, 2002). However, Heidke et al. (2018) developed and validated a sensitive and selective method that enables the quantification of LOPs in both speleothem and cave drip water samples. In this work, the techniques described by Heidke et al. (2018) were first applied to test samples, and then to actual cave samples. The speleothem samples were first dissolved in acid, and the acidic solution was extracted by solid-phase extraction (SPE). Then, the eluent was subjected to CuO oxidation in a microwave-assisted digestion method. Following this, the oxidised sample solutions were again extracted and enriched by SPE. Finally, LOPs were separated and detected by gas chromatography coupled to mass spectrometry (GC-MS). The great potential of this method is that it allows the analysis of the lignin composition of trace amounts of organic matter preserved in speleothems, combining the advantages of lignin analysis as a highly specific vegetation biomarker with the benefits of speleothems as terrestrial climate archives. In fact, lignin is a vegetation biomarker which owing to its specificity for higher plants can help to interpret other vegetation markers and geochemical records (Heidke et al., 2018).

The overarching purpose of this thesis was to establish an analytical method to extract, oxidize and quantify LOPs in speleothem samples. To do so, a first part of the experiment was dedicated to quantify the analytical blanks by splitting the procedure in five separate steps corresponding to nine “methodological” samples for statistics. These samples do not contain dissolved speleothem and underwent a different number of steps in the analysis. The goal was to identify which part(s) of the procedure was (were) most responsible for the contamination of the samples. Our results suggest that the contamination of samples is mainly caused by unpure air in the laboratory rather than by any specific chemical used or step of the method. For this reason, a careful selection of the period during which the analyses are conducted (for example, during months when the concentration of airborne pollen levels

is lower) or the use of a clean room can be of significant importance in obtaining more precise and reliable results.

Another objective of this work was to evaluate both signal-to-noise ratio and reproducibility of the results. This was achieved through the analysis of six “speleothem” (S) test samples. Three equivalent samples (S4, S5 and S6), each one containing about 1.6 g of a flowstone, were analysed together with three blank samples (S1, S2, and S3). The signal-to-noise ratio was computed by comparing the mean results of S1, S2, and S3 and the mean results of S4, S5 and S6. In contrast, the standard deviation and the coefficient of variation for S4, S5 and S6 provided insights into the relative reproducibility of the results. Samples containing dissolved speleothem exhibit LOP concentrations that are always at least one order (but usually at least two orders) of magnitude higher than those in the blank samples. Moreover, despite some fluctuations, the values obtained for S4, S5 and S6 always presented some overlap if considered within their respective uncertainty intervals.

Finally, the method described by (Heidke et al., 2018) was applied to 26 samples of 1.7 - 5.1 g of the RL18 flowstone collected in the Renella Cave, a small cave located in the northern Apuan Alps (Tuscany), Italy. In the recent years, this cave has been the object of study for paleoclimatic and paleoenvironmental reconstructions (e.g.: Drysdale et al., 2006; Chimenti et al., 2023). The goal here was to investigate the paleo-vegetation changes captured in the speleothem on centennial and millennial time scales. To further evaluate the potential of LOPs as a proxy for vegetational and environmental changes in the RL18 speleothem, a comparison between the LOP results and other proxies was undertaken. The curves of the sum parameter Σ8 and other LOPs parameters were examined together with the signals of stable isotopes ($\delta^{18}O$ and $\delta^{13}C$), the fluorescence emission wavelength, and the concentration of trace elements like Sr, Mg, P, and Zn, from the same sample.

Overall, our findings indicate minimal variability in the C/V and S/V ratios, suggesting a relatively consistent vegetation above the cave during the formation of the flowstone with a general dominance of angiosperm-derived plant material, both woody and non-woody, in comparison to gymnosperm material. This is likely to imply no major temperature change in the northern Apuan Alps during the time period under study. Nevertheless, a notable increase in total lignin content was observed at a depth of approximately 80 to 100 mm, marked by a peak in the Σ8 signal. Other proxies, namely stable isotope ratios and fluorescence emission wavelength, suggest that this maximum in total lignin content may be due to changes in the hydrological cycle, e.g. the amount of precipitation. A preliminary age model was used to date the depth layers containing the dramatic increase in the lignin content of the flowstone to approximately 10.7 - 11.3 ka. Wetter climatic conditions and low water residence time, inhibiting humification, have been proposed to be the potential mechanisms that caused LOP concentration to increase in the speleothem. In addition, it is notable that, from the middle to the youngest layers of the speleothem, a clear correlation between rising Mg concentration and isotope ratios, along with decreasing lignin content, points to the transition towards progressively drier climate over more recent times. Nevertheless, a paleoclimatic reconstruction is beyond the scope of this work, and before delving into speculation, it is essential to have a more robust and reliable age model available.

This Master's thesis is organised into six main sections. In section 2, Scientific Background, the foundational knowledge is presented, providing an overview of speleothems, the analysis of lignin and

other proxies, and the types of climate information that can be inferred from speleothem records. It also provides the fundamental principles of the techniques used throughout the study. The experimental setup and methodology used in the research are described in section 3, Experimental Section. In section 4, Results, the findings from the experimental work are presented for the test samples ("methodological" and "S" samples) first and for the cave samples (RL18 samples) next. In section 5, Discussion, the results are further described by offering an interpretative framework, exploring the implications of the findings and relating them to stable isotope signals, fluorescence analysis, and trace element records from the same sample. Finally, section 6, Summary and Conclusions, provides a concise synthesis of the key findings of the study, summarizing the main results and offering suggestions for future studies in this field.

2. Scientific background

2.1 Speleothems and climatic proxies

2.1.1 Speleothem formation and overview as paleoclimate archives

Underground voids, commonly referred to as "caves", are vast cavities formed by the dissolution of limestone or, less frequently, other more soluble rocks through the action of groundwater (Grotzinger & Jordan, 2014). The dissolution of limestone is facilitated by the presence of carbonic acid, which is produced when atmospheric carbon dioxide dissolves in rainwater. The infiltrating waters may also absorb a portion of the carbon dioxide emitted by plant roots, bacteria, and other soil organisms. When these carbon dioxide-enriched waters pass through the aeration zone and move towards the saturated zone, they dissolve the carbonates (Grotzinger & Jordan, 2014). More precisely, the soil CO_2 and water react to form a weak acid (hydrogencarbonate, HCO_3):

$$H_2O + CO_2 \rightarrow H^+ + HCO_3^-$$

which dissolves carbonate bedrock and carbonate soil clasts:

$$H^+ + HCO_3^- + CaCO_3 \rightarrow Ca^{2+}_{(aq)} + 2(HCO_3^-)_{(aq)}$$

Over time, the voids formed through dissolution expand, forming a network of cavities, both vertical and horizontal. A significant portion of the dissolution that leads to the development of an underground cavity system occurs within the saturated zone; here, the voids are filled with water, and dissolution takes place across the entire surface of the openings (Grotzinger & Jordan, 2014). As the water table lowers, the cavities that had formed within the saturated zone are exposed to the aeration zone and thus become filled with air. Under these conditions, if the CO_2 in the groundwater is greater than that in the cave air, water saturated with calcium carbonate may drip from the ceiling or along the walls and a portion of the carbon dioxide dissolved in the water is released into the cave's air (“degassing”) (Grotzinger & Jordan, 2014). The loss of carbon dioxide from the solution reduces the solubility of calcium carbonate, causing a small amount of calcium carbonate to precipitate (redeposit) from each water drop and accumulate as deposits on cave walls, ceilings and floors:

$$Ca^{2+}_{(aq)} + 2(HCO_3^-)_{(aq)} \rightarrow CaCO_3 + H_2O + CO_2$$

These secondary mineral deposits in caves are called speleothems (from the Greek words *spelaion* meaning "cave" and *thema* meaning "deposit". Distinct surface conditions cause different speleothem shapes and types (Leng, 2006), the main ones being:

- stalactites, which form as pointed pendants from water dropping from fractures located on the cave ceiling;
- stalagmites, which form from the ground toward the ceiling and are the "ground-up" counterparts of stalactites;
- flowstone, which are sheetlike deposits formed where water flows down the walls or along the floors of a cave.

Speleothems serve as valuable archives, since they record paleoenvironmental changes through a range of geochemical properties, allowing the application of a multiproxy approach (Regattieri et al., 2016). Mostly they can give information on the atmosphere, the soil and upper epikarst, the lower epikarst and cave, and the $CaCO_3$ precipitation (Leng, 2006).

Speleothems can be studied at a variety of time scales, from sub-annual to thousands of years, from the Pliocene to the present (Regattieri et al., 2016). Moreover, they are relatively frequent in all continents, except for Antarctica (Heidke et al., 2018).

Another advantage of speleothems is that they can usually be precisely dated with uranium-thorium (U/Th) or uranium-lead (U/Pb) methods. In particular, the U/Th technique calculates an age from the degree to which secular equilibrium has been restored between the radioactive isotope Th-230 and its radioactive parent U-234 within a sample and allows for sample dating over the last few hundred thousand years (Ruddiman, 2013).

Many processes drive speleothem formation. For example, microclimatic parameters, such as air pressure and flow and CO_2 concentration influence degassing rate and carbonate deposition and, consequently, speleothem growth. In many cases, to be able to interpret proxies, it is critical to study the current-day speleothem forming conditions. This practice is called “cave monitoring” (Leng, 2006).

Speleothems are mostly made of calcite, occasionally aragonite or calcite/aragonite interbeds (Leng, 2006). The mineralogical change between aragonite and calcite serves as a paleoenvironmental indicator itself, as aragonite typically forms during periods of reduced drip rates and increased water residence time within the karst aquifer. Consequently, the deposition of aragonite is often associated with drier climatic conditions (Frisia et al., 2002; Holzkämper et al., 2009). Also, the presence and the nature of interruption (hiatuses) and speleothem diagenesis have to be identified to build a proper chronology.

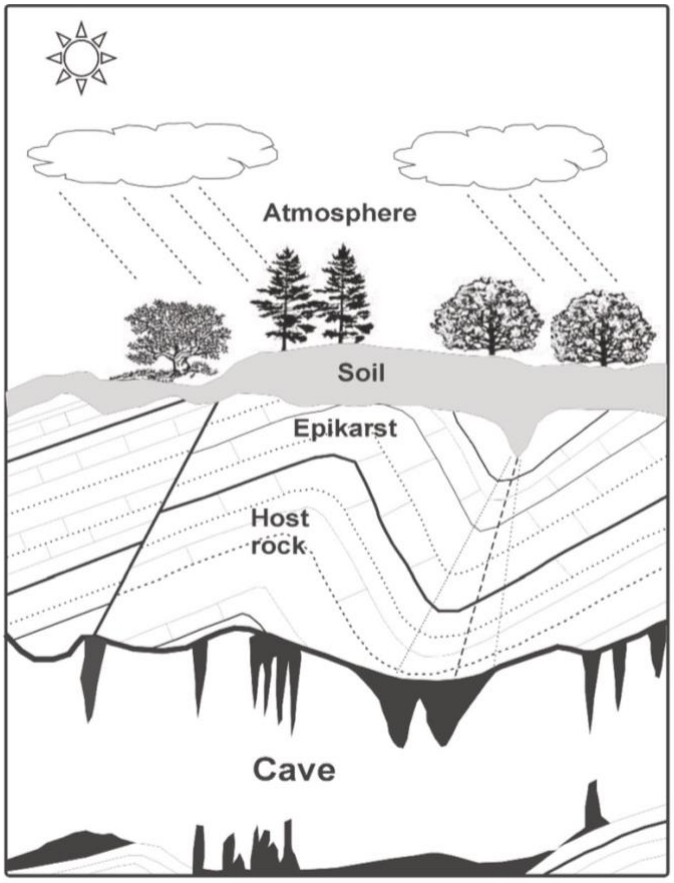

Figure 1. *Schematic diagram of a cave system illustrating several of the variables that can influence speleothem properties. From: Leng (2006).*

One important speleothem characteristic is its growth rate, which is primarily influenced by factors such as CO_2 supply in the seepage water, drip discharge, and temperature (Hellstrom & McCulloch, 2000; Genty et al., 2001; Borsato et al., 2015), even though subsurface temperatures vary only within a narrow range (Ruddiman, 2013). In general, speleothem growth phases indicate relatively wet and warm conditions. In fact, in order to grow speleothems need enough water in the soil to sustain the soil metabolism and the supply of CO_2 (Regattieri et al., 2016).

2.1.2 Isotopic composition

The stable oxygen and carbon isotope composition of speleothems ($\delta^{13}C$, $\delta^{18}O$) provides a valuable proxy for reconstructing past climatic conditions. The $\delta^{18}O$ in these calcium carbonate deposits is a proxy for the $\delta^{18}O$ of rainwater that was deposited at the surface and percolates through the soil and bedrock into the cave system. As such, the relative abundances of the two oxygen isotopes (^{18}O and ^{16}O) within these deposits serve as an indicator of atmospheric processes in the overlying environment (Leng, 2006). For instance, cave calcite deposits are frequently used as an index for the intensity of past monsoon circulations. At their peak, monsoons deliver large quantities of highly fractionated (^{18}O-deplected) water vapour, evaporated from the ocean and transported over considerable distances. In contrast, during periods of weaker monsoon activity, other local sources contribute ^{18}O-enriched rainwater to caves (Ruddiman, 2013). When calcite precipitation occurs in conditions close to isotopic equilibrium, the oxygen isotope composition of speleothems closely mirrors that of meteoric precipitation. However, the interpretation of $\delta^{18}O$ variations in continental carbonates is not straightforward, as it is influenced by a range of factors related to the hydrological cycle. These isotope effects, which occur during processes such as evaporation and precipitation, can lead to variations in $\delta^{18}O$ values across different locations. As a result, the paleoclimatic interpretation of $\delta^{18}O$ in speleothems can differ significantly depending on the dominant drivers of $\delta^{18}O$ in precipitation at specific sites. Thus, while $\delta^{18}O$ can serve as a valuable proxy for past climate conditions, its interpretation requires careful consideration of the specific climatic, environmental, and geological context of the study site (Leng, 2006).

Temporal variations in speleothem $\delta^{13}C$ provide significant potential for reconstructing climate-driven changes in both the nature and intensity of vegetation above a cave site. For instance, a shift between C3 (plants that use the Calvin cycle) and C4 (plants that use the Hatch-Slack cycle) vegetation can affect the $\delta^{13}C$ of the soil organic matter (Leng, 2006). This signal can be transmitted to the infiltrating water and then to speleothems. In regions where significant shifts in the relative proportions of C3 and C4 plants are not anticipated (such as the central-western Mediterranean, where C4 plants have not been documented during the Quaternary) the carbon isotope composition of speleothems can serve as an indicator of the varying contributions from organic (^{13}C-depleted; derived from biological activity in the soil) and inorganic (^{13}C enriched; from the bedrock) sources of CO_2.

A key consideration in speleothem research is that carbon isotope data should, whenever possible, be accompanied by relevant elemental data (e.g., Mg/Ca ratios) to assess alternative explanations for fluctuations in $\delta^{13}C$. For instance, strong correlations between carbon isotopes and Mg/Ca ratios may suggest that partial degassing of cave drip waters and calcite precipitation within the hydrological flow path above the cave (referred to as “prior calcite precipitation” and discussed in more details in sub-

section 2.1.3) could lead to elevated $\delta^{13}C$ values that are unrelated to changes in vegetation type or soil metabolism (Leng, 2006).

2.1.3 Fluorescence

Organic matter degradation in soil by bacteria is called humification. Degradation of organic matter produces three main kinds of acids, that can be identified according to their solubility in water and represent three different degrees of organic matter degradation (McGarry & Baker, 2000):

- humic acids (HA) are soluble in water at pHs higher than 2 and correspond to little degradation;
- fulvic acids (FA) are soluble in water at all pHs 2 and correspond to medium degradation;
- humins are insoluble in water at any pH 2 and correspond to great degradation.

Groundwater carries organic acids from the soil as it percolates. Then, these acids co-precipitate within speleothem calcite. The ratio between fulvic and humic acids in groundwater is dependent on water residence time and soil conditions, and it may reflect climate changes. When rainfall is higher or temperature cooler, humification is inhibited because compounds are flushed rapidly from soils, while under drier or warmer conditions, humification is more advanced (Swift et al., 1979).

Organic acids are particularly suitable for fluorescence analysis. Due to their different composition, fulvic and humic acids have different fluorescence properties. Different spectra obtained from a speleothem sample depend on the relative proportion of humic and fulvic acids, providing interesting insights into soil degradation and paleo hydrological conditions (McGarry & Baker, 2000). In general, wetter conditions cause a decrease in humification and shortening in the residence times of organic material in the soil, leading to a higher proportion of humic acids. Humic acids tend to exhibit fluorescence at higher wavelengths with lower emission intensity. Conversely, in drier conditions, prolonged residence times result in greater humification, with a higher proportion of fulvic acids. These, in turn, emit fluorescence at lower wavelengths and with greater intensity.

2.1.4 Trace elements

As already mentioned, the trace element composition of speleothems provides another valuable source of paleoclimatic information. The variations in the concentration of elements such as Mg, Sr, Ba, Al, Si, P, Y, and Zn, taking place on centennial to millennial timescales, are influenced by a complex interplay of environmental factors, including temperature, precipitation, and hydrological conditions (Regattieri et al., 2016). A multiproxy approach is needed, since interpreting trace element records in speleothems is often challenging, as the variability in elemental concentrations results from a range of interacting processes. These include atmospheric inputs, vegetation and soil influences, the karstic aquifer, primary speleothem crystal growth, and post-depositional alterations (Fairchild & Treble, 2009).

Discerning the relative contributions of various sources and processes and interpreting their potential climatic implications is a complex task that requires in-depth knowledge of the specific conditions of the individual cave settings. Nevertheless, by integrating information on local environmental and hydrological characteristics, derived from elemental records, with the broader paleoclimatic framework provided by other proxies, such as the stable isotope compositions, it is possible to construct more comprehensive temporal series. These integrated datasets enable a detailed investigation of the local paleoenvironmental response to regional and global climatic changes (Regattieri et al., 2016).

Magnesium, Sr, and Ba are primarily transported as dissolved ions in drip water, where they substitute for Ca in the carbonate crystal lattice (Fairchild & Treble, 2009). The partitioning of these elements between the solution and the solid phase is governed by a distribution coefficient (Morse & Bender, 1990), K_{tr}, which can vary with factors such as temperature, growth rate, crystal morphology, and the composition of the solution (Fairchild & Treble, 2009). A simple equation can be used to relate solution and mineral compositions:

$$(Tr/Ca)_{CaCO_3} = K_{tr}\ (Tr/Ca)_{solution}$$

where $(Tr/Ca)_{CaCO_3}$ and $(Tr/Ca)_{solution}$ are the molar ratio between trace element (Tr) and Ca in the solid and in the solution, respectively.

Fluctuations in the concentrations of these elements, particularly Mg, are often interpreted in paleohydrological contexts. Under low-flow conditions, degassing may occur in certain areas of the recharge system, leading to water supersaturation with respect to $CaCO_3$, which in turn results in calcite precipitation (Fairchild et al., 2000). Since the distribution coefficient for Mg is less than one ($K_{Mg} < 1$), the reduction in Ca is more significant than that of Mg, causing an increase in the Mg/Ca ratio in both the solution and the precipitating speleothem (Fairchild et al., 2000). This process is called prior calcite precipitation (PCP).

As previously mentioned, additional support for the occurrence of PCP may come from observing the enrichment of carbon isotopes. Lighter ^{12}C is preferentially lost during degassing, leading to a relative enrichment of ^{13}C in the solution (Fairchild & Treble, 2009).

Increases in the Mg/Ca ratio (i.e., higher Mg concentration assuming constant Ca levels) are thus associated with dry periods. In contrast, a decrease in Mg concentration can signal wetter conditions, which reduce PCP and shorten the water's residence time (Regattieri et al., 2016).

Strontium (Sr) and barium (Ba), like Mg, have distribution coefficients less than unity and can, therefore, be influenced by PCP. This effect is further evidenced by the positive correlation between Sr-Ba/Ca and Mg/Ca ratios (e.g.: Sinclair et al., 2012; Regattieri et al., 2014b). The incorporation of Sr and Ba into calcite has also been shown to be positively correlated with variations in speleothem growth rate (Treble et al., 2003), with a significant proportion of both Sr and Ba incorporated into more abundant crystal defect sites within the fast growing speleothem (Fairchild & Treble, 2009). However, the variability in the concentrations of these elements is influenced by several complex factors (Regattieri et al., 2016).

Other elements that are often analysed (Si, Al, P, Y, Zn) are likely to be transported primarily as detrital components rather than dissolved solutes in speleothems (Borsato et al., 2007; Fairchild & Treble, 2009). This detrital phase consists of mineral particles and organic colloids (complex heterogeneous aggregates between organic matter and other compounds), which are products of bedrock weathering and soil leaching. These particles are subsequently deposited either as macroscopically visible layers of mud or silt (Zhornyak et al., 2011) or, more commonly, as fine, microscopic particles that accumulate within individual layers of calcite (Fairchild et al., 2000).

The concentration of these elements is thought to be higher during periods of increased infiltration (Regattieri et al., 2016). Nevertheless, some differences in the distribution of elements transported as mineral particles or bounded to colloids can be observed and related to different environmental conditions.

For example, the phosphorus (P) content in speleothems has several potential sources, which depend largely on the specific characteristics of the cave environment. For instance, in areas where phosphorus-rich minerals, such as apatite, are present, P can come from the bedrock and be incorporated into the speleothem crystal lattice as part of P-rich phases, with the incorporation governed by a distribution coefficient (Frisia et al., 2012). However, several studies conducted in temperate ecosystems suggest that phosphorus in cave drip water mainly originates from the leaching of decomposing plant material (Treble et al., 2003; Borsato et al., 2007). Soluble hydrolyzed HPO_2, which is easily transported in pH-neutral groundwaters, is particularly mobile when it is chelated to organic colloids (e.g., Treble et al., 2003). Hence, the abundance of this element can be related to the vegetation cover above the cave: the greater the development and biological activity (vegetation above all), the greater the amount of P in the soil and waters. Phosphorus is a key element for the identification of annual cycles in speleothems, as well. During the summer months, pH conditions and microbial activity promote the accumulation of P in the upper horizons of the soil. Autumn precipitations then mobilize this phosphorus and transport it into the epikarst and in the speleothem recharge system. Incorporation into calcite results in the formation of fluorescent annual lamination (Borsato et al., 2007). In seasonal environments, the phosphorus content in speleothems is therefore commonly interpreted as a marker of surface biological productivity (Fairchild & Treble, 2009), reflecting changes in vegetation and soil conditions. Higher P concentrations are typically associated with increased primary productivity, and facilitated by higher water infiltration rates that transport P from the soil, as well as increased colloid transport, particularly during warmer and wetter periods (Regattieri et al., 2016).

The trivalent element Y behaves similarly to the heavy rare earth elements (Zhou et al., 2008). Yttrium, like P and Zn, is typically transported as part of the detrital fraction, either bound to mineral particles or organic colloids (Schimpf et al., 2011). In temperate regions with deep soil layers, these elements are believed to be primarily associated with organic colloids (Borsato et al., 2007), making them useful indicators of soil development and infiltration rates, despite their differences. A decrease in P, Y, and Zn concentrations is often interpreted as a deterioration in soil conditions (Regattieri et al., 2016). Silica (Si) and aluminium (Al) are thought to be mostly transported by mineral detritus. Their presence in a speleothem sample may be related to high infiltration rates, but also to greater catchment erosion (Regattieri et al., 2016).

2.1.5 Lignin

Lignin (see Figure 2), together with cellulose, constitutes one of the most important structural component of plant cell walls. These compounds play a crucial role by providing mechanical support and protection to the cell walls, as well as regulating plant growth processes. Furthermore, lignin is vital for resistance against microbial attacks and biomass degradation, and is impermeable to water (Schutyser et al., 2018). Lignin is a highly branched, amorphous polymer with a complex structure, primarily composed of three phenylpropanoid alcohol units known as monolignols, which are interconnected by C-C and C-O bonds (Vanholme et al., 2010):

- sinapyl alcohol (3,5-dimethoxy-4-hydroxycinnamyl alcohol);
- coniferyl alcohol (3-methoxy-4-hydroxycinnamyl alcohol);
- p-coumaryl alcohol (4-hydroxycinnamyl alcohol).

The distinction between these three alcohol units lies in the number of methoxy groups (-OCH_3) present on the phenolic nucleus (Schutyser et al., 2018). The proportion of alcohol units in lignin depends on the biomass source (i.e. the type of vegetation). Based on its origin, lignin can be classified into three types with varying monolignol contents: lignin from gymnosperm wood (e.g. pine, spruce) mainly consists of coniferyl alcohol, whereas lignin from angiosperm (e.g. birch, poplar) contains coniferyl and sinapyl alcohol. Instead, grass lignin (from non-woody vegetation and herbaceous biomass, like grasses, leaves and needles) is characterised by a higher proportion of p-coumaryl alcohol and ester-bound p-coumaric acid and ferulic acid (Boerjan et al., 2003; Vanholme et al., 2012).

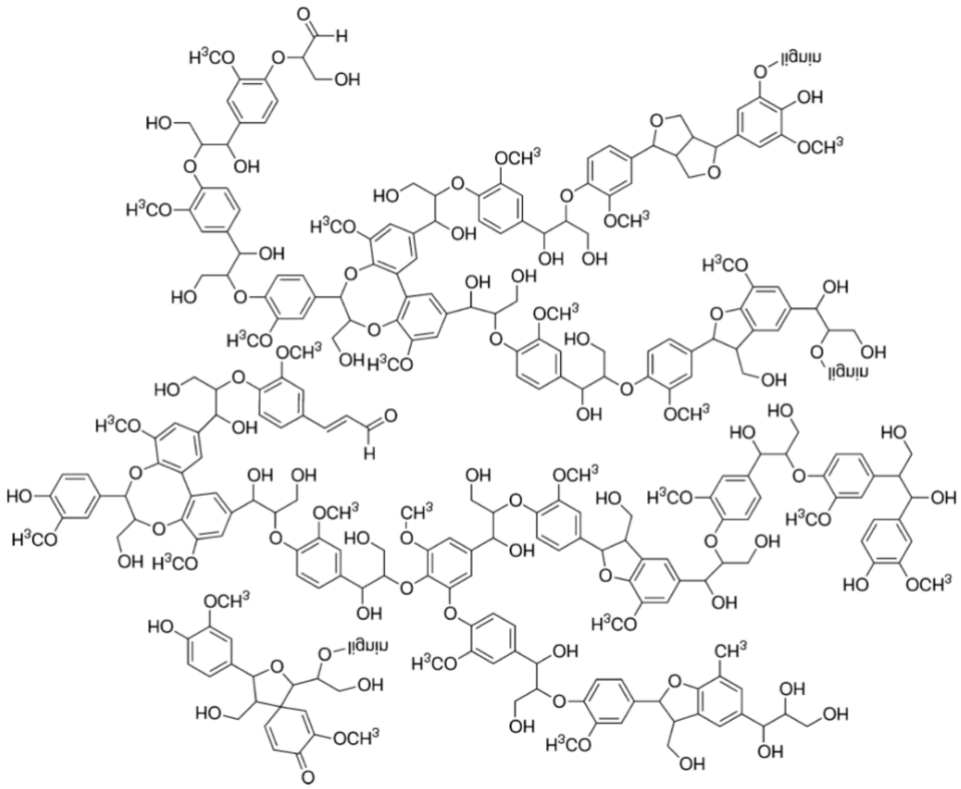

Figure 2. *Molecular structure of lignin. From Upton & Kask (2016).*

In order to perform analysis on the composition of lignin, the lignin polymer has to be broken down into monomers through oxidation known as lignin oxidation products (LOPs). A mild oxidation using CuO is often the preferred method. The guaiacyl phenylpropanoid from coniferyl alcohol is oxidized to vanillic acid, vanillin and acetovanillone (so-called V-group), the syringyl phenylpropanoid from sinapyl alcohol to syringic acid, syringaldehyde and acetosyringone (S-group), and the p-hydroxyphenyl phenylpropanoid from p-coumaryl alcohol to p-hydroxybenzoic acid, p-hydroxybenzaldehyde and p-hydroxyacetophenone (P-group) (Heidke et al., 2019). The 3,5 dihydroxybenzoic acid (3,5-Bd) is another product of lignin mild oxidation. The phenolic oxidation products are shown in Figure 3.

Lignin represents a significant portion of plant litter input (ca. 20%) into soils, contributing to soil organic matter, and is amongst the most studied macromolecules in natural environments (Thevenot et al., 2010). The microbial degradation of lignin is relatively slow, since only white-rot fungi can completely mineralise it to CO_2 in co-metabolism with other energy sources, whereas some other microorganisms

are only capable of producing structural changes in it (Kögel-Knabner, 2002). Although the debate on the exact fate of lignin in soils is still ongoing (Thevenot et al., 2010), its relative recalcitrance has led to lignin oxidation products being widely used as paleo-vegetation proxy in archives, such as peat, lake sediments and marine sediment cores, as a proxy for terrestrial input of plant biomass in natural waters, like rivers and oceans (Heidke et al., 2019). Lignin phenols in speleothems were first detected by Blyth & Watson (2009), and subsequent studies (Blyth et al., 2008; 2016) have emphasised the potential of LOPs as effective vegetation proxies in speleothems.

A method for the quantitative analysis of lignin as a paleo-vegetation proxy in both speleothems and cave drip water was developed by Heidke et al. (2018). The advantage of using lignin as a vegetation proxy lies in its exclusive production by vascular plants and not by microorganisms. Therefore, lignin is highly specific, and the risk of laboratory contamination is considerably lower compared to more ubiquitous substances, such as lipids (Heidke et al., 2019). Moreover, lignin analysis provides not only information on the abundance of vegetation but also insights into its specific type. In fact, lignin-derived products obtained after cupric oxide (CuO) oxidation and gas-chromatographic-mass-spectrometry analysis can be used as environmental biomarkers. As mentioned above, CuO oxidation yields a number of single-ring phenol compounds -which can be divided into four groups: vanillyl (V), syringyl (S), cinnamyl (C), and p-hydroxyl (P)- with their aldehyde, ketone and acid substitutions. The sum parameter Σ8, defined as

$$\Sigma 8 = C + S + V$$

and various characteristic ratios, such as the C- or S-to-V ratios, can be calculated, where C is defined as the sum of all lignin oxidation products of the C group, V as the sum of all lignin oxidation products of the V group, and S as the sum of all lignin oxidation products of the S group.

The Σ8 parameter is generally considered a quantitative measure of soil lignin: with increasing decomposition, Σ8 is usually decreasing (Thevenot et al., 2010). On the other hand, C- and S-to-V ratios are often used as source indicators. The molecular composition of lignins in soils, sediments, and speleothems can be related to major plant groups like angiosperms and gymnosperms (e.g.: Hedges & Mann, 1979; Heidke et al., 2021). The relationship between the S-to-V and C-to-V ratios in soils and sediments was observed to vary according to their source plants, indicating at least a partial preservation of characteristic lignin signatures from plants to soils and sediments (e.g.: Otto & Simpson, 2006). The sum of all lignin oxidation products of the P group, P, is not one of the parameters used to determine the source of lignin (Jex et al., 2014) because phenols of the p-hydroxyl group can originate from gymnosperm and non-woody angiosperm plant tissues, but from protein-rich organisms, as well, such as bacteria and plankton. However, despite some limitations, the P group of LOPs can be helpful when inferring information about the degradation status of the lignin (or soil organic matter, SOM) (e.g.: Goñi & Hedges, 1995; Qian et al., 2023). In fact, the P/(V+S) and 3,5-Bd/V ratios respectively increase with increasing pedogenesis and humification in soils, or diagenesis in sediments (e.g.: Goñi & Hedges, 1995; Dickens et al., 2007).

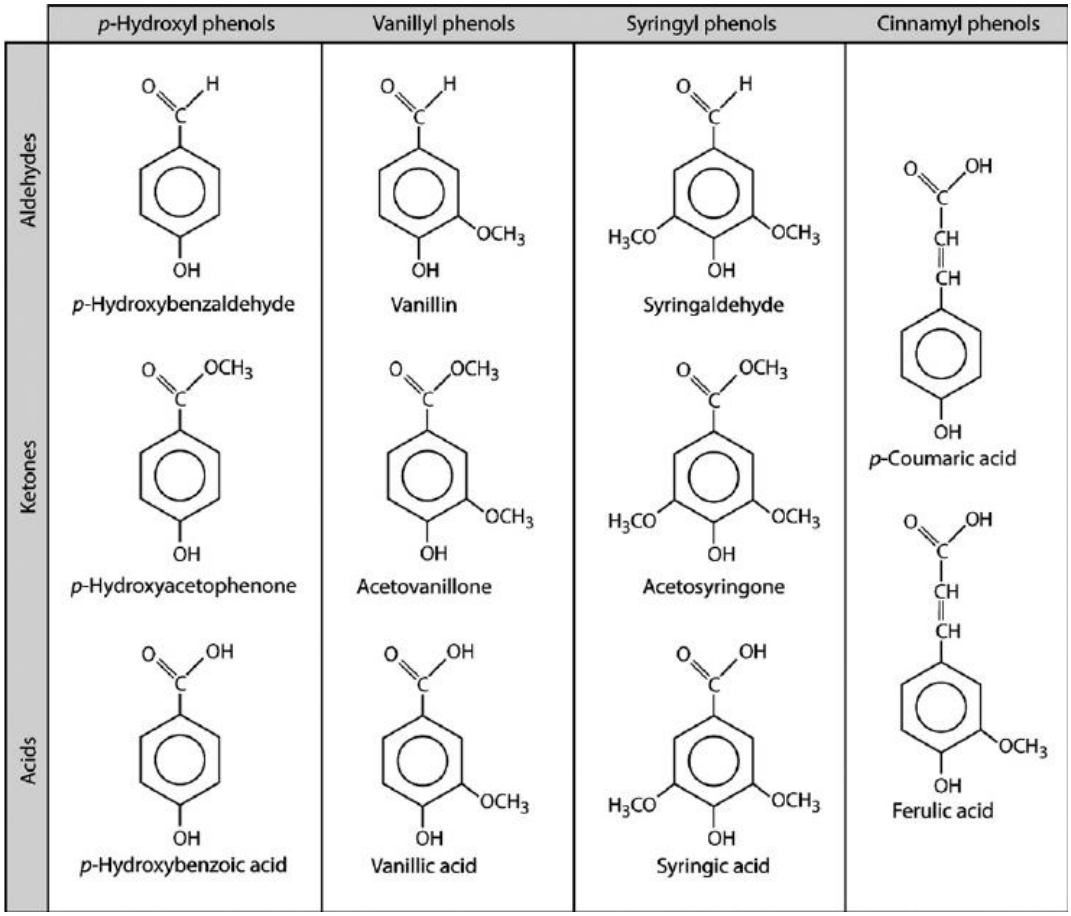

Figure 3. *Monomers of lignin produced by the alkaline CuO oxidation: P-type, V-type, S-type and C-type phenols. From Thevenot et al. (2010).*

Lignin composition in gymnosperm differs from that in angiosperm in the relative abundance of V, S, and C phenolic units. Gymnosperm wood is predominantly composed of V-units (approximately 80%) associated with C-units, whereas angiosperm wood contains roughly equal proportions of V and S units, also linked with C-units (Hedges & Mann, 1979). The relative proportions of V, S, and C units in soils, sediments and speleothems may thus enable the distinction of organic matter derived from angiosperm and gymnosperm taxa and provide insights into the source vegetation. Although the extent and the way in which these ratios are influenced by factors such as transport, microbial transformation, soil characteristics, land use, and interactions with mineral surfaces remain an ongoing area of research (e.g.: Thevenot et al., 2010; Jex et al., 2014), a higher C/V ratio is thought to indicate a higher contribution of non-woody vs. woody plant material, while a higher S/V ratio indicates a higher contribution of angiosperm vs. gymnosperm plant material (Hedges & Mann, 1979).

In a Holocene stalagmite from the Herbstlabyrinth cave in Germany, the concentrations of LOPs, along with the C/V and S/V ratios, were observed to co-vary with environmental fluctuations and showed correlations with other proxies, such as the concentrations of P, U, and Ba, as well as $\delta^{13}C$ values (Heidke et al., 2019). This study also identified seasonal variations in LOP concentrations in monthly dripwater samples from the Herbstlabyrinth, with lower concentrations in winter and higher concentrations in summer. Heidke et al. (2021) showed that the LOP signature of the vegetation overlying four different sites in New Zealand is at least partly preserved in dripwater and speleothem

samples. This is a necessary condition for using LOPs as a biomarker proxy for past vegetation changes.

Despite the advances made, several unresolved questions remain regarding the transport of lignin from the soil, through the karst system, and into the cave environment and speleothems. For example, the interaction of lignin with mineral surfaces can induce fractionation (Hernes et al., 2007, 2013), while factors such as land use, climate characteristics, and soil properties may also influence lignin degradation (Thevenot et al., 2010; Jex et al., 2014). These processes could potentially alter, at least partially, the original source-dependent LOP signatures, particularly the C/V and S/V ratios, thereby complicating their interpretation in terms of past vegetation dynamics. However, a clarification of all these aspects is beyond the scope of this work.

A schematic overview of the processes that may influence LOP signals is provided in Figure 4.

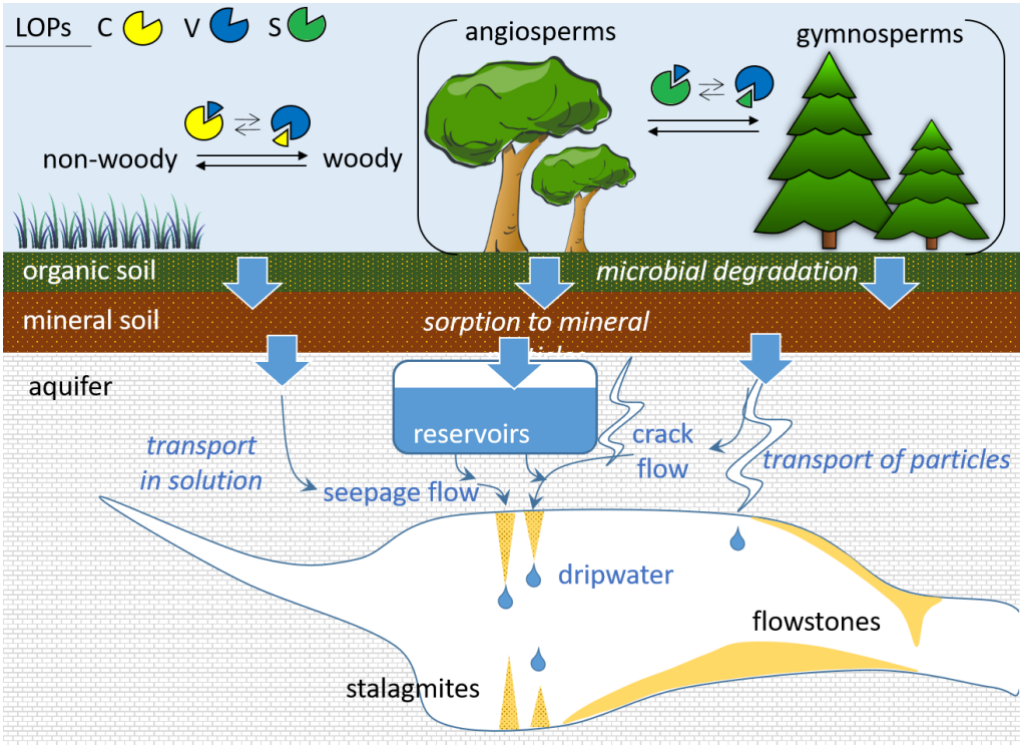

Figure 4. *Schematic representation of the different potential processes influencing the transport and degradation of LOPs in speleothems and cave dripwater. From Heidke et al. (2021).*

2.2 Fundamentals on the techniques used

2.2.1 Microwave-assisted alkaline CuO oxidation

Microwave radiation (MW) is part of the electromagnetic spectrum (EMS), and its wavelength goes from 1 m to 1 mm, which means that it is found between infrared and radio waves.

Before the advent of MW heating, most reactions employed conventional heat transfer equipment, such as heating jackets and oil baths. These methods are slower and usually depend on a temperature gradient transmitting heat to the inner parts of the apparatus. In contrast, MW energy is introduced into the reactor remotely and passes through the vessel walls, uniformly heating only the reactants and solvent rather than heating the vessel itself first. Rapid heating of substrates shortens the reaction time

and prevents over-reaction of the obtained products, reducing by-products and/or decomposition products (Mkumbuzi et al., 2023).

Oxidation with cupper oxide (CuO) is broadly used for the analysis of lignin in geochemical samples: there are many data sets to compare with, and this technique has been optimised many times in the past. For example, Goñi and Montgomery (2000) developed a microwave digestion method, which is the one that was used during this thesis project. Compared to previous procedures, this method has many advantages, such as a simplified extraction procedure, faster reaction times, the ability to accurately measure and control reaction conditions, added flexibility for the analyst, and a marked increase in the achievable sample throughput.

A known amount of fine CuO powder and a known amount of ferrous ammonium sulfate ($FeS(NH_4)2O_4$) are inserted to the reaction vessels containing the sample being analysed. Then, in an oxygen-free environment, a known amount of 2 N NaOH solution is added to each reaction vessel, as well, and then it is immediately capped. The ferrous ammonium sulfate is used to bind any remaining oxygen. The closed reaction vessels are placed in the rotating tray and loaded into the microwave. It has been found that the optimal temperature for the oxidation is 150°C and the optimal reaction time is 90 minutes (Goñi & Montgomery, 2000). Once the oxidation reactions are complete, the reaction vessels are allowed to cool, removed from the microwave, and can be opened.

Upon CuO oxidation, the lignin macromolecule undergoes hydrolysis, which results in the formation of several characteristic methoxylated phenols that are suitable for analysis by gas chromatography - mass spectrometry. More precisely, under the reaction conditions, phenols with aldehyde, ketone, and acid groups are obtained as the oxidation products of monolignols (i.e. lignin building blocks) with three carbon side chains present in the original polymer (Goñi & Montgomery, 2000), as described in more detail in the previous paragraph.

2.2.2 Gas chromatography – Mass spectrometry (GC – MS)

For the composition of this paragraph, some of the major manuals of analytic chemistry were used, such as “Analytical Chemistry: A Modern Approach To Analytical Science” by Mermet et al. (2004).

The detection and quantification of LOPs are often achieved through gas chromatography coupled with mass spectrometry (GC–MS), which is an analytical method that allows the identification of different substances, even in tiny amounts, within a test sample. A schematic representation of a GC-MS system includes a chromatograph, a mass spectrometer, and a data collection and analysis system, which together form the platform for the separation and (qualitative and quantitative) analysis of complex mixtures. The chromatograph consists of a sample injector, a system for the control of the temperature of the column, and a transfer line that allows the column effluent to enter the mass spectrometer. The mass spectrometer is composed of an ionisation chamber (ion source), a mass analyser, and an ion detector, all maintained under high vacuum. A schematic image of a GC-MS system including a component for electron ionisation is shown in Figure 5.

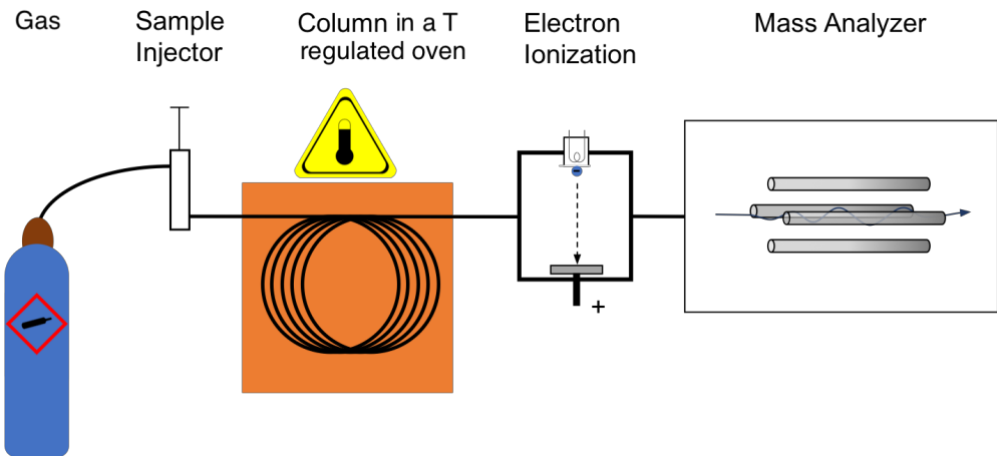

Figure 5. *Schematic representation of a GC-MS system with an electron ionisation system. Modified from: Cwszot, Kkmurray – File:Gcms_schematic.gif, CC BY 2.5, https://commons.wikimedia.org/w/index.php?curid=67620931*

The gas chromatograph utilises a capillary column whose properties regarding molecule separation depend on the column's dimensions (length, diameter, film thickness) and the phase properties. The chemical diversity among the molecules within a mixture and their relative affinities for the stationary phase of the chromatographic column facilitate their separation as the sample progresses through the column. The molecules are retained by the column and subsequently eluted at different time intervals, referred to as the retention time. This temporal separation enables the downstream mass spectrometer to capture, ionise, accelerate, deflect, and detect the ionised molecules separately. The mass spectrometer analyses these molecules by fragmenting them into ionised components, which are then separated within a magnetic sector based on their mass-to-charge ratio (m/z). The detection is typically achieved through an electron multiplier, which essentially converts the ionised mass fragments into an electrical signal that is then detected. The pattern of ionised fragments of a molecule is called mass spectrum, and the most common method of ionisation is electron ionisation (EI). In the EI technique, the molecules enter into the MS where they are bombarded with free electrons emitted from a filament, causing the molecule to fragment in a characteristic and reproducible way. This so-called "hard ionisation" technique leads to the generation of numerous fragments with low mass-to-charge ratios (m/z), while few, if any, molecules remain close to their molecular mass. The molecular fragmentation pattern is influenced by the electron energy applied to the system, typically set at 70 eV (electronvolts). The use of 70 eV standardises the process, allowing for effective comparison of the resulting spectra with reference spectra from libraries, using, for example, software provided by the instrument manufacturer.

The use of these two components, GC and MS, together allows a much finer degree of substance identification than either unit used separately. In fact, it is not possible to accurately identify a particular molecule by gas chromatography or mass spectrometry alone because the mass spectrometry process normally requires a very pure sample, while gas chromatography using a traditional detector cannot differentiate between multiple molecules that happen to have the same retention time. This leads to the co-elution of two or more molecules. The combination of both techniques, GC and MS, dramatically reduces the chance of error.

A mass spectrometer is commonly used in one of two modes: full scan or selective ion monitoring (SIM). Most GC-MS instruments can perform both functions, either separately or simultaneously, depending on the specific configuration of the instrument. The quantification of a substance is achieved by comparing the relative abundances of atomic masses within the generated spectrum. The identification process is generally automated using a software, provided a list of potential elements is specified.

A "full spectrum" analysis considers all the peaks present in the spectrum. In contrast, selective ion monitoring (SIM) focuses only on specific ions that are associated with a particular compound. Certain ion fragments are entered into the instrument method, and only those fragments are detected by the mass spectrometer. This approach operates on the assumption that, at a given retention time, a specific set of ions is characteristic of a distinct substance. SIM is a rapid and efficient technique, particularly when prior information about the sample is available or when only a few specific compounds need to be detected. As the amount of information gathered about the ions in a given gas chromatographic peak decreases, the detection limit is lower and the sensitivity of the analysis increases. Thus, SIM allows for the detection and measurement of a smaller quantity of a compound; however, the degree of certainty regarding the identity of the compound is reduced. To further increase the confidence in the result, it is important to ensure that the ion ratios of the various mass fragments align with those of a known reference standard. On the other hand, full scan MS is useful in determining unknown compounds in a sample and provides more information than SIM when it comes to confirming or resolving molecules.

3. Experimental section

3.1 Chemicals and materials

Copper(II) oxide (97 %) was purchased from ThermoFischer Scientific, while ammonium iron(II) sulfate hexahydrate (≥99 %) was purchased from Sigma-Aldrich.
Methanol (MeOH) and n-hexane (HEX) (96%) were purchased from Scharlau Science Group.
Dichloromethane (DCM) was purchased from Merck KgaA.
Solid-phase extraction columns (CHROMABOND HLB, 60 µm, column volume/adsorbent weight: 3 mL / 60 mg) were purchased from MACHEREY-NAGEL.

3.2 Methods with the test samples

Figure 6 is a process chart illustrating the overall test sample preparation procedure, the different steps of which will be described in detail in the following sections. Overall, the analysis follows the one described in Heidke et al. (2018). In addition to some speleothem samples, multiple blank samples were also performed at this stage of the study. It is important to note that this part of the analysis took place in July 2024. A descriptive summary of the test samples and the steps of the process each of them underwent can be found in Table 1.

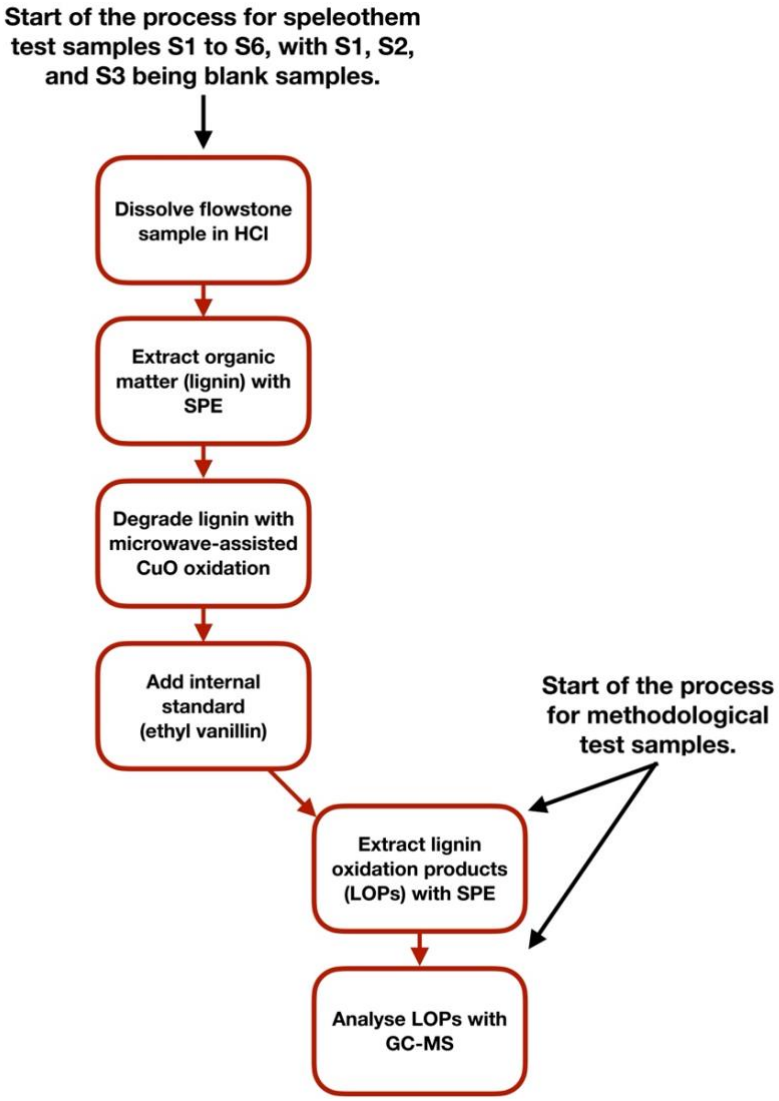

Figure 6. *Process chart of the overall analysis of test samples. A detailed description of the individual steps is given in the sub-sections of Sect. 3.2.*

Table 1. *List of test samples with description of the process steps each of them underwent*

Sample ID	Dissolved flowstone sample in HCl	Extraction of organic matter with SPE	Microwave-assisted CuO oxidation	Addition of internal standard	Extraction of LOPs with SPE (see Table 2 and 3)	Drying step 1 (before transfer into brown vials)	Drying step 2 (after transfer into brown vials)	Dilution
Blank_vial	No	No	No	No	No	No	Concentrator (1hour) + N_2 stream (5 minutes)	15 µL of pyridine + 15 µL of BTSFA
MeOH_1	No	No	No	No	No	Concentrator (ca. 45 minutes)	Concentrator (ca. 10 minutes)	15 µL of pyridine + 15 µL of BTSFA
MeOH_2	No	No	No	No	No	Concentrator (ca. 45 minutes)	Concentrator (ca. 10 minutes)	15 µL of pyridine + 15 µL of BTSFA
C+MeOH_1	No	No	No	No	Yes	Concentrator (ca. 45 minutes)	Concentrator (ca. 10 minutes)	15 µL of pyridine + 15 µL of BTSFA
C+MeOH_2	No	No	No	No	Yes	Concentrator (ca. 45 minutes)	Concentrator (ca. 10 minutes)	15 µL of pyridine + 15 µL of BTSFA
C+MeOH+dry	No	No	No	No	Yes	No	Concentrator (1hour) + N_2 stream (5 minutes)	15 µL of pyridine + 15 µL of BTSFA
C+HCl+MeOH_1	No	No	No	No	Yes	Concentrator (ca. 45 minutes)	Concentrator (ca. 10 minutes)	15 µL of pyridine + 15 µL of BTSFA
C+HCl+MeOH_2	No	No	No	No	Yes	Concentrator (ca. 45 minutes)	Concentrator (ca. 10 minutes)	15 µL of pyridine + 15 µL of BTSFA
C+HCl+MeOH_3	No	No	No	No	Yes	Concentrator (ca. 45 minutes)	Concentrator (ca. 10 minutes)	15 µL of pyridine + 15 µL of BTSFA
S1	No	Yes	Yes	Yes	Yes	No	Concentrator (1hour) + N_2 stream (5 minutes)	60 µL of pyridine + 60 µL of BTSFA
S2	No	Yes	Yes	Yes	Yes	No	Concentrator (1hour) + N_2 stream (5 minutes)	60 µL of pyridine + 60 µL of BTSFA
S3	No	Yes	Yes	Yes	Yes	No	Concentrator (1hour) + N_2 stream (5 minutes)	60 µL of pyridine + 60 µL of BTSFA
S4	Yes ca. 1.6 g	Yes	Yes	Yes	Yes	No	Concentrator (1hour) + N_2 stream (5 minutes)	60 µL of pyridine + 60 µL of BTSFA
S5	Yes ca. 1.6 g	Yes	Yes	Yes	Yes	No	Concentrator (1hour) + N_2 stream (5 minutes)	60 µL of pyridine + 60 µL of BTSFA
S6	Yes ca. 1.6 g	Yes	Yes	Yes	Yes	No	Concentrator (1hour) + N_2 stream (5 minutes)	60 µL of pyridine + 60 µL of BTSFA

3.2.1 Solid-phase extraction in methodological test samples

In geochemical analysis involving chemical separation steps for sample preparation, preconditioning cartridges is a critical step to ensure that they function as intended, providing accurate, reproducible, and contaminant-free results. Cartridges, especially those used for sample preparation, can contain trace impurities from manufacturing or storage that would introduce noise or biases into the analysis, affecting the accuracy and reliability of results. Thus, preconditioning ensures that the cartridge is clean and ready for use with the sample. Additionally, preconditioning helps equilibrate the cartridge with the solvents or reagents used in the analysis, ensuring that the cartridge behaves consistently across different samples. This leads to more reproducible and reliable results. Moreover, for procedures like solid-phase extraction, preconditioning can help improve the retention efficiency of target analytes by removing any previously retained compounds or conditioning the sorbent to interact more effectively with the analytes of interest. This results in higher recovery rates and more precise measurements.

A summary of the single steps of the solid-phase extraction for each methodological test sample is shown in Table 2.

At first, a total of five SPE cartridges were preconditioned with 3 mL of MeOH followed by 3 mL of ultrapure water, which was acidified to pH 1.

Onto the first two cartridges, 3 mL of MeOH was loaded, which filled the test tubes below (samples named “C+MeOH_1” and “C+MeOH_2”, respectively, see Table 1.

In contrast, 3.3 mL of HCl 6N were loaded onto the other three cartridges (samples named “C+HCl+MeOH_1”, “C+HCl+MeOH_2”, and “C+HCl+MeOH_3”, respectively, see Table 1). These three cartridges were then washed with 6 mL of acidified ultrapure water and dried for about 15 minutes by sucking ambient air through the cartridges using a vacuum manifold. To ensure both the proper functioning of the vacuum manifold and a minimised risk of contamination that could potentially affect the integrity of the sample, a layer of aluminium foil was placed at the top of the cartridges, above their openings. It served as a simple protective barrier, preventing excessive external contamination from entering the cartridges, while still permitting the necessary airflow for an efficient operation of the vacuum system.

Finally, 3 mL of MeOH were loaded onto these three cartridges and filled the test tubes below.

Moreover, 1.8 mL of MeOH were added directly into two test tubes (samples named “MeOH_1” and “MeOH_2”, respectively, see Table 1).

Next, the test tubes, which were seven in total were dried inside a RVC 2-18 Cdplus (Martin Christ Gefriertrocknungsanlagen GmbH, Germany) concentrator, in a vacuum environment at 60°C, for about 40 to 50 minutes, depending on the time needed by each sample to reach dryness.

Then, the residue was redissolved in 300 µL of ethyl acetate ($C_4H_8O_2$) and the solution was transferred into 1.5 mL brown vials using a different Pasteur pipette for each sample. The goal of this drying plus redissolution step was to concentrate LOPs in a lesser volume of solvent before transferring the solution into the brown vials to be stored for later analyses.

Finally, the solvent was evaporated to dryness inside the concentrator in ca. 10 minutes.

Once the solutions were completely dry, the residues were redissolved in 15 µL of pyridine, which is a basic heterocyclic organic compound with the chemical formula C_5H_5N, and 15 µL of Bis(trimethylsilyl)trifluoroacetamide (BTSFA) were added to each vial.

3.2.2 Preparation of speleothem test samples

A sample of 9.4 g of the RL18 flowstone from the Renella Cave, Italy, was used during this part of the experiments. Detailed information on flowstone RL18 is included in Zhornyak et al. (2011) and is summarized in sub-section 3.3.1.

The speleothem piece was dissolved in 30 mL of hydrochloric acid (6N HCl) and left to dissolve overnight at room temperature. During the rest of the analysis, only half of this solution was used, i.e. about 15 mL containing ca. 4.7 g of speleothem.

Table 2. *Descriptive summary of the solid-phase extraction in methodological test samples.*

Sample ID	Cartridges preconditioning	Speleothem sample	Acid load onto the cartridges	Cartridges wash	Cartridges drying	MeOH load
Blank_vial	No use of cartridges	No	No use of cartridges	No use of cartridges	No use of cartridges	1 mL onto the brown vial
MeOH_1	No use of cartridges	No	No use of cartridges	No use of cartridges	No use of cartridges	3 mL onto the test tube
MeOH_2	No use of cartridges	No	No use of cartridges	No use of cartridges	No use of cartridges	3 mL onto the test tube
C+MeOH_1	3 mL of MeOH + 3 mL of acidified ultrapure water	No	No	No	No	3 mL onto the cartridges
C+MeOH_2	3 mL of MeOH + 3 mL of acidified ultrapure water	No	No	No	No	3 mL onto the cartridges
C+MeOH+dry	3 mL of MeOH + 3 mL of acidified ultrapure water	No	No	No	15 minutes of vacuum manifold	2 mL onto the cartridges
C+HCl+MeOH_1	3 mL of MeOH + 3 mL of acidified ultrapure water	No	3.3 mL of HCl 6N	6 mL of acidified ultrapure water	15 minutes of vacuum manifold	3 mL onto the cartridges
C+HCl+MeOH_2	3 mL of MeOH + 3 mL of acidified ultrapure water	No	3.3 mL of HCl 6N	6 mL of acidified ultrapure water	15 minutes of vacuum manifold	3 mL onto the cartridges
C+HCl+MeOH_3	3 mL of MeOH + 3 mL of acidified ultrapure water	No	3.3 mL of HCl 6N	6 mL of acidified ultrapure water	15 minutes of vacuum manifold	3 mL onto the cartridges

3.2.3 Solid-phase extraction of organic matter in dissolved speleothem test solution

In this phase, 6 SPE cartridges were preconditioned with 3 mL of MeOH followed by 3 mL of ultrapure water, which was acidified to pH 1. Onto the first three cartridges (samples named “S1”, “S2”, and “S3”, respectively, which were blank samples), 3 mL of HCl 6N were loaded.

Onto the other three cartridges (samples named “S4”, “S5”, and “S6”, respectively, see Table 1.) ca 5 mL of diluted flowstone solution was loaded onto the cartridges using a different Pasteur pipette for each sample. The drip rate of the cartridges was about 1 drop s^{-1}. The cartridges were then washed with 6 mL of acidified ultrapure water and dried for about 30 minutes by sucking ambient air through the cartridges using a vacuum manifold, with a layer of aluminium foil placed at the top of the cartridges, above the openings. Then, the lignin in the samples was eluted with 2 mL of MeOH, which allowed the substances of interest to be transferred from the cartridges into the test tubes below. The content of the

tubes was then transferred into the microwave reaction vessels, using ca. 1 mL of MeOH to rinse the test tubes. The vessels were placed inside a drying oven at 60°C for the solvent to evaporate to dryness. A summary of the single steps of the solid-phase extraction for each speleothem test sample is shown in Table 3.

Table 3. *Descriptive summary of the solid-phase extraction in speleothem test samples.*

Sample ID	Cartridges preconditioning	Speleothem sample	Acid load onto the cartridges	Cartridges wash	Cartridges drying	MeOH load
S1	3 mL of MeOH + 3 mL of acidified ultrapure water	No	3 mL of HCl 6N	6 mL of acidified ultrapure water	30 minutes of vacuum manifold	2 mL onto the cartridges
S2	3 mL of MeOH + 3 mL of acidified ultrapure water	No	3 mL of HCl 6N	6 mL of acidified ultrapure water	30 minutes of vacuum manifold	2 mL onto the cartridges
S3	3 mL of MeOH + 3 mL of acidified ultrapure water	No	3 mL of HCl 6N	6 mL of acidified ultrapure water	30 minutes of vacuum manifold	2 mL onto the cartridges
S4	3 mL of MeOH + 3 mL of acidified ultrapure water	Yes ca. 1.6 g	5 mL of flowstone solution diluted in HCl 6N	6 mL of acidified ultrapure water	30 minutes of vacuum manifold	2 mL onto the cartridges
S5	3 mL of MeOH + 3 mL of acidified ultrapure water	Yes ca. 1.6 g	5 mL of flowstone solution diluted in HCl 6N	6 mL of acidified ultrapure water	30 minutes of vacuum manifold	2 mL onto the cartridges
S6	3 mL of MeOH + 3 mL of acidified ultrapure water	Yes ca. 1.6 g	5 mL of flowstone solution diluted in HCl 6N	6 mL of acidified ultrapure water	30 minutes of vacuum manifold	2 mL onto the cartridges

3.2.4 Microwave-assisted CuO oxidation

Lignin phenols were analyzed via CuO oxidation following the method published by (Goñi & Montgomery, 2000).

20 mL Perfluoroalkoxy alkanes (PFA) vessels were used as reaction vessels, each of which was loaded, in addition to the sample solution, with 100 mg of copper oxide (CuO), about 50 mg of Ammonium iron(II) sulfate hexahydrate ($FeS(NH_4)2O_4$), and 6 mL of an alkaline solution (2 M NaOH aqueous solution). To operate in an environment free from oxygen, which could lead to overoxidation of the lignin oxidation products, a glovebox was used. A glovebox is a sealed container designed to allow the manipulation of objects where a separate atmosphere is desired, in our case, an atmosphere without oxygen. The glovebox is equipped with gloves integrated into its sides or front, allowing the user to insert their hands into the gloves and perform tasks inside the box while maintaining an airtight seal and preventing any breach of containment. The vessels and the NaOH aqueous solution were placed inside the glove box. Then, the NaOH aqueous solution was purged by pumping nitrogen (N_2) to remove dissolved oxygen until a concentration of less than 1% was reached in the whole glove box. The NaOH solution bubbling step is important, as most samples are sensitive to the presence of O_2 in the reaction solution. Finally, 6 mL of NaOH aqueous solution was added to each vessel and they were capped before being extracted from the glovebox to ensure an inert gas atmosphere inside them.

The well-sealed vessels were then placed in the high-pressure segment rotor of the microwave oven. The microwave-assisted CuO oxidation procedure was performed using a MARS 6 Microwave Digestion System (CEM Corporation, USA) was used with a high-pressure segment rotor and a temperature sensor that utilizes Light Emitting Technology (LET) to measure the temperature inside one reaction vessel. The temperature was increased to 150°C in 10 minutes and then held at 150 ◦C for 90 min. The vessels were then allowed to cool down to room temperature overnight.

Directly after opening the vessels, 50 µL of a 7,824 ng μg^{-1} standard solution of ethyl vanillin was added as an internal standard into each sample to estimate recovery rates. Ethyl vanillin is particularly suitable as an internal standard because it is an artificial compound. Hence, it has very low blank values and does not occur in natural samples (Heidke et al., 2018).

Next, the reaction solutions were transferred into centrifuge tubes, and the reaction vessels were rinsed twice with 3 mL of NaOH aqueous solution. The combined solutions were centrifuged in a VWR Mega Star 1.6 centrifuge for 2 min at 2000 rpm to separate the liquid solution from the copper particles. Next, the supernatant was carefully decanted into test tubes already containing 4 mL of concentrated HCl each, in order to be acidified to pH 1.

3.2.5 Solid-phase extraction of LOPs in oxidized solutions

The conditioning, loading, washing, and drying steps of the SPE cartridges were similar to those described in Sect. 2.2.3. A total of seven SPE cartridges were preconditioned with 3 mL of MeOH followed by 3 mL of ultrapure water, which was acidified to pH 1. The oxidised solutions were loaded onto six of the preconditioned cartridges using a different Pasteur pipette for each sample, while nothing was loaded into the seventh cartridge (sample named "C+MeOH+dry", see Table 1). The drip rate of the cartridges was about 1 drop s^{-1}. The introduction of the C+MeOH+dry sample aims to investigate the eventual contamination introduced by the usage of the vacuum manifold. The six cartridges onto which acid was loaded, were then washed with 6 mL of acidified ultrapure water. Next, all the cartridges were dried for about 15 minutes by sucking ambient air through the cartridges using a vacuum manifold, with a layer of aluminium foil placed at the top of the cartridges, above the openings.

Lignin oxidation products in the samples were eluted with 1.6 mL of MeOH, which allowed the transfer of the substances of interest from the cartridges directly into 1 mL brown vials placed below.

Moreover, 1 mL of MeOH was injected directly into one 1 mL brown vial (sample named "Blank_vial", see Table 1).

The solvent inside the eight vials was partially evaporated inside the RVC 2-18 Cdplus concentrator, in a vacuum environment at 60°C, for about an hour. Then, to accelerate the drying step, the remaining solvent was evaporated to dryness under a gentle stream of N_2 at 55°C in ca. 5 minutes. Once the solutions were completely dry, the residue of samples S1 to S6 was redissolved in 60 µL of pyridine and 60 µL of BTSFA. In contrast, the residue of samples C+MeOH_dry and Blank_vial was redissolved in 15 µL of pyridine and 15 µL of BTSFA each.

3.2.6 GC-MS analysis

The quantification of CuO oxidation products was carried out on a gas chromatography-mass spectrometry (GC-MS), using a 7820A Gas Chromatograph coupled with a 5977B Mass Selective Detector (all by Agilent Technologies) in single ion monitoring (SIM). To separate LOPs, the GC-MS was equipped with a Trajan SGE 30 m × 320 µm (0.25 µm-thick film) PB-1 capillary column. The oven temperature ramp was set from 100°C to 300°C at a rate of 4°C/min with a hold time of 10 minutes.

CuO oxidation products analysed include 3,5-dihydroxybenzoic acid (3,5-Bd) and 11 lignin phenols:

- vanillyl phenols (V): vanillin (Vl), acetovanillone (Vn), and vanillic acid (Vd);
- syringyl phenols (S): syringaldehyde (Sl), acetosyringone (Sd), and syringic acid (Sn);

- cinnamyl phenols I: p-coumaric acid (pCd) and ferulic acid (Fd)
- the p-hydroxyl phenols (P): p-hydroxybenzoic acid (Pd), p-hydroxybenzaldehyde (Pl), and p-hydroxyacetophenone (Pn).

Quantification of lignin phenols was achieved through calibration curves obtained from commercially available standards (Sigma-Aldrich).

3.3 Methods applied to the analysis of the RL 18

Figure 8 is a process chart illustrating the overall sample preparation procedure, the different steps of which will be described in detail in the following sections. Overall, the analysis follows the one described in Heidke et al. (2018) and took place in October and November 2024. During the procedure, some modifications have been applied compared to what is described in Sect. 3.2, but the instrumentation, such as the microwave and the gas chromatography-mass spectrometry (GC-MS), were the same. Nevertheless, differences, when present, are always mentioned in the following sections.

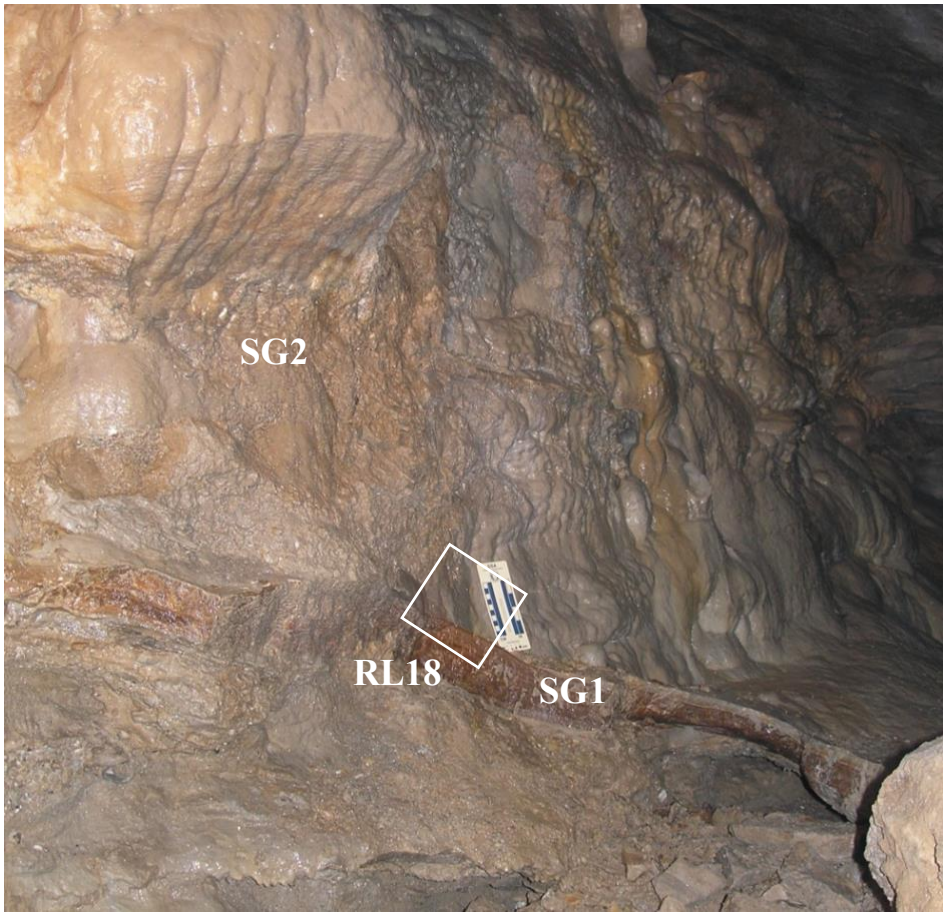

Figure 7. *Sampling position of RL18 in Renella cave. Courtesy of Eleonora Regattieri.*

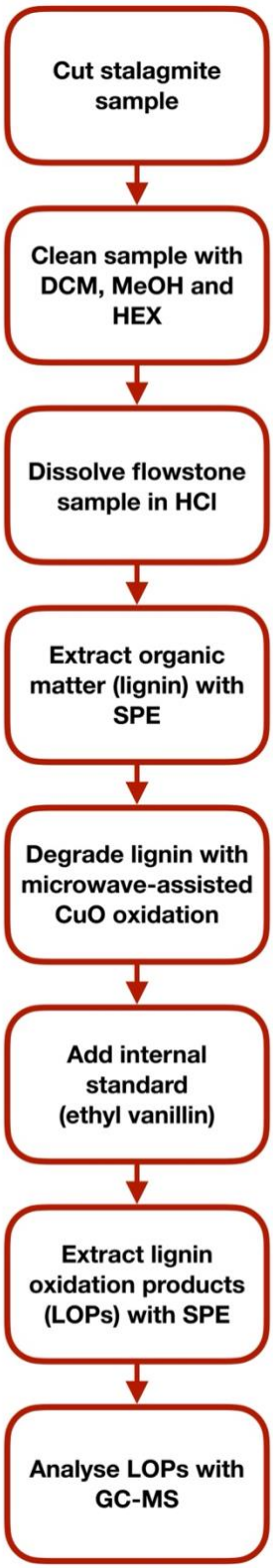

Figure 8. *Process chart of the overall sample preparation procedure. A detailed description of the individual steps is given in the sub-sections of Sect. 3.3.*

3.3.1 Sampling and preparation of flowstone samples

Detailed information on flowstone RL18 is included in Zhornyak et al. (2011) and is summarised in this paragraph. Flowstone RL18 from the Renella Cave, central Italy, reaches up to ca 15 cm in thickness and overlies a lithologically heterogeneous (polygenetic) sandy-gravel layer, comprising marble and basement (phyllitic) elements (clastic layer SG1, see Figure 7). RL18 is a predominantly dark-brown, well-laminated flowstone. The lowest U/Th age of RL18 suggests that its formation started before ca 12.5 ka, and its deposition ceased at ca 8 ka. Thus, the stalagmite spans the transition from the Pleistocene to the Holocene. About 1 cm at the base is composed of a grey sand-rich calcite, which is separated from the main dark-brown section by a layer of grey sand (Figure 9). This is the only evidence of growth interruption. The top of flowstone RL18 is partially covered by a second clastic layer comprising mainly cemented sands (layer SG2, Figure 7 and Figure 9) with a composition similar to SG1, but finer-grained and containing mud layers probably indicative of standing-water deposition after flood events. The SG2 layer currently forms a shelf in certain areas of the chamber. The presence of layer SG2 at the top of RL18 is particularly relevant, since, nowadays, the cave experiences intermittent flooding of the lower galleries, but there is no sign of recent flooding in the higher galleries where RL18 was collected. Zhornyak et al. (2011) suggest that SG2 formed during a period of elevated cave stream discharge and sediment transport into the cave when flood events were sufficiently intense to submerge the majority of the cave, thereby allowing sedimentation.

A part of flowstone RL18, spanning from 0 to 124 mm of depth, was cut along the growth axis in pieces ca 4 mm thick. This part of the sample preparation was performed at the Institute of Geosciences and Earth Resources (IGG) in Pisa, Italy. A total of 25 different samples from RL18, whose information is listed in Table 4, were sent from IGG to the Institute of Polar Sciences (ISP) in Bologna, where the rest of the analysis was conducted.

Figure 9. *RL18 flowstone from the Renella cave. Courtesy of Eleonora Regattieri.*

To clean the flowstone samples, each sample was covered in methanol (MeOH) and placed in an ultrasonic cleaner for approximately one minute. The solvent was discarded, and the sample was further cleaned using dichloromethane (DCM) and finally hexane (HEX). The first two solvents, being polar, were effective in removing polar contaminants, while hexane, a non-polar solvent, was used to eliminate non-polar impurities. Once, the samples were dried, they were weighed (see Table 1) and placed in clean Falcon tubes for further processing.

To dissolve the samples, 3 mL of hydrochloric acid (HCl) was added for every gram of speleothem material present in each Falcon tube. The acid was introduced carefully and gradually, 1 mL at a time, in order to avoid, as much as possible, the loss of material due to possible overflow from the tube caused by the strong decarbonisation reaction that occurs during the process. The samples were left to dissolve overnight at room temperature.

Table 4. *List of RL18 flowstone samples*

Sample ID	Depth (± 1 mm)	Mass (± 0.001 g)
RL 18-1	0 – 4	4.961
RL 18-2	5 – 9	4.893
RL 18-3	10 – 14	5.140
RL 18-4	15 – 19	4.519
RL 18-5	20 – 24	4.683
RL 18-5b	25 – 29	3.159
RL 18-6	30 – 34	3.838
RL 18-7	35 – 39	4.154
RL 18-8	40 – 44	3.026
RL 18-9	45 – 49	3.777
RL 18-10	50 – 54	3.021
RL 18-11	55 – 59	3.467
RL 18-12	60 – 64	2.940
RL 18-13	65 – 69	2.656
RL 18-14	70 – 74	2.515
RL 18-15	75 – 79	2.059
RL 18-16	80 – 85	2.900
RL 18-17	86 – 90	1.794
RL 18-18	91 – 95	1.795
RL 18-19	96 – 101	3.344
RL 18-20	101 – 105	2.581
RL 18-21	106 – 109	3.677
RL 18-22	110 – 114	2.206
RL 18-23	115 – 118	2.456
RL 18-24	119 – 123	1.742

3.3.2 Solid-phase extraction of organic matter in dissolved flowstone solution

The SPE cartridges were preconditioned with 3 mL of MeOH followed by 6 mL of ultrapure water, which was acidified to pH 1. For the first three cartridges, 3 mL of MeOH followed by only 3 mL (instead of 6 mL) of ultrapure water were used for the preconditioning. These cartridges were used for one first blank sample and the first two flowstone samples (RL 18-1 and RL 18-2). No evident difference was present in the results of these three samples compared to all the others, but it was deemed more prudent to use 6 mL of acidified ultrapure water during the preconditioning instead of 3 mL. This decision was made to ensure a more thorough rinsing process.

The diluted flowstone solution was loaded onto the cartridges using a different Pasteur pipette for each sample. The drip rate of the cartridges was about 1 drop s^{-1}. The cartridges were then washed with 6 mL of acidified ultrapure water and dried for about 1 minute by sucking ambient air through the cartridges using a vacuum manifold, with a layer of aluminium foil placed at the top of the cartridges, above the openings. In addition to the 25 speleothems samples, 5 blank samples were produced as well. For these, the procedure was analogous, but instead of the dissolved sample, 6 mL of pure acid was loaded onto the cartridges. The lignin in the samples was eluted with 2.2 mL of MeOH, which allowed to transfer of the substances of interest from the cartridges into the test tubes below. The content of the tubes was then transferred into the microwave reaction vessels, using 0,700 mL of MeOH to rinse the test tubes. The solvent was evaporated to dryness under a gentle stream of N_2.

3.3.3 Microwave-assisted CuO oxidation

PFA vessels with a capacity of 20 mL were used as reaction vessels, each of which was loaded, in addition to the sample solution, with 100 mg of CuO, about 50 mg di $FeS(NH_4)_2O_4$, and 6 mL of alkaline solution (2 M NaOH aqueous solution). To operate in an environment free from oxygen, which could lead to overoxidation of the lignin oxidation products, a glovebox was used, as described in Subsection 3.2.4.

The well-sealed vessels were then placed in the high-pressure segment rotor of the microwave oven, processing 12 samples at a time. Having a total of 30 samples (25 speleothems samples and 5 blank samples), the third round of microwave-assisted CuO oxidation was performed with the rotor holding 6 vessels containing samples and six vessels filled with 100 mg of CuO, about 50 mg di $FeS(NH_4)_2O_4$, and 6 mL of the 2 M NaOH aqueous solution. The temperature was increased to 150°C in 10 minutes and then held at 150 ◦C for 90 min.

Afterwards, the vessels were allowed to cool down to room temperature. Then, the solution of each vessel was carefully transferred into 50 mL Falcon tubes, and 50 µL of a 7,824 ng μg^{-1} standard solution of ethyl vanillin was added as an internal standard into each tube. The combined solutions were centrifuged for 2 min at 1000 rpm and the supernatant was decanted into 8 mL brown vials.

3.3.4 Solid-phase extraction of LOPs in oxidized solutions

The content of the 30 different 8 mL brown vials was transferred into 30 different bigger glass vials, and the 2 M NaOH aqueous solution was added in order to reach the same volume inside each vial, which corresponded to the volume of the vial that was the fullest. Then, the oxidized solutions were acidified to pH 1 by adding 2 mL of HCl. The conditioning, loading, washing, and drying steps of the SPE cartridges were similar to those described in Sect. 2.3.2. The SPE cartridges were preconditioned with 6 mL of MeOH followed by 6 mL of ultrapure water, which was acidified to pH 1. The oxidized solutions were loaded onto the cartridges using a different Pasteur pipette for each sample. The drip rate of the cartridges was about 1 drop s^{-1}. The cartridges were then washed with 6 mL of acidified ultrapure water and dried for about 1 minute by sucking ambient air through the cartridges using a vacuum manifold, with a layer of aluminium foil placed at the top of the cartridges, above the openings. Lignin oxidation products in the samples were eluted with 4.5 mL (6 mL for the first samples) of MeOH, which allowed

the transfer of the substances of interest from the cartridges into the test tubes below. The solvent was evaporated to dryness under a gentle stream of N_2 at 55°C.

Once the solutions were completely dry, the residue was redissolved using 300 µL of pyridine and an ultrasonic cleaner. Finally, using a different Pasteur pipette for each sample, the solutions were transferred into 1.5 mL brown vials, adding 15 µL of BTSFA, as well.

3.3.5 GC-MS analysis

The quantification of CuO oxidation products was carried out on a gas chromatography-mass spectrometry (GC-MS) in single ion monitoring (SIM). To separate LOPs, the GC-MS was equipped with a Trajan SGE 30 m × 320 µm (0.25 µm-thick film) PB-1 capillary column. The oven temperature ramp was set from 100°C to 300°C at a rate of 4°C/min with a hold time of 10 minutes.

CuO oxidation products analysed include 3,5-dihydroxybenzoic acid (3,5-Bd) and 11 lignin phenols:

- vanillyl phenols (V): vanillin (Vl), acetovanillone (Vn), and vanillic acid (Vd);
- syringyl phenols (S): syringaldehyde (Sl), acetosyringone (Sd), and syringic acid (Sn);
- cinnamyl phenols I: p-coumaric acid (pCd) and ferulic acid (Fd)
- the p-hydroxyl phenols (P): p-hydroxybenzoic acid (Pd), p-hydroxybenzaldehyde (Pl), and p-hydroxyacetophenone (Pn).

Quantification of lignin phenols was achieved through calibration curves obtained from commercially available standards (Sigma-Aldrich).

4. Results

In this section and the appendix, the tables containing all the values measured by the GC-MS are shown. The errors for all results presented in this work were calculated using the law of the propagation of uncertainty. In the following chapters, the names of the detected phenols will be abbreviated as follows:

- 3,5-Bd = 3,5-dihydroxybenzoic acid

P group:

- Pd = p-hydroxybenzoic acid
- Pl = p-hydroxybenzaldehyde
- Pn = p-hydroxyacetophenone

V group:

- Vd = vanillic acid
- Vl = vanillin
- Vn = acetovanillone

S group:

- Sd = syringic acid
- Sl = syringaldehyde
- Sn = acetosyringone

C group:

- pCd = trans-p-coumaric acid
- Fd = trans-ferulic acid

4.1 Test samples

Each step in the analytical sample preparation method includes the risk of positive or negative artefacts, especially if large amounts of chemicals are added or multiple decanting processes are done. Hence, the sample preparation was divided into several parts to inspect which chemical or phase of the analysis could cause major contamination. The different methodological test samples underwent different procedures, and Figure 10 shows the peak area detected by the GC-MS for each phenol in the methodological test samples. When more than one sample was performed for a specific sample type (such as for “MeOH”) the average between the n samples was calculated and used for further analysis. The blank values of each phenol and fully listed in Table 5 and Table 6.

As one could expect, “C+HCl+MeOH” samples, which underwent all analysis steps are often more contaminated than other samples. However, this is not always the case. The "blank vial" sample is also highly contaminated despite being a sample that has undergone virtually no processing (see Table 1 and Table 2). When it comes to certain specific phenols (e.g., 3,5-Bd and Pd), the "blank vial" sample is even more contaminated than the "C+HCl+MeOH" sample. Therefore, in light of contamination that seems unrelated to the number of processing steps or chemicals employed, it can be concluded that the majority of the contamination is likely due to impure air in the laboratory rather than any specific stage of the sample preparation, and it is distributed randomly among the methodological test samples.

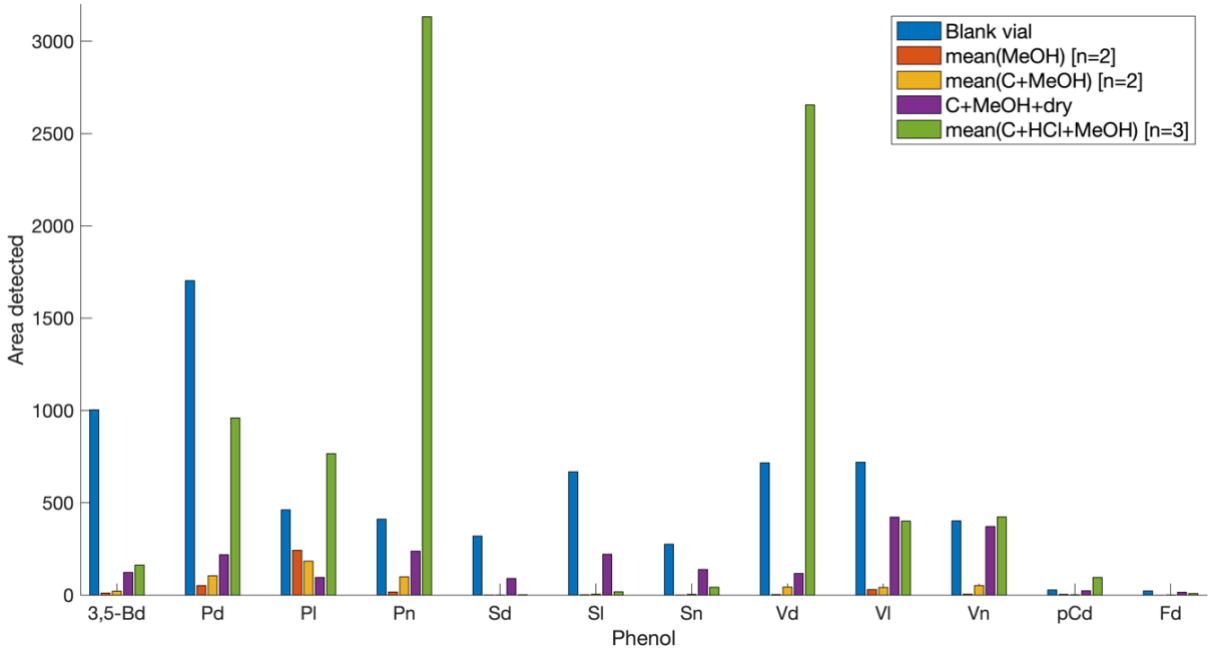

Figure 10. *Peak area detected by the GC-MS for the 12 LOPs in methodological samples (eventually averaged over n samples) that underwent different numbers of analysis steps. See Table 1 and Table* ***2****.*

Due to the randomness in the contamination, the methodological samples can be considered virtually equivalent and be used to evaluate the most present phenols. To do so, for each phenol of the P, C, V, and S group, the blank values of all methodological samples were summed, and the results obtained were plotted as piechart (see Figure 11, left). A piechart showing the total LOPs group proportions is also shown (see Figure 11, right).

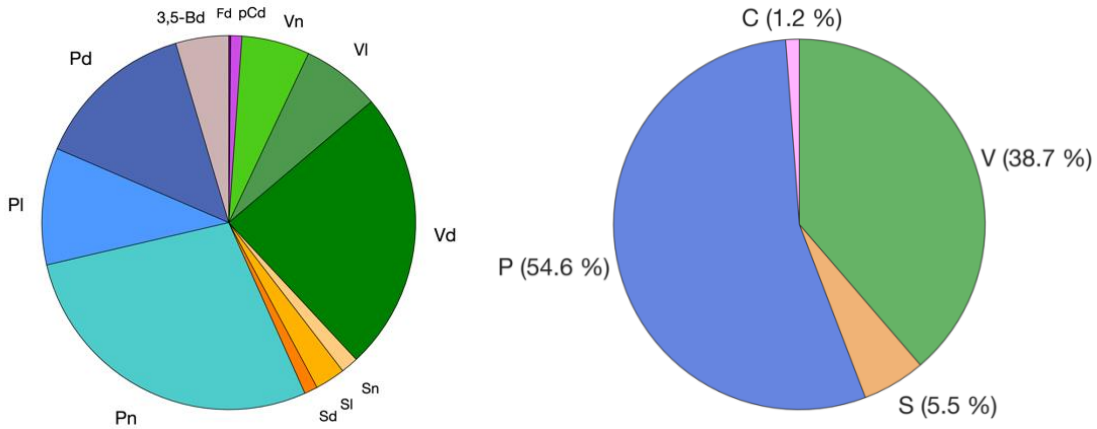

Figure 11. *Left: single phenol proportions in all methodological test samples. Right: LOP's groups proportions in all methodological test samples.*

Table 5. *Areas measured by the GC-MS for the methodological test samples.*

Sample ID	Pl	Pn	Vl	Vn	Pd	Sl	Sn	Vd	3,5-Bd	Sd	pCd	Fd
Blank_vial	462	411	720	402	1703	668	275	716	1004	319	28	22
MeOH_1	256	19	33	6	62	2	1	2	14	3	7	0
MeOH_2	228	13	27	3	41	2	1	3	8	0	2	0
C+MeOH_1	304	63	31	32	76	3	3	73	16	2	2	2
C+MeOH_2	65	135	51	70	134	7	6	14	26	1	2	0
C+MeOH+dry	95	238	422	372	219	221	139	117	123	90	23	15
C+HCl+MeOH_1	953	2899	463	476	843	23	39	2939	114	0	91	11
C+HCl+MeOH_2	1134	3528	548	549	916	20	44	2727	146	2	99	11
C+HCl+MeOH_3	210	2971	193	246	1118	9	44	2302	228	3	99	1

Table 6. *Areas measured by the GC-MS for the methodological and blank test samples averaged over n samples.*

Sample ID	Pl	Pn	Vl	Vn	Pd	Sl	Sn	Vd	3,5-Bd	Sd	pCd	Fd
Blank_vial (n=1)	462	411	720	402	1703	668	275	716	1004	319	28	22
MeOH (n=2)	242	16	30	5	51	2	1	3	11	1	4	0
C+MeOH (n=2)	184	99	41	51	105	5	4	44	21	1	2	1
C+MeOH+dry (n=1)	95	238	422	372	219	221	139	117	123	90	23	15
C+HCl+MeOH (n=3)	766	3133	401	424	959	17	42	2656	162	2	96	8
S blanks (n=3)	4932	8664	3694	802	7983	450	89	727	605	210	1934	4

Table 7. *Areas measured by the GC-MS for the speleothem test samples (S1, S2, and S3 are blank samples) with mean, standard deviation, standard error on the mean, and coefficient of variance expressed as percentage.*

Sample ID	Pl	Pn	Vl	Vn	Pd	Sl	Sn	Vd	3,5-Bd	Sd	pCd	Fd
S1	4989	7373	5739	1145	8258	495	69	1224	805	231	882	6
S2	5421	8756	2374	643	7771	467	125	278	668	268	1028	3
S3	4384	9862	2969	619	7921	388	74	679	342	132	3890	3
Mean	4932	8664	3694	802	7983	450	89	727	605	210	1934	4
Standard deviation	521	1247	1796	297	249	56	31	475	238	71	1696	2
Standard error on the mean	301	720	1037	172	144	32	18	274	137	41	979	1
Coefficient of variation (%)	11	14	49	37	3	12	35	65	39	34	88	42
S4	25444	112289	237849	168643	542285	324763	166505	268031	549659	193205	19646	30043
S5	34414	139155	290941	196157	557571	375534	186383	264455	566772	201474	20885	32877
S6	28081	117109	221292	157537	480088	287465	154030	237485	416321	167736	13359	24849
Mean	29313	122851	250027	174112	526648	329254	168973	256657	510917	187471	17963	29256
Standard deviation	4610	14324	36386	19882	41040	44206	16317	16699	82368	17584	4036	4071
Standard error on the mean	2662	8270	21008	11479	23694	25522	9421	9641	47555	10152	2330	2351
Coefficient of variation (%)	16	12	15	11	8	13	10	7	16	9	22	14
Ratio (in %) mean blank/mean speleothem	17%	7%	1%	<1%	2%	<1%	<1%	<1%	<1%	<1%	11%	<1%

The summed blank values reflect the natural occurrence of the different analytes. The highest blank values have been found for the p-hydroxyacetophenone, vanillic acid, p-hydroxybenzoic acid, and p-hydroxybenzaldehyde. The p-hydroxy group is known to originate not only from lignin but also from protein-rich materials, such as bacteria (Jex et al., 2014). For this reason, the P group phenols are usually not used as proxies for the source of lignin. Vanillin and its oxidised form, vanillic acid, are commonly employed as fragrances and flavourings in food, cosmetics, and household cleaning products. As such, these compounds could also be introduced into the sample via the laboratory air or from detergents used to clean the laboratory equipment.

The values of the integrated peak area detected by the GC-MS of each phenol for the speleothem (S) test samples are listed in Table 7, together with the mean, standard deviation, standard error on the mean, and coefficient of variation (also known as the relative standard deviations. The coefficient of variation, expressed as a percentage, is computed by multiplying by 100 the ratio of the standard deviation and the mean of each analyte. S1, S2, and S3 are blank samples, while S4, S5, and S6 contained some dissolved speleothem. If the percentages plotted in Figure 11 are calculated again, this time including S1, S2, and S3, one can see that the inclusion of S blank test samples produces a not negligible increase in the relative abundance of pCd (and, consequently, of the C group). These results are illustrated in Figure 12. The reason for this enhanced pCd value could be that the S samples underwent a three times longer cartridge drying step compared to methodological test samples. We believe that this caused a rise in the pCd contamination level, since p-coumaric acid is an important component of pollen (Hu et al., 1999; Tareq & Ohta, 2015). More precisely, pCd is highly present in sporopollenin (Fraser et al., 2012; Montgomery et al., 2016), a major constituent of pollen and fungal spores. It is important to note that these analyses were conducted in July, a period during which the air is particularly rich in pollen. Consequently, para-coumaric acid might have been introduced into the S blank test samples through laboratory unpure air. These results led us to perform a much shorter drying step (about one minute) when analysing the RL18 samples.

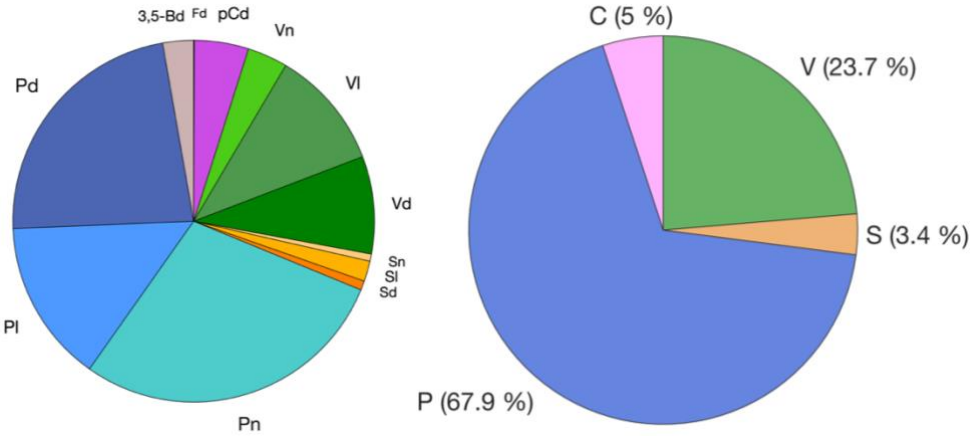

Figure 12. *Left: single phenol proportions in all methodological test samples and S1, S2, and S3 samples. Right: LOP's groups proportions in all methodological test samples and S1, S2, and S3 samples.*

An additional indication that the contamination of the samples primarily occurred due to the laboratory unpure air rather than during any specific step is provided by the random distribution of the values of the ratio (listed in Table 8) between the areas detected for the methodological samples, and the mean

area detected for S1, S2, and S3. In most cases, the mean area for the S blank test samples is much larger than the areas detected in the case of the methodological samples. This can be easily explained by the fact that S samples had more chance of being contaminated, since they underwent a longer analysis. Nevertheless, there are cases in which a specific phenol is present in a much bigger amount in methodological samples (for examples, Fd in the “blank vial” sample).

Table 8. *Ratios between the areas detected for the methodological samples (averaged over n samples) and the mean area detected for S1, S2, and S3.*

Sample ID	Pl	Pn	Pd	Vl	Vn	Vd	Sl	Sn	Sd	pCd	Fd	3,5-Bd
Blank_vial (n=1)	0.09	0.05	0.21	0.19	0.50	0.98	1.49	3.08	1.52	0.01	5.26	1.66
MeOH (n=2)	0.05	<0.01	0.01	0.01	0.01	<0.01	<0.01	0.01	0.01	<0.01	<0.01	0.02
C+MeOH (n=2)	0.04	0.01	0.01	0.01	0.06	0.06	0.01	0.05	0.01	<0.01	0.18	0.03
C+MeOH+dry (n=1)	0.02	0.03	0.03	0.11	0.46	0.16	0.49	1.55	0.43	0.01	3.48	0.20
C+HCl+MeOH (n=3)	0.16	0.36	0.12	0.11	0.53	3.65	0.04	0.47	0.01	0.05	1.82	0.27

In Table 7, the mean values and some other statistics for each phenol of the three S blanks are shown. The blank value varied from sample to sample, which is reflected in the standard deviations of the blank values given in Table 7, but tends to be much smaller than that of the speleothem samples S4, S5, and S6. The ratio of the mean blank value and the mean speleothem value, expressed as a percentage, is always less than or equal to 2%, except for three phenols: Pl, Pn, and pCd. One can rectify for this contamination by neglecting the P group of LOPs and reducing the time in the cartage drying step. The fact that the GC-MS efficiently detected a much higher amount of LOPs in the samples that contained the dissolved sediment is evident from the plots in Figure 13, where the areas of the LOP groups in the blank samples (S1, S2, and S3) is represented next to the areas of the LOP groups in the S4, S5, and S6 samples. The areas obtained for S4, S5, and S6 are about two orders of magnitude larger than those obtained for S1, S2, and S3. In S4, S5, and S6, we found a similar amount of S-group LOPs and V-group LOPs, with a modest predominance of S-group LOPs. In contrast, a much smaller area was detected for the C-group LOPS. In contrast, when it comes to blank samples, the largest area detected is the one for V-group LOPs, followed by that for C-group LOPs. Blank samples, therefore, contain a much smaller amount of S-group LOPs compared to the speleothem dissolved in S4, S5, and S6. In Figure 25, in the appendix, the LOP groups area for all the blank S test samples (i.e. S1, S2, and S3) are shown in a linear scale to allow for better visualisation of the contribution of the LOP groups to the total area.

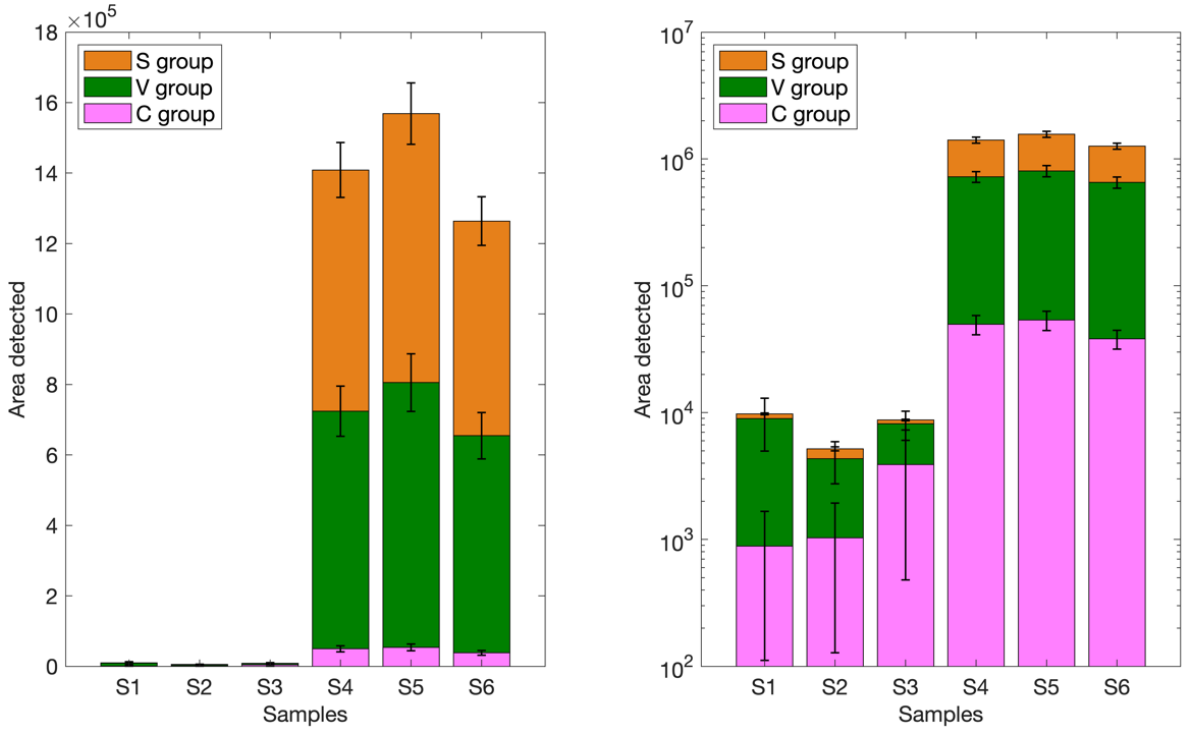

Figure 13. *Left: LOP groups area for all the S test samples. S1, S2, and S3 are blank samples, while S4, S5, and S6 contained dissolved flowstone. The height of the columns represents the sum of the LOP concentrations, Σ8, and the different colours show the contribution of the C-, S- and V-group LOPs. Right: Same plot, but the y-axis is in logarithmic scale.*

As already mentioned, another goal of the test samples analysis was the evaluation of the repeatability of the sample preparation and analysis method. For this reason, 9.4 g of the RL18 flowstone were dissolved in 30 mL of HCl, and half of this solution, i.e. about 15 mL containing ca. 4.7 g of speleothem, was divided into the three samples S4, S5, and S6.

To convert areas detected by the GC-MS to concentration in mg g^{-1}, external calibration with a standard solution containing ethyl vanillin was performed. The calibration function was obtained using a power regression method. The concentrations of the single LOPs (in mg g^{-1}) obtained for samples S4, S5, and S6 are shown in Table 9, together with some basic statistics (mean values, standard deviations and coefficients of variation). The coefficient of variation is then used as the percentage of uncertainty to attribute to each single value. In contrast, the error on the mean is calculated as the ratio of the standard deviation and the square root of the number of averaged samples n (in this case, n=3). The coefficients of variation ranged from 6 % to 13 %. The trans-ferulic acid has the highest coefficients of variation among the studied phenols, mainly because its concentration is low. For the p-hydroxy group, the relative standard deviations are also generally high, but these analytes were not used for the determination of LOP parameters. The variability can be caused by the CuO oxidation step, which is known to cause relatively high variability even in samples with high lignin content (for example, Hedges & Mann, 1979, with relative standard deviations ranging between 3% and more than 80%).

By summing the values in Table 9, the concentration for the S, C, V, and P group LOPs for samples S4, S5, and S6 and for their mean are computed. The sum of all eight LOPs (Σ8) is also calculated. These results are listed in Table 10 and plotted in Figure 14.

Table 9. *Concentration of LOPs (in mg g^{-1}) in samples S4, S5, and S6 with some basic statistics: mean values, standard deviations and coefficients of variation expressed in percentage.*

Sample ID	Pl (mg g^{-1})	Pn (mg g^{-1})	Vl (mg g^{-1})	Vn (mg g^{-1})	Pd (mg g^{-1})	Sl (mg g^{-1})	Sn (mg g^{-1})	Vd (mg g^{-1})	3,5-Bd (mg g^{-1})	Sd (mg g^{-1})	pCd (mg g^{-1})	Fd (mg g^{-1})
S4	0.021 ± 0.002	0.045 ± 0.004	0.032 ± 0.002	0.042 ± 0.003	0.047 ± 0.005	0.100 ± 0.007	0.062 ± 0.006	0.054 ± 0.005	0.076 ± 0.005	0.086 ± 0.009	0.066 ± 0.005	0.018 ± 0.002
S5	0.026 ± 0.003	0.052 ± 0.005	0.035 ± 0.003	0.046 ± 0.003	0.054 ± 0.005	0.107 ± 0.008	0.070 ± 0.007	0.060 ± 0.005	0.079 ± 0.005	0.09 ± 0.01	0.071 ± 0.006	0.019 ± 0.003
S6	0.022 ± 0.002	0.045 ± 0.004	0.030 ± 0.002	0.040 ± 0.003	0.045 ± 0.004	0.092 ± 0.007	0.057 ± 0.006	0.051 ± 0.004	0.070 ± 0.004	0.074 ± 0.008	0.061 ± 0.005	0.015 ± 0.002
Mean	0.023 ± 0.001	0.047 ± 0.003	0.032 ± 0.001	0.043 ± 0.002	0.049 ± 0.003	0.100 ± 0.004	0.063 ± 0.004	0.055 ± 0.003	0.075 ± 0.003	0.084 ± 0.005	0.066 ± 0.003	0.017 ± 0.001
Standard deviation	0.003	0.004	0.002	0.005	0.007	0.007	0.005	0.005	0.009	0.005	0.002	0.002
Coefficient of variation	11 %	10 %	7 %	8 %	10 %	7 %	10 %	8 %	6 %	11 %	8 %	13 %

Table 10. *Concentrations (in mg g^{-1}) of the S, C, V, and P group LOPs and the sum of all eight LOPs (Σ8) in samples S4, S5, and S6 and their mean.*

Sample	S group (mg g^{-1})	C group (mg g^{-1})	V group (mg g^{-1})	P group (mg g^{-1})	Σ8 (mg g^{-1})
S4	0.18 ± 0.02	0.039 ± 0.004	0.15 ± 0.01	0.17 ± 0.01	0.38 ± 0.03
S5	0.20 ± 0.02	0.042 ± 0.005	0.17 ± 0.01	0.18 ± 0.02	0.41 ± 0.04
S6	0.17 ± 0.02	0.034 ± 0.004	0.14 ± 0.01	0.16 ± 0.01	0.35 ± 0.03
Mean	0.18 ± 0.02	0.038 ± 0.004	0.16 ± 0.01	0.17 ± 0.01	0.38 ± 0.03

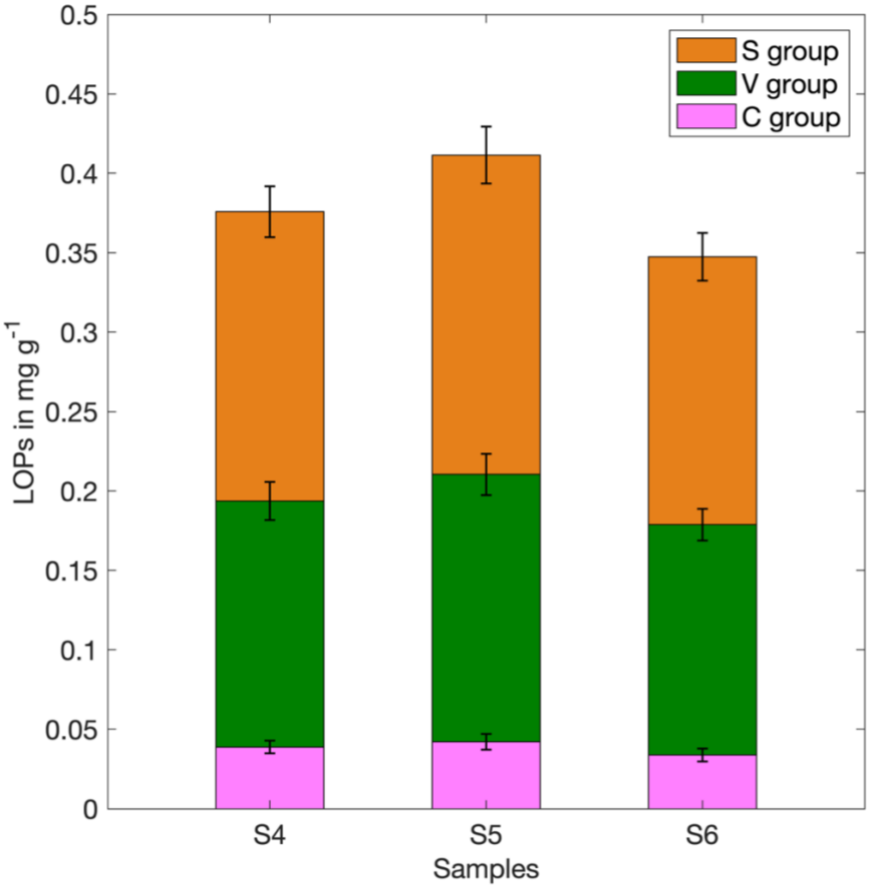

Figure 14. *LOPs concentration (in mg g^{-1}) in the speleothem test samples S4, S5, and S6. The height of the columns represents the sum of the LOP concentrations, Σ8, and the different colours show the contribution of the C-, S- and V-group LOPs.*

4.2 Cave samples (RL18 samples)

To evaluate and eventually eliminate the influence of possible contamination sources on the results, five reagent blanks, which had undergone all preparation steps, were analysed with the RL18 samples. The mean values and the standard deviations of the five reagent blanks are shown in Table 11. The blank values varied from sample to sample (they are all listed in Table A2, in the appendix), which is reflected in the standard deviations of the blank values given in Table 11. Note that the preparation of blank 1 occurred on a different day compared to the others. Moreover, in Table 11, one can find the smallest value detected for each LOP among the RL18 samples and the ratio, for each LOP, of the blank mean area to the minimum area detected for the RL18 samples. This ratio provides an estimation of the relative maximum weight that, for each phenol, the contribution of contamination had in our samples on average.

In Figure 15, the mean area for the five blank samples and the lowest area among the RL18 samples for each LOP are shown. It is evident that, for every phenol, with Pl being the only exception, the difference between the two areas is at least one order of magnitude.

To ensure that the measured peak area is caused only by the analyte, the concentrations of LOPs measured in these reagent blanks, i.e. the corresponding peak area of the reagent blank measurement, could be subtracted from the concentrations measured in the samples. However, we decided not to apply this subtraction, since the uncertainty intervals computed using the coefficient of variation inferred from test samples S4, S5, and S6 (see Table 9) are much higher than the mean peak areas of the reagent blanks.

The blank values shown in Table A2, in the appendix, reflect once again the natural occurrence of the different analytes. The highest blank values have been found for the p-hydroxy group, vanillin, and vanillic acid. Since the P group phenols are not used to reconstruct the source of lignin, its relatively high contamination is not a matter of concern in this study.

***Table 11**. Mean area detected for the five blank samples, their standard deviation, minimum area detected for the RL18 samples and ratios between the blank mean area and the minimum RL18 sample area.*

	3,5-Bd	**Pd**	**Pl**	**Pn**	**Sd**	**Sl**	**Sn**	**Vd**	**Vl**	**Vn**	**pCd**	**Fd**
Blanks mean	52 ± 17	1238 ± 674	1309 ± 309	170 ± 160	13 ± 9	21 ± 19	4 ± 4	97 ± 19	111 ± 54	20 ± 25	12 ± 15	3 ± 1
Blanks *standard deviations*	29	1167	534	277	16	34	8	33	94	44	25	2
RL18 samples minimum	1465 ± 88	41798 ± 4180	5025 ± 553	6869 ± 687	5376 ± 591	9447 ± 661	4740 ± 474	9109 ± 728	8779 ± 615	3902 ± 312	774 ± 62	343 ± 45
Ratio (Blanks mean / Samples minimum)	0.04	0.03	0.26	0.03	<0.01	<0.01	<0.01	0.01	0.01	0.01	0.02	0.01

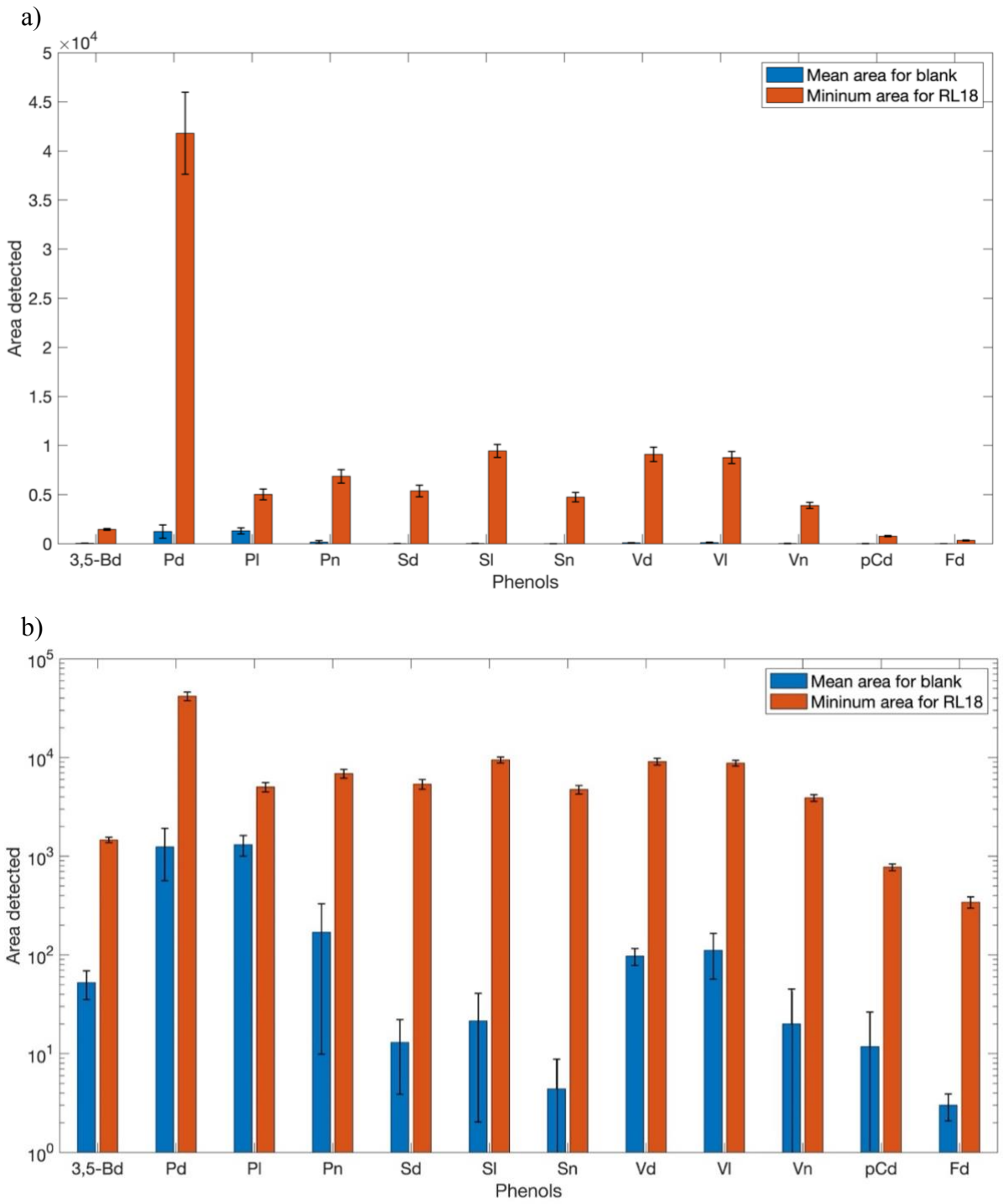

Figure 15. *a) Mean (n=5) area for the five blank samples and lowest area among the RL18 samples for each LOP with error bars. b) Same plot but the y-axis is in logarithmic scale.*

To convert the areas measured by the GC-MS to concentration in mg g^{-1}, external calibration with a standard solution containing ethyl vanillin was performed. The calibration function was obtained using a power regression method. The concentrations of the single LOPs (in mg g^{-1}) obtained for the RL18 samples are shown in Table A3, in the appendix, while the concentrations of the S-, C-, and V- groups of LOPs are listed in Table 12, together with the sum of all eight LOPs (Σ8) in the RL18 samples and the ratios C/V and S/V. The concentrations of the S-, C-, and V- groups of LOPs and the Σ8 parameter are also plotted against the mean depth of the flowstone sample in Figure 16 and Figure 17.

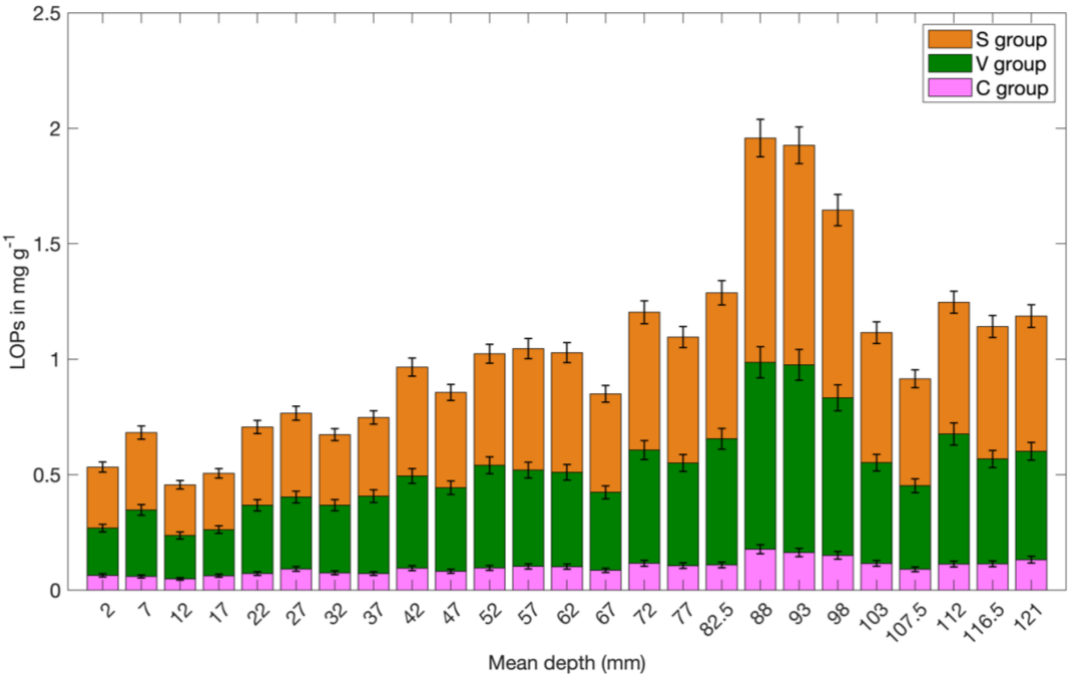

Figure 16. *LOP concentration (in mg g^{-1}) against the mean depth of each RL18 sample. The height of the columns represents the sum of the LOP concentrations, Σ8, and the different colours show the contribution of the C-, S- and V-group LOPs.*

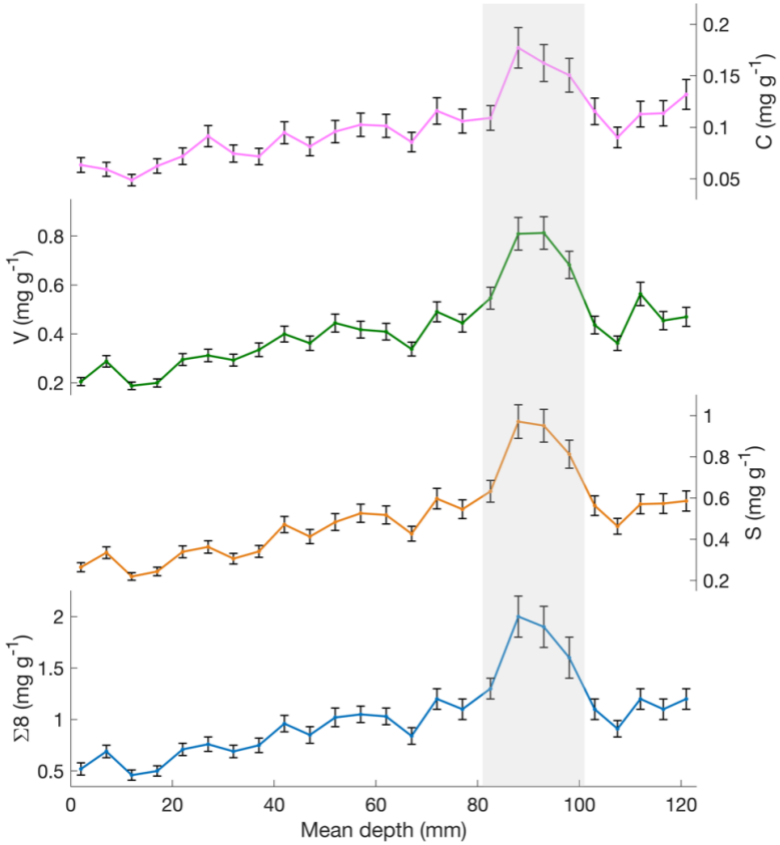

Figure 17. *Concentrations (in mg g^{-1}) of the S-, C-, and V- groups of LOPs and sum of all eight LOPs (Σ8) against the mean depth of each RL18 sample. The grey area highlights the depth range characterised by an increase in all the concentrations. Note that the y-axes are different.*

Table 12. *Concentrations (in mg g^{-1}) of the S, C, and V group LOPs, the sum of all eight LOPs (Σ8) and the ratios C/V and S/V in the RL18 samples.*

Sample ID	Mean depth (mm)	S Group (mg g^{-1})	C Group (mg g^{-1})	V Group (mg g^{-1})	Sigma (mg g^{-1})	C/V	S/V
RL 18-1	2	0.26 ± 0.03	0.063 ± 0.007	0.20 ± 0.02	0.52 ± 0.06	0.031 ± 0.06	1.29 ± 0.21
RL 18-2	7	0.34 ± 0.03	0.059 ± 0.007	0.29 ± 0.02	0.69 ± 0.06	0.021 ± 0.04	1.17 ± 0.19
RL 18-3	12	0.22 ± 0.02	0.049 ± 0.006	0.19 ± 0.02	0.46 ± 0.05	0.026 ± 0.05	1.17 ± 0.19
RL 18-4	17	0.24 ± 0.02	0.062 ± 0.007	0.20 ± 0.02	0.50 ± 0.05	0.031 ± 0.06	1.22 ± 0.20
RL 18-5	22	0.34 ± 0.03	0.072 ± 0.008	0.30 ± 0.02	0.71 ± 0.06	0.024 ± 0.05	1.15 ± 0.19
RL 18-5b	27	0.36 ± 0.03	0.09 ± 0.01	0.31 ± 0.03	0.76 ± 0.07	0.029 ± 0.06	1.16 ± 0.19
RL 18-6	32	0.31 ± 0.03	0.075 ± 0.008	0.30 ± 0.02	0.69 ± 0.06	0.025 ± 0.05	1.05 ± 0.17
RL 18-7	37	0.34 ± 0.03	0.072 ± 0.008	0.34 ± 0.03	0.75 ± 0.07	0.021 ± 0.04	1.02 ± 0.17
RL 18-8	42	0.47 ± 0.04	0.09 ± 0.01	0.40 ± 0.03	0.96 ± 0.08	0.024 ± 0.05	1.18 ± 0.20
RL 18-9	47	0.41 ± 0.04	0.081 ± 0.009	0.36 ± 0.03	0.85 ± 0.08	0.023 ± 0.04	1.14 ± 0.19
RL 18-10	52	0.48 ± 0.04	0.10 ± 0.01	0.44 ± 0.04	1.02 ± 0.09	0.022 ± 0.04	1.09 ± 0.18
RL 18-11	57	0.53 ± 0.04	0.10 ± 0.01	0.42 ± 0.03	1.05 ± 0.08	0.025 ± 0.05	1.26 ± 0.21
RL 18-12	62	0.52 ± 0.04	0.10 ± 0.01	0.41 ± 0.03	1.03 ± 0.08	0.025 ± 0.05	1.27 ± 0.21
RL 18-13	67	0.43 ± 0.04	0.07 ± 0.01	0.34 ± 0.03	0.84 ± 0.08	0.025 ± 0.05	1.26 ± 0.21
RL 18-14	72	0.60 ± 0.05	0.12 ± 0.01	0.49 ± 0.04	1.2 ± 0.1	0.024 ± 0.05	1.22 ± 0.20
RL 18-15	77	0.55 ± 0.05	0.11 ± 0.01	0.44 ± 0.04	1.1 ± 0.1	0.024 ± 0.05	1.23 ± 0.20
RL 18-16	83	0.63 ± 0.05	0.11 ± 0.01	0.55 ± 0.04	1.3 ± 0.1	0.020 ± 0.04	1.16 ± 0.19
RL 18-17	88	0.97 ± 0.08	0.18 ± 0.02	0.81 ± 0.07	2.0 ± 0.2	0.022 ± 0.04	1.20 ± 0.20
RL 18-18	93	0.95 ± 0.08	0.16 ± 0.02	0.81 ± 0.07	1.9 ± 0.2	0.020 ± 0.04	1.17 ± 0.19
RL 18-19	98	0.81 ± 0.08	0.15 ± 0.02	0.68 ± 0.06	1.6 ± 0.2	0.022 ± 0.04	1.19 ± 0.20
RL 18-20	103	0.56 ± 0.05	0.12 ± 0.01	0.44 ± 0.04	1.1 ± 0.1	0.026 ± 0.05	1.29 ± 0.21
RL 18-21	108	0.46 ± 0.04	0.09 ± 0.01	0.36 ± 0.03	0.91 ± 0.08	0.025 ± 0.05	1.28 ± 0.21
RL 18-22	112	0.57 ± 0.05	0.11 ± 0.01	0.56 ± 0.05	1.2 ± 0.1	0.020± 0.04	1.01 ± 0.17
RL 18-23	117	0.57 ± 0.05	0.11 ± 0.01	0.45 ± 0.04	1.1 ± 0.1	0.025 ± 0.05	1.26 ± 0.21
RL 18-24	121	0.59 ± 0.05	0.13 ± 0.01	0.47 ± 0.04	1.2 ± 0.1	0.028 ± 0.05	1.25 ± 0.21

Between ca. 80 and 100 mm depth, a very evident peak is visible in both the Σ8 signal and in the curves of the C, V, and S group LOPs. Thus, the increase in the total content of lignin in the corresponding layers of the flowstone is due to a rise in the concentration of all the groups of LOPs. In Figure 18 the sum of all eight LOPs (Σ8) and the ratios C/V and S/V are plotted against the mean depth of the flowstone sample.

The trend of the ratios C/V and S/V is fairly constant along the entire flowstone depth under study, and no noteworthy features are detected in conjunction with the peak in the Σ8 signal. The C/V ratios of the speleothem samples were all between 0.2 and 0.4, and the S/V ratios were all above 1.0, which suggests a significant contribution of woody and nonwoody angiosperm plant material, compared to gymnosperm plant material.

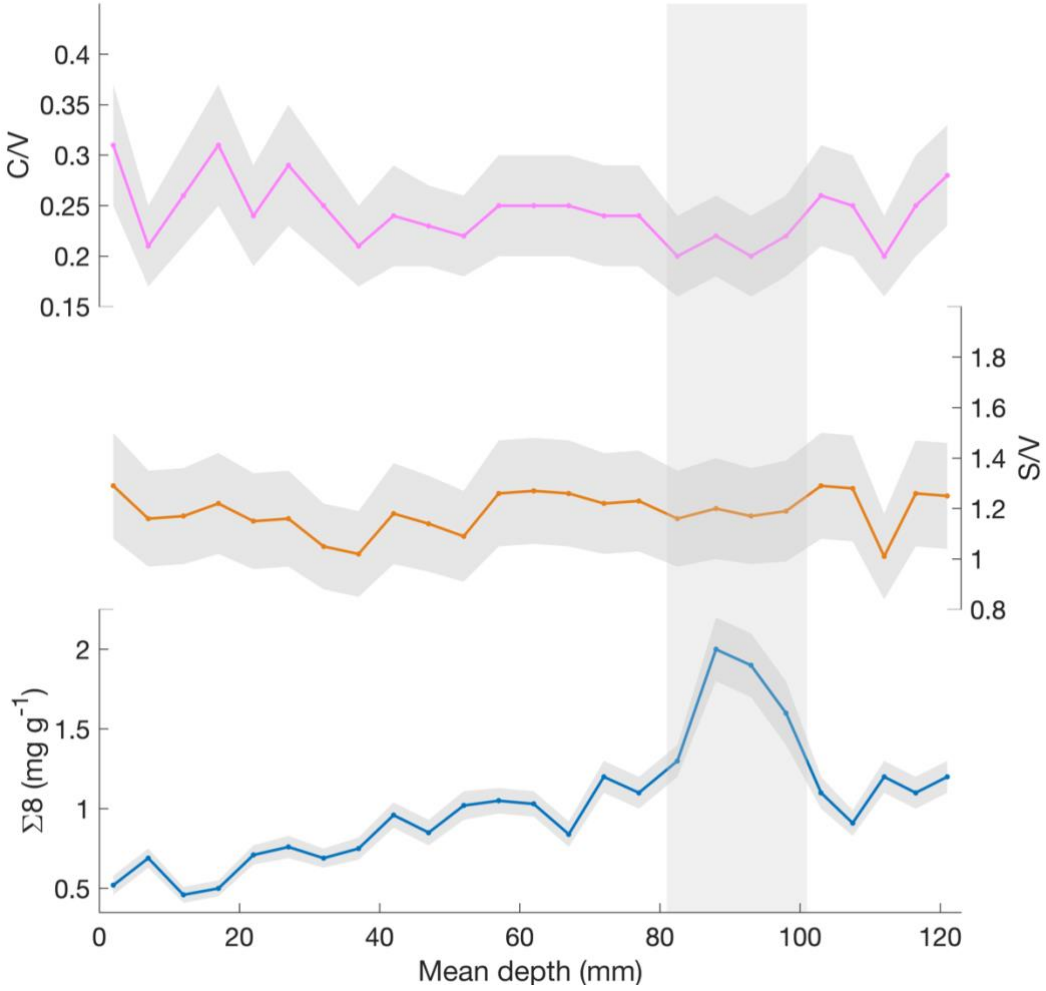

Figure 18. *Sum of all eight LOPs (Σ8) and the ratios C/V and S/V against the mean depth of each RL18 sample. The grey area highlights the depth range characterised by an increase in Σ8. Note that the y-axes are different.*

Finally, both the ratios 3,5-Bd/V and P/(V+S) have been used as a characteristic indicator of the lignin (or soil organic matter, SOM) degradation status (e.g.: Goñi & Hedges, 1995; Qian et al., 2023), since the degradation process leads to a selective loss of methoxy groups in S- and V-type lignin phenols without affecting the p-hydroxy phenols. These quantities must be interpreted with caution for several reasons. Firstly, p-hydroxyphenols are not solely produced by the oxidation of lignin. Like LOPs from

the P group, also the 3,5-Bd phenol can originate from autochthonous brown macroalgae (Goñi & Hedges, 1995). Furthermore, the type and source of vegetation influence both the P/(V+S) and 3,5-Bd/V ratios (Qian et al., 2023).

Despite these downsides, it is still interesting to observe the trends of these ratios, which are presented in Figure 19. Although the two curves exhibit very different behaviours, both appear to reach a minimum, albeit not pronounced, at the same depth at which the peak in Σ8 is found.

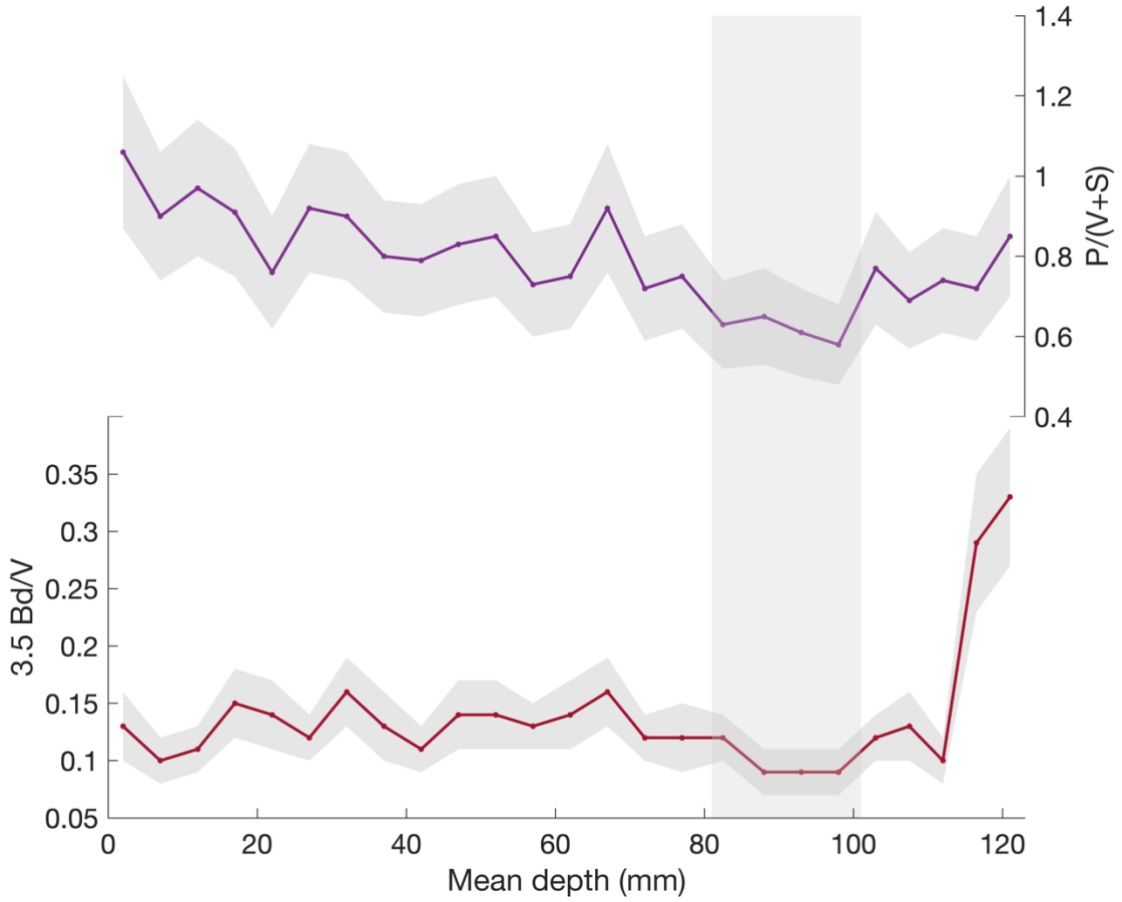

Figure 19. *3,5-Bd/V ratio and P/(V+S) ratio against the mean depth of each RL18 sample. The grey area highlights the depth range characterised by an increase in Σ8. Note that the y-axes are different.*

5. Discussion

5.1 Test samples

The test sample analysis had multiple objectives. The first and more basic one was to familiarise with the procedure. Secondly, we were interested in investigating if it was possible to optimise the different steps and if there was one specific step responsible for a consistent part of the sample contamination. In addition, another relevant aim was to compare the results of the analyses applied to blank samples (S1, S2, and S3) with those of the samples (S4, S5, and S6) containing the speleothem under study, i.e. the RL18 flowstone. This was done in order to estimate the signal-to-noise ratio. Finally, we wanted to assess the reproducibility of this type of analysis by looking at the S4, S5, and S6 results, which we would expect to be very similar.

As inferable from Figure 10, no single step in the analysis appears to be particularly more susceptible to contamination than the others. However, all stages of the process are potentially vulnerable to contamination. Consequently, it is strongly recommended to carry out these measurements either during the winter months, when less pollen is present in the air, or within a controlled environment, such as a clean room. This would mitigate the risk of airborne contaminants affecting the results, ensuring a higher level of reliability and precision in the data obtained.

The methodology developed by Heidke et al. (2018) proved to be highly effective, as it enables the quantification of lignin in speleothems with an exceptionally high signal-to-noise ratio, even when working with limited sample quantities (less than 2 g). In Table 7, the mean values and the standard deviations of the area detected by the GC-MS for each phenol were listed for both the three S blank samples (S1, S2, and S3) and the three speleothem test samples S4, S5, and S6. For all LOPs, the blank mean tends to be significantly smaller than the mean of S4, S5, and S6. The ratio of the mean blank value and the mean speleothem value, expressed as a percentage, is always less than or equal to 2%, except for three phenols: Pl, Pn, and pCd. These results suggest that, for the majority of phenolic compounds, the contamination level is minimal, ensuring the reliability of the data. Also, the exceptions noted for Pl, Pn, and pCd can be easily overcome. Indeed, the P group LOPs are not typically used as proxies for studying the source of lignin, as these phenolic compounds also originate from sources other than lignin, such as bacteria and plankton (Jex et al., 2014). This broad range of potential sources complicates the use of these phenols as definitive indicators of lignin origin. On the other hand, the trans-p-coumaric acid was most likely introduced into our samples due to contaminated laboratory air. The analyses were conducted in July, a period when airborne pollen concentrations are particularly high. Since pollen contains significant levels of pCd (Hu et al., 1999; Tareq & Ohta, 2015), it is plausible that this compound entered samples through inadvertent exposure to the surrounding environment. The S test samples were particularly rich in pCd compared to the methodological test samples probably because the cartridges used for the S test samples were subjected to a longer drying step (ca. 30 minutes, compared to ca. 15 minutes for the methodological test samples). When analysing the RL18 samples, we decided to significantly shorten the drying step duration to approximately one minute to reduce the likelihood of impure air being drawn into the cartridges by the vacuum manifold. To further mitigate the contamination from trans-p-coumaric acid, it is sufficient to conduct such analyses either

during a more appropriate period, such as winter, when pollen levels are typically lower (as we did for the RL18 samples), or inside an environment more adequately isolated from external contamination sources, for example, a clean room.

As shown in Table 7, the evaluation of the reproducibility of the result obtained through this method yielded favourable results. Equivalent samples provided outcomes that varied from sample to sample, which is reflected in the standard deviations listed in Table 7. Still, when considered within their respective uncertainty intervals, the values always presented some overlap. This indicates a good degree of consistency and reliability in the analytical procedure. The computed coefficients of variation were found to be variable across the different LOPs, with an average value of 9%, which is an acceptable degree of uncertainty in most cases.

5.2 Cave samples (RL18 samples)

5.2.1 Lignin concentration and origin: Σ8, the C/V ratio, and S/V ratio

Analysing the LOP concentration in the RL18 flowstone, the most outstanding result is probably the pronounced peak in the parameter Σ8, which is the sum of LOPs from the C-, S- and V-groups, and it is used to infer the total lignin concentration. In Figure 20, the parameter Σ8 is plotted against both the mean depth of the samples and the age, in kilo years ago, of the corresponding layer estimated with a preliminary age model.

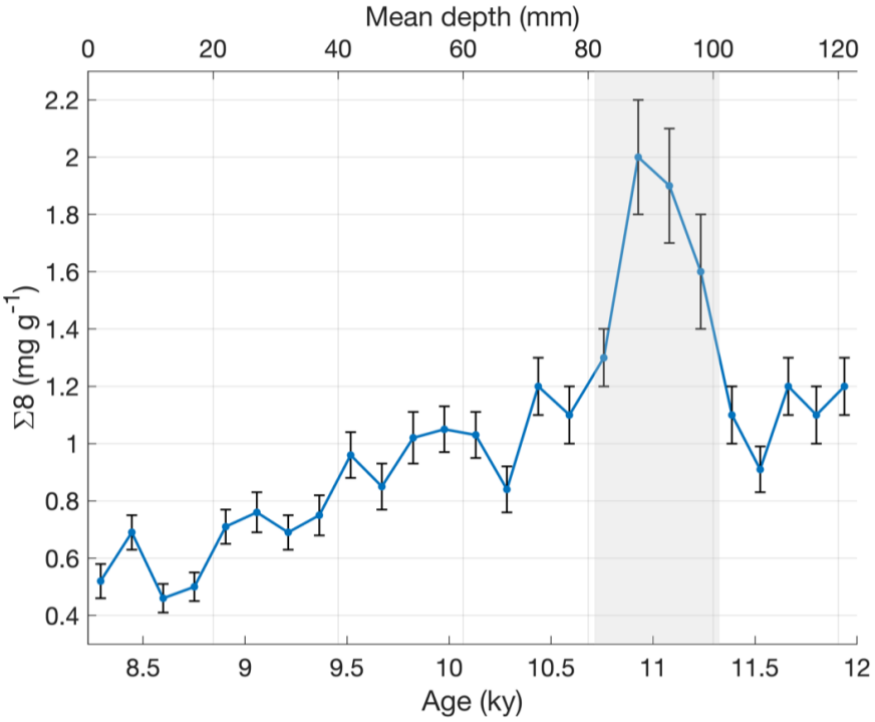

Figure 20. *Concentrations (in mg g^{-1}) of sum of all eight LOPs (Σ8) against both the mean depth and the age of each RL18 sample. The grey area highlights the range of the Σ8 peak. Note that the one shown is just a preliminary depth model.*

The peak observed in the Σ8 signal indicates a rise in the total lignin content in the soil during the period corresponding to this particular depth interval, but this may have multiple explanations. According to the preliminary depth model, this peak corresponds to a temporal range that stretches from ca. 10.7 ka

until about 11.3 ka. This period coincides with the early stages of the Holocene, which was characterised by notable environmental, ecological and climatic changes, including rising temperatures and shifting precipitation patterns. Hence, the peak in the Σ8 curve could be due to an increase in the amount of the total vegetation in the area overlying the cave. The increased concentration of LOPs within this interval could also be indicative of a more intensive degradation of plant material, possibly due to increased microbial activity. Its cause could also lie in changes in hydrological conditions, such as increased rainfall, which might influence both the transport of lignin in the soil and the rate of lignin degradation. Further research, including more refined dating, would be required to confirm the exact cause and timing of this peak. For the time being, it may be useful to attempt to interpret the Σ8 curve by comparing it with other proxies, such as isotopes, fluorescence, and trace elements (see the following paragraphs).

Figure 21 shows the C/V ratio versus the S/V ratio for all samples. The regions for different plant types are based on the analysis of different plant species (Hedges & Mann, 1979). Gymnosperm woody samples contain mainly V-group LOPs. Angiosperm woody samples contain V- and S-group LOPs, but almost no C-group LOPs. Gymnosperm non-woody samples contain V- and C-group LOPs, but almost no S-group LOPs. Angiosperm nonwoody samples contain all three groups of LOPs and thus show a wide range of C/V and S/V ratios. All our samples plot in a quite narrow area that corresponds to that of angiosperm woody material and angiosperm non-woody material. Nevertheless, it is important to keep in mind that these regions are just broadly defined and are based on a limited number of analyses and a restricted range of different plant species, and these presumptions surely need to be supported by a complete analysis of the flowstone and a comparison with the other proxy data. In addition, a comparison with Holocene pollen records from the area may also help confirm these preliminary results.

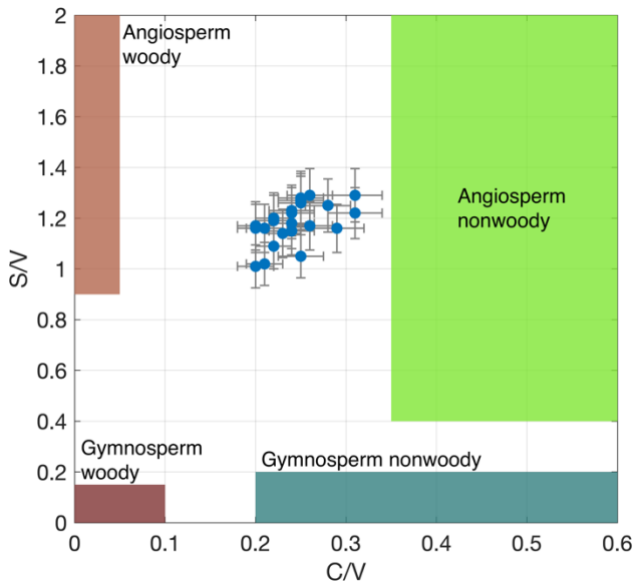

Figure 21. *Lignin oxidation parameters S/V vs. C/V of all RL18 samples and regions for different sample types defined by Hedges & Mann (1979).*

The C/V and S/V ratios were found to be fairly constant along the entire flowstone depth under study, suggesting that the vegetation type growing in the area above the cave did not experience significant changes during the speleothem's growth period. Thus, the increase in the total lignin content in the

speleothem (inferable from the peak in Σ8) was likely not accompanied by any change in the plant groups, mainly angiosperm, that produced such lignin.

5.2.3 Precipitation intensity: $\delta^{18}O$, $\delta^{13}C$, and Mg/Ca ratio

In Figure 22, the stable isotope composition ($\delta^{18}O$ and $\delta^{13}C$), magnesium (Mg), and the sum parameter Σ8 are shown against the mean depth of the RL18 samples.

The $\delta^{18}O$ and $\delta^{13}C$ curves in Figure 22 exhibit a strong positive correlation. Despite several marked oscillations, from a depth of 120 mm to approximately a depth of 50 mm, both $\delta^{18}O$ and $\delta^{13}C$ decrease, while in the layers above 50 mm, the two isotope records show a trend toward less negative values. In contrast, Σ8 generally decreases throughout the length of the RL18 core, with the large peak around 90 mm depth being the most remarkable exception.

In the central Mediterranean, changes in the $\delta^{18}O$ of continental carbonates are primarily associated with variations in regional hydrological conditions, particularly in precipitation levels. Lower $\delta^{18}O$ values occur during wetter periods, and precipitation is enriched in ^{18}O during drier periods (Regattieri et al., 2016). The O isotope signal suggests higher precipitation during the period corresponding to the first half of the speleothem growth, with a consistent trend of decreasing in rainfall during the second half.

The $\delta^{13}C$ record is thought to relate to soil and vegetation development above the cave (Regattieri et al., 2016). In the central-western Mediterranean, the carbon isotope composition of speleothems can serve as an indicator of the varying contributions of organic and inorganic CO_2 sources. During periods of increased temperature and precipitation, there is typically a corresponding enhancement in vegetation development and biological activity within the soil. This increased biological activity leads to a higher supply of organic CO_2, which is reflected by lower $\delta^{13}C$ values in the speleothem deposits. Conversely, when temperature and precipitation decrease, vegetation reduces and biological activity in the soil declines. This results in a lower supply of organic CO_2 and a longer residence time of water in the recharge system, which further limits the contribution of organic CO_2. These conditions are usually associated with higher $\delta^{13}C$ values in the speleothems. Thus, the $\delta^{13}C$ curve further supports the interpretation of a wetter period corresponding to the older half of the flowstone and a drier period during the formation of the younger half of the speleothem.

Corresponding with the peak of Σ8 (at approximately 90 mm depth, light grey area in Figure 22), the isotopic curves indicate an increase in the precipitation. In the following period, precipitation increases again, but the pattern is not mimicked by increase in Σ8. The trend toward reduced precipitation starting at ca. 60 mm depth also corresponds to a similar trend of decreasing Σ8.

Although an even clearer correlation between Σ8, $\delta^{18}O$, and $\delta^{13}C$ would be desirable, these proxies suggest a positive relationship between precipitation intensity and the total lignin content in the corresponding layers of the flowstone. The peak in Σ8 could therefore be, at least in part, attributable to hydrological causes.

The correlation between the isotopic signals and Mg appears to be moderate in the older portion of the flowstone. Instead, in the upper half of the speleothem, the trend toward higher Mg values (which correspond to increasing Mg/Ca ratio assuming constant Ca levels) corresponds to increases in the isotope ratios, supporting the notion of a drier climate associated with a decrease in Σ8.

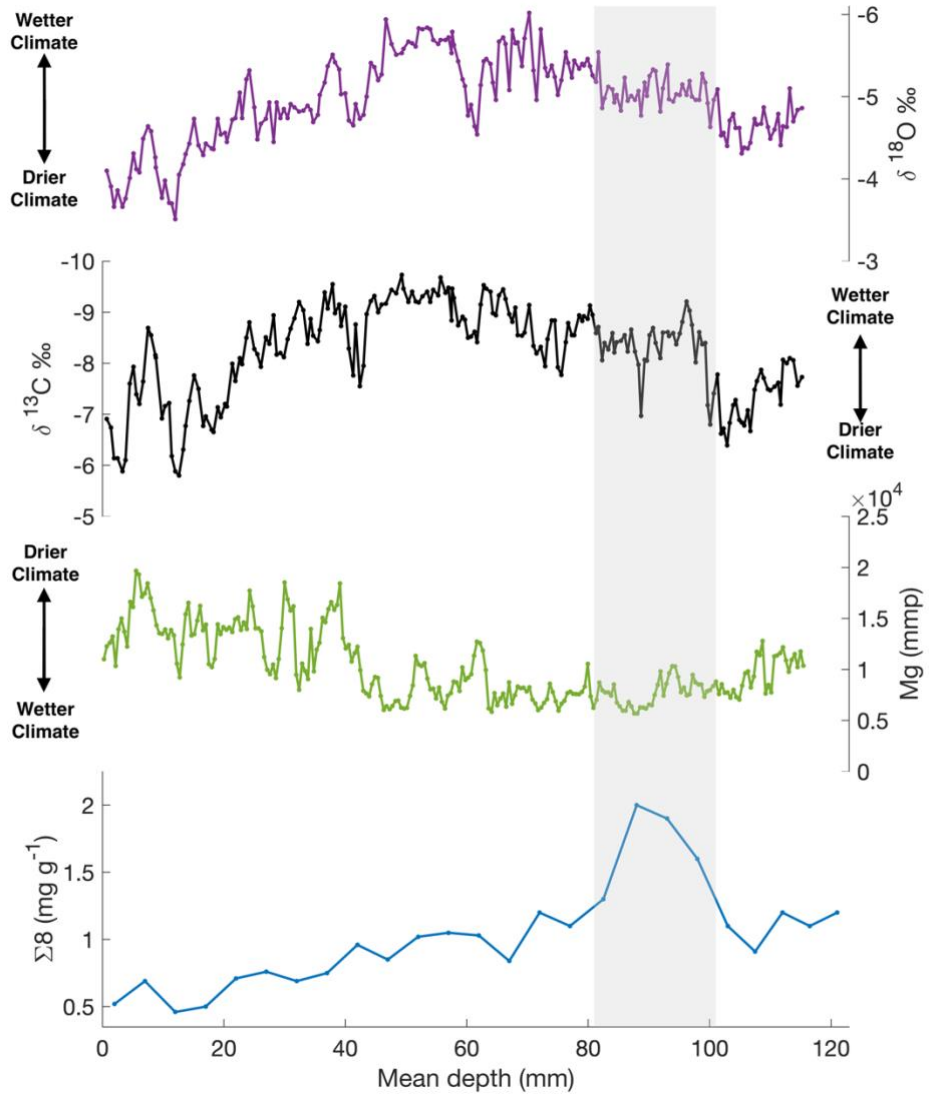

Figure 22. *Comparison of $\delta^{18}O$, $\delta^{13}C$, Mg, and Σ8. All plotted against the mean depth of the RL18 samples. The light grey bar highlights the main peak in the Σ8 records. Note: the y-axes of the isotope plots are inverted.*

5.3.2 Humification: fluorescence analysis, P/(V+S) ratio, and 3,5-Bd/V ratio

The intensity and spectral characteristics of speleothem fluorescence are influenced by the quantity and type of organic acids (fulvic and humic acids) incorporated into the calcite matrix. Humic acids are more complex and are typically formed earlier in the decay process compared to fulvic acids, which are indicative of a later stage of organic degradation. In general, cooler or wetter conditions cause a decrease in humification or shortening in the residence times of organic material in the soil, leading to a higher proportion of humic acids. Humic acid tends to exhibit fluorescence at higher wavelengths with lower emission intensity. Conversely, in drier conditions, prolonged residence times result in greater humification, with a higher proportion of fulvic acids. These, in turn, emit fluorescence at lower wavelengths and with greater intensity (McGarry & Baker, 2000). Therefore, assuming no major temperature changes, an increase in the wavelength of the emitted fluorescence is associated to wetter conditions inhibiting humification. Conversely, drier conditions cause longer residence times, increased humification and shorter emission wavelengths. This relationship was further demonstrated for Renella

speleothems by Drysdale et al. (2006) where the same proxies, namely stable isotope, trace element, and organic fluorescence data, were used.

In Figure 23, the fluorescence emission wavelength is compared with the 3,5-Bd/V ratio, the $\delta^{13}C$ signal, and the Σ8 parameter. The general trend of the emission wavelength is consistent with the $\delta^{13}C$ and Σ8 patterns, especially for the precipitation increase at 100 mm depth that correspond to the increase in lignin content, with decreasing isotope ratio (i.e. wetter conditions) correlating with an increase in emission wavelength (λ). Also, the precipitation reduction from 20 mm to the top of the flowstone corresponds to a slight increase in the emission λ, and to the decreasing trend of the Σ8 parameter.

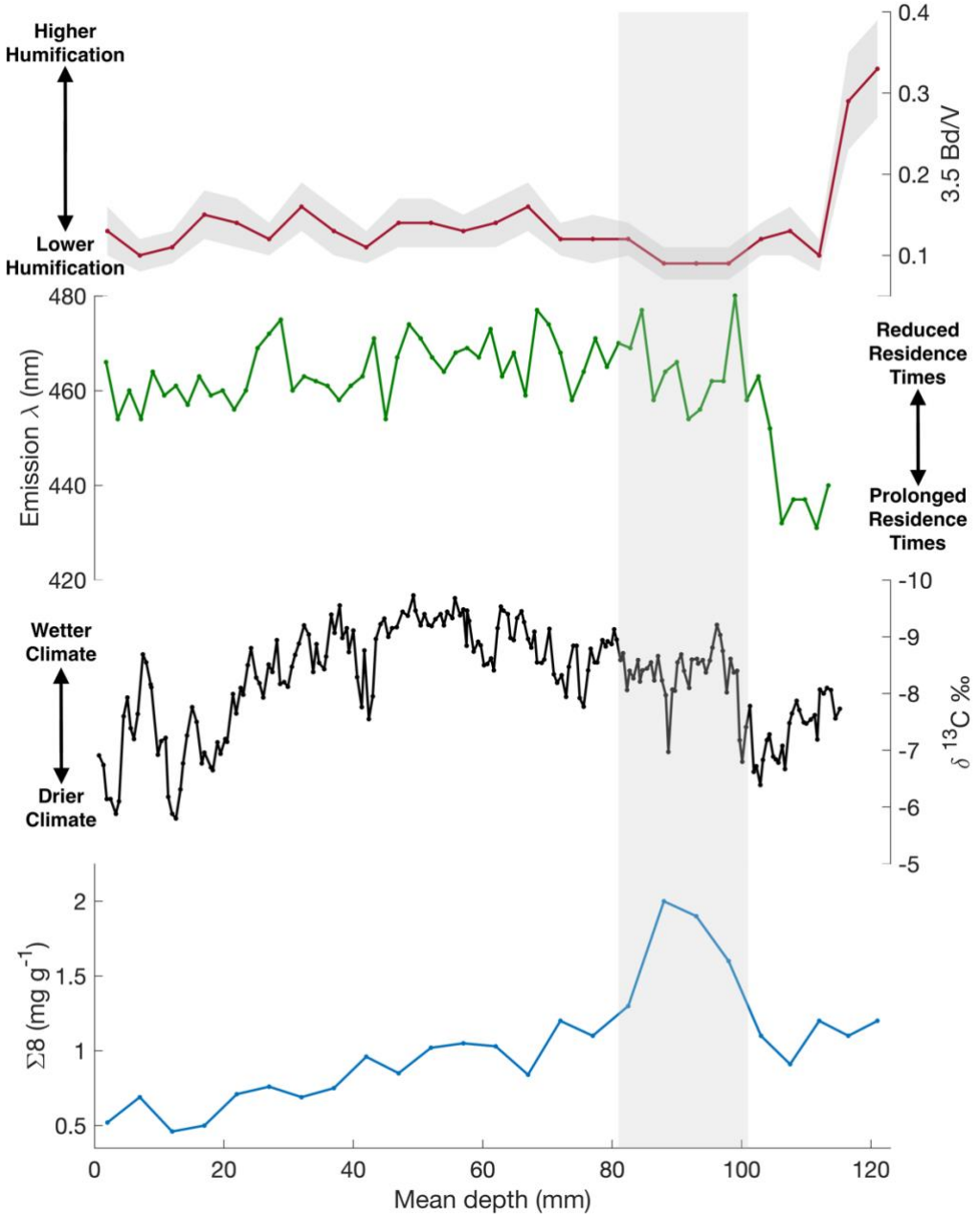

Figure 23. *Comparison of 3,5-Bd/V ratio, peak fluorescence emission wavelength (λ), $\delta^{13}C$, and Σ8. All plotted against the mean depth of the RL18 samples. The grey bar highlights the main peak in the Σ8 records. Note: the y-axis of the $\delta^{13}C$ plot is inverted.*

The P/(V+S) and 3,5-Bd/V ratios increase with increasing pedogenesis and humification in soils or diagenesis in sediments (e.g.: Goñi & Hedges, 1995; Dickens et al., 2007). Both ratios are shown in Figure 19, but only the 3,5-Bd/V ratio is present in Figure 23 because it is considered more reliable, since the P group of LOPs is subject to larger uncertainties. Overall, both the 3.5-Bd/V ratio and the peak fluorescence emission wavelength exhibit a relatively constant trend, despite some fluctuations, over most of the speleothem depth.

Noteworthy, the two curves show opposite behaviours during the precipitation increase at 100 mm depth: the 3.5-Bd/V ratio decreases significantly, while the emission wavelength increases dramatically, but with a spatial lag. This is probably largely due to the averaging effects of the relatively large (4.5 mm diameter) spot size of the fiber-optic probe used in the fluorescence measurements (Drysdale et al., 2006) and large sample volumes needed to perform LOPs analyses. Although it is not possible to extrapolate clear information from the comparison of these two signals, if one assumes that the changes in the two curves are roughly synchronous, their interpretation remains consistent. Specifically, the fluorescence data indicate a prevalence of less evolved humic acids, which corresponds to shorter residence times, while the 3.5Bd/V ratio suggests that humification is less advanced.

5.2.4 Trace elements

When analysing trace element records in speleothems, the primary objectives are the evaluation of the potential influence of local factors, such as sources and transport mechanisms, on the variability and distribution of each element; the determination of whether trace element fluctuations align with previous paleohydrological interpretations; and the investigation of the connections between local environmental conditions and broader regional and global climate changes. Nevertheless, climate conditions inferred from speleothem properties are closely linked to local climatology, and any proposed connections between local and global climate changes are inherently based on assumptions about the teleconnections that govern these interactions (Regattieri et al., 2016).

A detailed description of the trace element signals is beyond the scope of this study. The aim here is a purely qualitative and preliminary assessment of the trace element curves, intending to identify potential correlations between the concentrations of the different elements and between them and Σ8.

During dry periods, typically characterised by low-flow conditions, an increase in Mg, Sr, and Ba is usually observed, while Ca tends to remain more constant. This results in a positive correlation between the Sr/Ca, Ba/Ca, and Mg/Ca ratios. In Figure 24, the concentrations of Sr and Ba exhibit a signal that decreases slightly between the older and more recent layers of the speleothem, which apprears in desagreement with the hypothesis that the most recent period of flowstone formation was characterised by reduced rainfall. However, Sr and Ba's trends might be easily caused by factors other than changes in the amount of rain, for example variations in the growth rate. Moreover, both elements, yet Sr in particular, shows slightly higher values between approximately 80 and 100 mm depth, coinciding with the peak in Σ8. In contrast, the Mg curve exhibits a markedly different behaviour, generally increasing in the more recent layers and supporting the idea of a drier climate occuring in that time period, with no significant correlation between Mg and either Sr or Ba.

It is believed that the concentrations of Si, Al, P, Y, and Zn tend to be higher during periods of increased infiltration. Additionally, an increase in P is often indicative of greater biological activity, while an

increase in Al may also be associated with higher catchment erosion. Finally, a decrease in the concentrations of P, Y, and Zn is frequently interpreted as a sign of deterioration in soil conditions.

The curves for Al, P, Y, and Zn display large fluctuations throughout the speleothem depth, except in the layers between 0 and approximately 30 mm: the youngest samples appear to have almost negligible concentrations of these elements. Furthermore, Y and Zn show relatively high values corresponding to the peak in Σ8 at around 90 mm depth. However, both Y and Zn, as well as P, exhibit a minimum at approximately 93 mm depth. The increase in the lignin content within the RL18 speleothem thus seems to have occurred during a period of greater water infiltration into the cave (possibly accompanied by less deterioration in soil conditions). However, this period was not without interruptions, which are recorded and evident in the trace element curves but not in the Σ8 signal, likely due to its lower spatial (and temporal) resolution, resulting from the need for larger sample sizes to perform LOPs analyses.

In general, the trace element curves do not appear to provide easily interpretable insights nor clear indications regarding the conditions that led to the variations in the lignin content in the analysed flowstone. To reduce the number of variables, it would certainly be beneficial to have a more reliable age model, which would allow for a more precise temporal placement of the Σ8 peak.

5.2.5 Further remarks

With a Σ8 value of ca. 0.46 - 2 mg per g of stalagmite (see Table 12, the LOP concentration of the RL18 flowstone samples was of the same order of magnitude as the typical concentration of sediment samples (e.g., Σ8 is 0.15-0.75 mg per g of stalagmite in Tareq et al., 2011)). Because of these high concentrations, a smaller amount of speleothem would have been enough to be above the CG-GM sensitivity. Therefore, each one of the samples listed in Table 4 could have been divided into two separate samples.

Room for improvement lies also in adding the standard solution of ethyl vanillin to each sample just after the microwave-assisted oxidation, before transfering the solution from the vessels to the centrifuge tubes. We did it when working with the test samples but not when analysing the cave samples. This is important for maximising the accuracy with which we can estimate the correction factor, that includes diluition and recovery, of our samples.

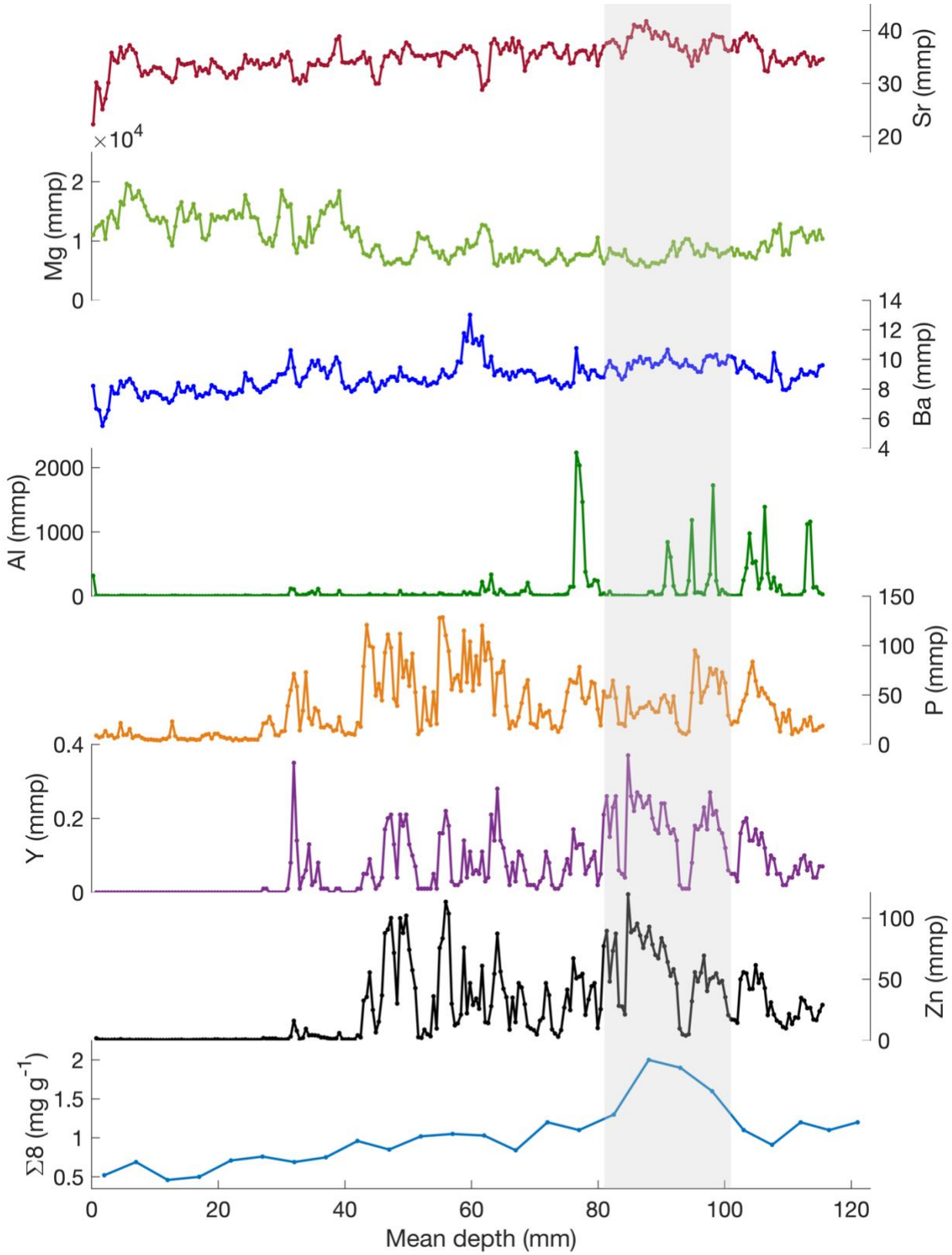

Figure 24. *Comparison of trace elements (from top: Mg, S, Ba, Al, P, Y, and Zn) and Σ8, plotted against the mean depth of the RL18 samples. The trace elements curves are 20 pts. running averages. The grey bar highlights the peak in the Σ8 records.*

6. Summary and conclusions

Speleothems such as stalagmites, stalactites and flowstones are secondary carbonate accumulations deposited in caves by degassing of cave drip-waters that are supersaturated with respect to calcium carbonate. These cave deposits made of $CaCO_3$ preserve several relevant climatic signals, e.g. isotope composition, carbonate petrography, annual band thickness, trace element ratios, luminescence and organic molecular signals (Leng, 2006; Ruddiman, 2013). In fact, since speleothems form within the hydrological cycle, they record environmental and climate conditions occurring at the time of their formation and have many properties that can be used as proxies for paleo reconstructions (Regattieri et al., 2016). For instance, the stable isotope concentrations provide useful information (e.g., temperature, amount, source) about climate-driven changes in the isotope composition of meteoric water that falls on a cave site. Fluorescence changes in speleothems provide insights into the degree of humification of organic matter in the overlying soil, with variations in peak emission wavelengths reflecting shifts in climatic conditions, such as rainfall and temperature (Drysdale et al., 2006). Fluorescence intensity reflects the amount of organic matter present, while the emission wavelength, is specific to the molecule and, therefore, can be used to differentiate between different types of organic matter (Blyth et al., 2008). On the other hand, geochemical variations in trace elements are influenced by shifts in hydrological input, fluctuations in the supply and transport of catchment erosion products to the cave and changes in the overlying soil and vegetation (Regattieri et al., 2016).

In recent years, lignin in speleothems has been recognised as a promising paleo-vegetation proxy because it is produced exclusively by vascular plants and represents one of the main constituents of wood and woody plants (Boerjan et al., 2003; Jex et al., 2014). In addition, the analysis of lignin has the distinct advantage that it can provide information about not only the abundance but also the type of vegetation. The microbial degradation of lignin in the soil is relatively slow. Hence, due to its relative stability, lignin oxidation products (LOPs) are becoming widely used as a paleo-vegetation proxy in climate archives (Jex et al., 2014).

Lignin is a complex biomacromolecule primarily consisting of methoxylated phenol units linked by ether (C-O) and carbon (C-C) bonds (Goñi & Montgomery, 2000). Lignin from gymnosperms (soft wood) consists mainly of guaiacyl units, whereas lignin from angiosperms (hard wood) contains both guaiacyl and syringyl units. Grasses and non-woody plant parts like leaves and needles are constituted from comparable amounts of guaiacyl, syringyl and p-hydroxyphenyl units. Moreover, p-coumaric acid and ferulic acid can be ester-bound to the terminal hydroxyl groups of the propyl side chains, especially in grass lignin (Boerjan et al., 2003; Vanholme et al., 2012). To study the lignin composition of a sample, the lignin polymer is oxidatively degraded into monomeric LOPs. A frequent method is CuO oxidation. The guaiacyl unit is oxidized to vanillic acid, vanillin and acetovanillone (which compose the V-group), the syringyl unit is oxidized to syringic acid, syringaldehyde and acetosyringone (S-group), while ferulic acid and p-coumaric acid form the C-group. Additionally, the p-hydroxyphenyl unit is oxidised to p-hydroxybenzoic acid, p-hydroxybenzaldehyde and p-hydroxyacetophenone (P-group). However, since P-group LOPs can also originate from sources other than lignin, such as soil microorganisms or the degradation of protein-rich material, they are usually not used as vegetation proxies (Jex et al., 2014; Heidke et al., 2021).

After the oxidation, the gas-chromatographic-mass-spectrometry (GC-MS) analysis of derived phenolic CuO-oxidation products is a commonly used method for characterisation and quantification of lignin. While the parameter Σ8, which is the sum of LOPs from the C-, S- and V-groups, is used to infer the total lignin concentration, the ratios of the different LOP groups, C/V and S/V, are used to investigate the type of lignin. A higher C/V ratio is an indication of a higher contribution of non-woody (compared to woody plant) material, and a higher S/V ratio is an indication of a higher contribution of angiosperm (compared to gymnosperm plant) material (Hedges & Mann, 1979).

Recent studies (Heidke et al., 2018, 2019) showed that trace concentrations of lignin oxidation products can be quantified in dripwater and speleothems and that LOP concentrations and C/V and S/V ratios tend to correlate with other geochemical proxies of the same samples. This strongly suggests a co-variation with environmental changes, even though many uncertainties still exist regarding the transport of lignin from the soil, through the karst system, and into the cave and speleothem formations (Heidke et al., 2021).

The method developed by Heidke et al., (2018) holds significant potential, as it effectively combines the advantages of lignin analysis, which serves as a highly specific biomarker for vegetation, with the utility of speleothems as valuable terrestrial climate archives.

In this thesis paper, we applied this method to multiple blank samples, and to several samples containing 1.6 to 5.1 g of speleothem dissolved in acid. More specifically, these samples included three speleothem test samples (S4, S5, and S6) and 25 cave samples (from the flowstone RL18). The method included several steps: first, the acidic solution is subjected to solid-phase extraction (SPE). Then, the eluate is treated with CuO oxidation through a microwave-assisted digestion procedure. The sample solutions are then re-extracted and enriched via SPE. Finally, LOPs are separated and detected using GC-MS.

The objectives of this work were, first of all, to examine the settings that maximise the results of the method developed by (Heidke et al., 2018) and to assess if its sensitivity is high enough to detect and quantify LOPs with a sufficient temporal resolution to reveal centennial to millennial climate changes. To identify which stage(s) of the analysis contributed most significantly to sample contamination, the method was tested on nine “methodological” samples, which did not contain dissolved speleothem material and underwent varying numbers of procedural steps. The LOP concentrations in the methodological samples were not proportional to the number of steps each of them underwent, but reflected the natural occurrence of the different analytes. These results suggest that contamination is primarily due to impure air within the laboratory, rather than specific chemicals or procedural steps. Consequently, careful selection of the analysis period (for instance, during months with lower airborne pollen levels) or the use of a clean room could be crucial in obtaining more precise and reliable results. The signal-to-noise ratio of the results was calculated by comparing the mean results of the speleothem test samples (S4, S5, and S6) with those of blank samples (S1, S2, and S3) which had undergone all sample preparation steps. Our findings show that speleothem samples consistently exhibit LOP concentrations at least one order (and often two orders) of magnitude higher than those in the blank samples. Despite some fluctuations, the values for S4, S5, and S6 overlapped within their respective uncertainty intervals, indicating satisfactory reproducibility of the analysis. These encouraging results

support the idea of analysing LOPs in speleothem for paleo-vegetation reconstruction using the method developed by Heidke et al. (2018) with sufficient confidence even when the speleothem quantity is limited (less than 2 g).

Secondly, one aim of this thesis was to present the results of the application of the lignin analysis method developed by Heidke et al. (2018) to the RL 18 flowstone, collected in the Renella Cave, Central Italy. Renella is a small, shallow cave located on the western side of the Apuan Alps, which opens at 275 m a.s.l., is 200 m long, and has been the subject of paleoclimatic and paleoenvironmental studies in the last few decades (e.g., Drysdale et al., 2006; Chimenti et al., 2023).

Finally, we were interested in investigating if and how the LOP signal in the studied speleothem varies with climatic and vegetational changes by comparing the record with other established proxy signals, such as trace elements and stable isotopes, from the same sample. Given the complex nature of the geochemical changes recorded in speleothems, such as atmospheric inputs, vegetation and soil influences, the karstic aquifer, and post-depositional alterations, a multiproxy approach is needed to gain a detailed understanding of the environmental evolution at the cave site under study over the time spanned by the samples (Regattieri et al., 2016).

Overall, our results show little variability in the C/V and S/V ratios and therefore in the type of lignin sources during the period of formation of the flowstone. This might suggest either reduced changes in vegetation or a reservoir effect within the critical zone due to the leaching of pre-aged soil-derived organic material. However, it was possible to infer both a dramatic increase in the total lignin content at a depth of about 80 to 100 mm (identifiable by the peak in Σ8 signal) and a general predominance of angiosperm plant material (both woody and non woody), compared to gymnosperm plant material. This increase in LOP corresponds to an increase in the precipitation (shown by the stable isotope records) and to a decrease in water residence time highlighted (shown by fluorescence data). Since the type vegetation present in the area above the cave did not change during the period under study, as demonstrated by the little variability in the C/V and S/V ratios, it can be assumed that no major temperature changes occurred. This further supports the interpretation of the increase in the wavelength of the emitted fluorescence as associated to wetter conditions inhibiting humification (correspondent to the peak in Σ8).

From about half of the speleothem to its youngest layers, there is a very significant agreement between increasing Mg and isotope ratios, slightly increasing emission λ, and decreasing lignin total content. This good coherence among different proxies indicates a trend of progressively drier climate in more recent times.

Furthermore, a preliminary age model was applied to date the depth layers displaying a significant increase in lignin content to around 10.7–11.3 ka. Some hypotheses have been suggested regarding the mechanisms driving this rise in LOPs, however, a comprehensive paleoclimatic reconstruction falls outside the scope of this thesis.

Comparing the Σ8 curve with fluorescence and trace element signals, the increase in lignin content within the RL18 speleothem seems to have occurred during a period of enahnced water infiltration into the cave, potentially coupled with less degradation of soil conditions conditions and leaching of lignin from soil organic matter. However, this process was probably not continuous, as evidenced by the trace

element concentrations, but not by the Σ8 signal. This discrepancy may be attributed to the lower spatial and temporal resolution of the Σ8 signal.

Overall, the climatic proxies generally align and despite not providing definitive insights into the specific conditions responsible for the observed variations in lignin content, offer coherent hypotheses for explaining such changes. To further improve the reliability of these interpretations, a more robust age model would be advantageous, as it would enable precise temporal alignment of the Σ8 peak and easier interpretation of the vegetation-climate response.

References

Blyth, A. J., Baker, A., Collins, M. J., Penkman, K. E. H., Gilmour, M. A., Moss, J. S., Genty, D., & Drysdale, R. N. (2008). Molecular organic matter in speleothems and its potential as an environmental proxy. *Quaternary Science Reviews*, *27*(9), 905–921. https://doi.org/10.1016/j.quascirev.2008.02.002

Blyth, A. J., Hartland, A., & Baker, A. (2016). Organic proxies in speleothems – New developments, advantages and limitations. *Quaternary Science Reviews*, *149*, 1–17. https://doi.org/10.1016/j.quascirev.2016.07.001

Blyth, A. J., & Watson, J. S. (2009). Thermochemolysis of organic matter preserved in stalagmites: A preliminary study. *Organic Geochemistry*, *40*(9), 1029–1031. https://doi.org/10.1016/j.orggeochem.2009.06.007

Boerjan, W., Ralph, J., & Baucher, M. (2003). Lignin biosynthesis. *Annual Review of Plant Biology*, *54*, 519–546. https://doi.org/10.1146/annurev.arplant.54.031902.134938

Borsato, A., Frisia, S., Fairchild, I. J., Somogyi, A., & Susini, J. (2007). Trace element distribution in annual stalagmite laminae mapped by micrometer-resolution X-ray fluorescence: Implications for incorporation of environmentally significant species. *Geochimica et Cosmochimica Acta*, *71*(6), 1494–1512. https://doi.org/10.1016/j.gca.2006.12.016

Borsato, A., Frisia, S., & Miorandi, R. (2015). Carbon dioxide concentration in temperate climate caves and parent soils over an altitudinal gradient and its influence on speleothem growth and fabrics. *Earth Surface Processes and Landforms*, *40*, 1158–1170. https://doi.org/10.1002/esp.3706x

Chimenti, M., Natali, S., Giannecchini, R., Zanchetta, G., Baneschi, I., Doveri, M., Isola, I., & Piccini, L. (2023). Hydrogeochemistry and Isotopic Composition of Waters in the Renella Cave (Central Italy): New Insights into Groundwater Dynamics. *Water*, *15*(9), Article 9. https://doi.org/10.3390/w15091764

Dickens, A. F., Gudeman, J. A., Gélinas, Y., Baldock, J. A., Tinner, W., Hu, F. S., & Hedges, J. I. (2007). Sources and distribution of CuO-derived benzene carboxylic acids in soils and sediments. *Organic Geochemistry*, *38*(8), 1256–1276. https://doi.org/10.1016/j.orggeochem.2007.04.004

Drysdale, R., Zanchetta, G., Hellstrom, J., Maas, R., Fallick, A., Pickett, M., Cartwright, I., & Piccini, L. (2006). *Late Holocene drought responsible for the collapse of Old World civilizations is recorded in an Italian flowstone*. https://www.researchgate.net/publication/200179569_Late_Holocene_drought_responsible_for_the_collapse_of_Old_World_civilizations_is_recorded_in_an_Italian_flowstone

Fairchild, I. J., & Baker, A. (2012). *Speleothem Science: From Process to Past Environments*. John Wiley & Sons, Ltd., Chichester, UK. https://doi.org/10.1002/9781444361094

Fairchild, I. J., Borsato, A., Tooth, A. F., Frisia, S., Hawkesworth, C. J., Huang, Y., McDermott, F., & Spiro, B. (2000). Controls on trace element (Sr–Mg) compositions of carbonate cave waters: Implications for speleothem climatic records. *Chemical Geology*, *166*(3), 255–269. https://doi.org/10.1016/S0009-2541(99)00216-8

Fairchild, I. J., Smith, C. L., Baker, A., Fuller, L., Spötl, C., Mattey, D., McDermott, F., & E.i.m.f. (2006). Modification and preservation of environmental signals in speleothems. *Earth-Science Reviews*, *75*(1), 105–153. https://doi.org/10.1016/j.earscirev.2005.08.003

Fairchild, I. J., & Treble, P. C. (2009). Trace elements in speleothems as recorders of environmental change. *Quaternary Science Reviews*, *28*(5), 449–468. https://doi.org/10.1016/j.quascirev.2008.11.007

Fraser, W. T., Scott, A. C., Forbes, A. E. S., Glasspool, I. J., Plotnick, R. E., Kenig, F., & Lomax, B. H. (2012). Evolutionary stasis of sporopollenin biochemistry revealed by unaltered Pennsylvanian spores. *New Phytologist*, *196*(2), 397–401. https://doi.org/10.1111/j.1469-8137.2012.04301.x

Frisia, S., Borsato, A., Drysdale, R. N., Paul, B., Greig, A., & Cotte, M. (2012). A re-evaluation of the palaeoclimatic significance of phosphorus variability in speleothems revealed by high-resolution synchrotron micro XRF mapping. *Climate of the Past*, *8*(6), 2039–2051. https://doi.org/10.5194/cp-8-2039-2012

Frisia, S., Borsato, A., Fairchild, I. J., McDermott, F., & Selmo, E. M. (2002). Aragonite-Calcite Relationships in Speleothems (Grotte De Clamouse, France): Environment, Fabrics, and Carbonate Geochemistry. *Journal of Sedimentary Research*, *72*(5), 687–699. https://doi.org/10.1306/020702720687

Gałuszka, A., Migaszewski, Z. M., & Namieśnik, J. (2017). The role of analytical chemistry in the study of the Anthropocene. *TrAC Trends in Analytical Chemistry*, *97*, 146–152. https://doi.org/10.1016/j.trac.2017.08.017

Genty, D., Baker, A., & Vokal, B. (2001). Intra- and inter-annual growth rate of modern stalagmites. *Chemical Geology*, *176*(1), 191–212. https://doi.org/10.1016/S0009-2541(00)00399-5

Giorio, C., Kehrwald, N., Barbante, C., Kalberer, M., King, A. C. F., Thomas, E. R., Wolff, E. W., & Zennaro, P. (2018). *Prospects for reconstructing paleoenvironmental conditions from organic compounds in polar snow and ice*. https://doi.org/10.17863/CAM.21119

Goñi, M. A., & Hedges, J. I. (1995). Sources and reactivities of marine-derived organic matter in coastal sediments as determined by alkaline CuO oxidation. *Geochimica et Cosmochimica Acta*, *59*(14), 2965–2981. https://doi.org/10.1016/0016-7037(95)00188-3

Goñi, M. A., & Montgomery, S. (2000). Alkaline CuO oxidation with a microwave digestion system: Lignin analyses of geochemical samples. *Analytical Chemistry*, *72*(14), 3116–3121. https://doi.org/10.1021/ac991316w

Grotzinger, J., & Jordan, T. H. (2014). *Understanding Earth: Seventh Edition*. Macmillan Learning.

Hedges, J. I., & Mann, D. C. (1979). The characterization of plant tissues by their lignin oxidation products. *Geochimica et Cosmochimica Acta*, *43*(11), 1803.

Hedges, J. I., & Parker, P. L. (1976). Land-derived organic matter in surface sediments from the Gulf of Mexico. *Geochimica et Cosmochimica Acta*, *40*(9), 1019–1029. https://doi.org/10.1016/0016-7037(76)90044-2

Heidke, I., Hartland, A., Scholz, D., Pearson, A., Hellstrom, J., Breitenbach, S. F. M., & Hoffmann, T. (2021). Lignin oxidation products in soil, dripwater and speleothems from four different sites in New Zealand. *Biogeosciences*, *18*(7), 2289–2300. https://doi.org/10.5194/bg-18-2289-2021

Heidke, I., Scholz, D., & Hoffmann, T. (2018). Quantification of lignin oxidation products as vegetation biomarkers in speleothems and cave drip water. *Biogeosciences Discussions*, 1–23. https://doi.org/10.5194/bg-2018-253

Heidke, I., Scholz, D., & Hoffmann, T. (2019). Lignin oxidation products as a potential proxy for vegetation and environmental changes in speleothems and cave drip water – a first record from the Herbstlabyrinth, central Germany. *Climate of the Past*, *15*(3), 1025–1037. https://doi.org/10.5194/cp-15-1025-2019

Hellstrom, J. C., & McCulloch, M. T. (2000). Multi-proxy constraints on the climatic significance of trace element records from a New Zealand speleothem. *Earth and Planetary Science Letters*, *179*(2), 287–297. https://doi.org/10.1016/S0012-821X(00)00115-1

Hernes, P. J., & Benner, R. (2002). Transport and diagenesis of dissolved and particulate terrigenous organic matter in the North Pacific Ocean. *Deep Sea Research Part I: Oceanographic Research*, *49*(12), 2119–2132. https://doi.org/10.1016/S0967-0637(02)00128-0

Hernes, P. J., Kaiser, K., Dyda, R. Y., & Cerli, C. (2013). Molecular Trickery in Soil Organic Matter: Hidden Lignin. *Environmental Science & Technology*, *47*(16), 9077–9085. https://doi.org/10.1021/es401019n

Hernes, P. J., Robinson, A., & Audfenkampe, A. (2007). Fractionation of lignin during leaching and sorption and implications for organic matter "'freshness"'. *Geophysical Research Letters - GEOPHYS RES LETT*, *34*. https://doi.org/10.1029/2007GL031017

Holzkämper, S., Holmgren, K., Lee-Thorp, J., Talma, S., Mangini, A., & Partridge, T. (2009). Late Pleistocene stalagmite growth in Wolkberg Cave, South Africa. *Earth and Planetary Science Letters*, *282*(1), 212–221. https://doi.org/10.1016/j.epsl.2009.03.016

Hu, F. S., Hedges, J. I., Gordon, E. S., & Brubaker, L. B. (1999). Lignin biomarkers and pollen in postglacial sediments of an Alaskan lake. *Geochimica et Cosmochimica Acta*, *63*(9), 1421–1430. https://doi.org/10.1016/S0016-7037(99)00100-3

Jex, C., Pate, G., Blyth, A., Spencer, R., Hernes, P., Khan, S., & Baker, A. (2014). Lignin biogeochemistry: From modern processes to Quaternary archives. *Quaternary Science Reviews*, *87*, 46–59. https://doi.org/10.1016/j.quascirev.2013.12.028

Kögel-Knabner, I. (2002). The macromolecular organic composition of plant and microbial residues as inputs to soil organic matter. *Soil Biology and Biochemistry*, *34*(2), 139–162. https://doi.org/10.1016/S0038-0717(01)00158-4

Leng, M. (2006). *Isotopes in Palaeoenvironmental Research*. Springer. https://doi.org/10.1007/1-4020-2504-1

McDermott, F. (2004). Palaeo-climate reconstruction from stable isotope variations in speleothems: A review. *Quaternary Science Reviews*, *23*(7), 901–918. https://doi.org/10.1016/j.quascirev.2003.06.021

McGarry, S., & Baker, A. (2000). Organic acid fluorescence: Applications to speleothem palaeoenvironmental reconstruction. *Quaternary Science Reviews*, *19*, 1087–1101. https://doi.org/10.1016/S0277-3791(99)00087-6

Mermet, J.-M., Otto, M., Valcarcel, M., Kellner, R., & Widmer, H. M. (2004). *Analytical Chemistry: A Modern Approach To Analytical Science* (2° edizione). Vch Verlagsgesellschaft Mbh.

Mkumbuzi, E., Pillay, M. N., & Zyl, W. E. van. (2023). Reaction mechanisms in microwave-assisted lignin depolymerisation in hydrogen-donating solvents. *Green Processing and Synthesis*, *12*(1). https://doi.org/10.1515/gps-2023-0154

Montgomery, W., Potiszil, C., Watson, J. S., & Sephton, M. A. (2016). Sporopollenin, a Natural Copolymer, is Robust under High Hydrostatic Pressure. *Macromolecular Chemistry and Physics*, *217*(22), 2494–2500. https://doi.org/10.1002/macp.201600142

Morse, J. W., & Bender, M. L. (1990). Partition coefficients in calcite: Examination of factors influencing the validity of experimental results and their application to natural systems. *Chemical Geology*, *82*, 265–277. https://doi.org/10.1016/0009-2541(90)90085-L

Otto, A., & Simpson, M. (2006). Evaluation of CuO oxidation parameters for determining the source and stage of lignin degradation in soil. *Biogeochemistry*, *80*, 121–142. https://doi.org/10.1007/s10533-006-9014-x

Qian, Z., Fan, Z., Peng, W., Du, H., & Hu, P. (2023). Source to Sink of Lignin Phenols in a Subtropical Forest of Southwest China. *Forests*, *14*(9), 1701. https://doi.org/10.3390/f14091701

Quiers, M., Perrette, Y., Chalmin, E., Fanget, B., & Poulenard, J. (2015). Geochemical mapping of organic carbon in stalagmites using liquid-phase and solid-phase fluorescence. *Chemical Geology*, *411*, 240–247. https://doi.org/10.1016/j.chemgeo.2015.07.012

Regattieri, E., Zanchetta, G., Drysdale, R. N., Isola, I., Hellstrom, J. C., & Dallai, L. (2014b). Lateglacial to Holocene trace element record (Ba, Mg, Sr) from Corchia Cave (Apuan Alps, central Italy): Paleoenvironmental implications. *Journal of Quaternary Science*, *29*(4), 381–392. https://doi.org/10.1002/jqs.2712

Regattieri, E., Zanchetta, G., Drysdale, R. N., Isola, I., Woodhead, J. D., Hellstrom, J. C., Giaccio, B., Greig, A., Baneschi, I., & Dotsika, E. (2016). Environmental variability between the penultimate deglaciation and the mid Eemian: Insights from Tana che Urla (central Italy) speleothem trace element record. *Quaternary Science Reviews*, *152*, 80–92. https://doi.org/10.1016/j.quascirev.2016.09.027

Richards, D. A., & Dorale, J. A. (2003). Uranium-series Chronology and Environmental Applications of Speleothems. *Reviews in Mineralogy and Geochemistry*, *52*(1), 407–460. https://doi.org/10.2113/0520407

Ruddiman, W. (2013). *Earth's Climate: Past and Future* (Third edition). W. H. Freeman.

Schimpf, D., Kilian, R., Kronz, A., Simon, K., Spötl, C., Wörner, G., Deininger, M., & Mangini, A. (2011). The significance of chemical, isotopic, and detrital components in three coeval stalagmites from the superhumid southernmost Andes (53°S) as high-resolution palaeo-climate proxies. *Quaternary Science Reviews*, *30*(3), 443–459. https://doi.org/10.1016/j.quascirev.2010.12.006

Scholz, D., & Hoffmann, D. (2008). 230Th/U-dating of fossil corals and speleothems. *E&G Quaternary Science Journal*, *57*(1/2), 52–76. https://doi.org/10.3285/eg.57.1-2.3

Schutyser, W., Renders, T., Bosch, S. V. den, Koelewijn, S.-F., Beckham, G. T., & Sels, B. F. (2018). Chemicals from lignin: An interplay of lignocellulose fractionation, depolymerisation, and upgrading. *Chemical Society Reviews*, *47*(3), 852–908. https://doi.org/10.1039/C7CS00566K

Sinclair, D. J., Banner, J. L., Taylor, F. W., Partin, J., Jenson, J., Mylroie, J., Goddard, E., Quinn, T., Jocson, J., & Miklavič, B. (2012). Magnesium and strontium systematics in tropical speleothems from the Western Pacific. *Chemical Geology*, *294–295*, 1–17. https://doi.org/10.1016/j.chemgeo.2011.10.008

Standley, L. J., & Kaplan, L. A. (1998). Isolation and analysis of lignin-derived phenols in aquatic humic substances: Improvements on the procedures. *Organic Geochemistry*, *28*(11), 689–697. https://doi.org/10.1016/S0146-6380(98)00041-2

Swift, M. J., Heal, O. W., Anderson, J. M., & Anderson, J. M. (1979). *Decomposition in Terrestrial Ecosystems*. Oxford, Blackwell Scientific Publications.

Tareq, S. M., Kitagawa, H., & Ohta, K. (2011). Lignin biomarker and isotopic records of paleovegetation and climate changes from Lake Erhai, southwest China, since 18.5 ka BP. *Quaternary International*, *229*. https://doi.org/10.1016/j.quaint.2010.04.014

Tareq, S. M., & Ohta, K. (2015). Lignin and Isotope Signatures in Pollen: A Caveat of Lignin Phenol Biomarker for Reconstructing Paleovegetation. *Asian Journal of Water, Environment and Pollution*, *12*, 1–9. https://doi.org/10.3233/AJW-2015-12_1_02

Tareq, S. M., Tanaka, N., & Ohta, K. (2004). Biomarker signature in tropical wetland: Lignin phenol vegetation index (LPVI) and its implications for reconstructing the paleoenvironment. *The Science of the Total Environment*, *324*(1–3), 91–103. https://doi.org/10.1016/j.scitotenv.2003.10.020

Thevenot, M., Rumpel, C., & Dignac, M.-F. (2010). *Fate of lignins in soils: A review*.

Treble, P., Shelley, J. M. G., & Chappell, J. (2003). Comparison of high resolution sub-annual records of trace elements in a modern (1911–1992) speleothem with instrumental climate data from southwest Australia. *Earth and Planetary Science Letters*, *216*(1), 141–153. https://doi.org/10.1016/S0012-821X(03)00504-1

Upton, B. M., & Kasko, A. M. (2016). Strategies for the Conversion of Lignin to High-Value Polymeric Materials: Review and Perspective. *Chemical Reviews*, *116*(4), 2275–2306. https://doi.org/10.1021/acs.chemrev.5b00345

Vanholme, R., Demedts, B., Morreel, K., Ralph, J., & Boerjan, W. (2010). Lignin biosynthesis and structure. *Plant Physiology*, *153*(3), 895–905. https://doi.org/10.1104/pp.110.155119

Vanholme, R., Morreel, K., Darrah, C., Oyarce, P., Grabber, J. H., Ralph, J., & Boerjan, W. (2012). Metabolic engineering of novel lignin in biomass crops. *The New Phytologist*, *196*(4), 978–1000. https://doi.org/10.1111/j.1469-8137.2012.04337.x

Zhang, T., Li, X., Sun, S., Lan, H., Du, P., & Wang, M. (2013). Determination of lignin in marine sediment using alkaline cupric oxide oxidation-solid phase extraction-on-column derivatization-gas chromatography. *Journal of Ocean University of China*, *12*. https://doi.org/10.1007/s11802-011-1936-z

Zhornyak, L. V., Zanchetta, G., Drysdale, R., Hellstrom, J., Isola, I., Regattieri, E., Piccini, L., Baneschi, I., & Couchoud, I. (2011). Stratigraphic evidence for a “pluvial phase” between ca 8200–7100 ka from Renella cave (Central Italy). *Quaternary Science Reviews*, *30*, 409–417. https://doi.org/10.1016/j.quascirev.2010.12.003

Zhou, H., Chi, B., Lawrence, M., Zhao, J., Yan, J., Greig, A., & Feng, Y. (2008). High-resolution and precisely dated record of weathering and hydrological dynamics recorded by manganese and rare-earth elements in a stalagmite from Central China. *Quaternary Research*, *69*(3), 438–446. https://doi.org/10.1016/j.yqres.2008.02.005

Appendix

Table A1. *Areas for LOPs' groups and the sum of all eight LOPs (Σ8) obtained by summing the areas detected for the single phenols by the GC-MS. For the blank samples, the mean among S1, S2, and S3 is also reported.*

Sample		S group	C group	V group	P group	Σ8
S1		795	888	8108	20620	9791
S2		861	1032	3294	21948	5187
S3		594	3893	4267	22167	8754
	Mean	750	1938	8108	21579	7911
S4		$(6.8 \pm 0.8) \cdot 10^5$	$(5.0 \pm 0.9) \cdot 10^4$	$(6.7 \pm 0.7) \cdot 10^5$	$(6.8 \pm 0.6) \cdot 10^5$	$(1.4 \pm 0.2) \cdot 10^6$
S5		$(7.6 \pm 0.9) \cdot 10^5$	$(5.4 \pm 0.9) \cdot 10^4$	$(7.5 \pm 0.7) \cdot 10^5$	$(7.3 \pm 0.7) \cdot 10^5$	$(1.6 \pm 0.2) \cdot 10^6$
S6		$(6.1 \pm 0.7) \cdot 10^5$	$(3.8 \pm 0.7) \cdot 10^4$	$(6.2 \pm 0.6) \cdot 10^5$	$(6.3 \pm 0.6) \cdot 10^5$	$(1.3 \pm 0.1) \cdot 10^6$

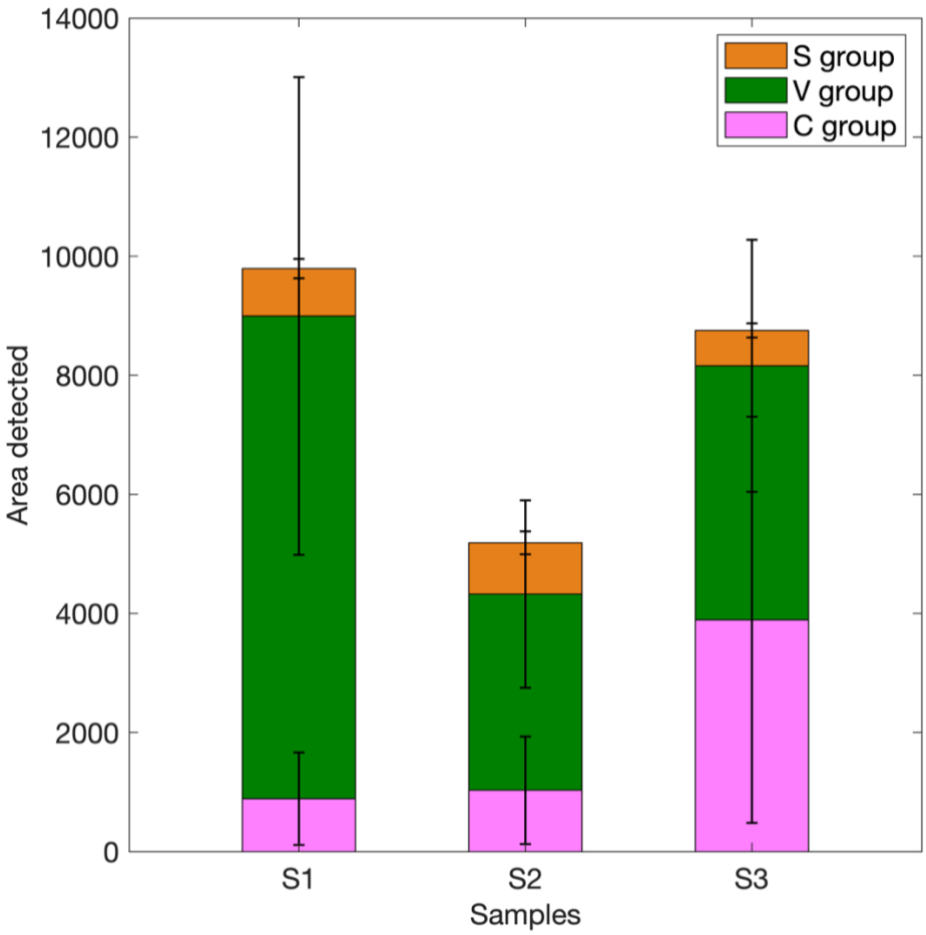

Figure 25. *LOP groups area for the blank S test samples: S1, S2, and. The height of the columns represents the sum of the LOP concentrations, Σ8, and the different colours show the contribution of the C-, S- and V-group LOPs.*

Table A2. *Areas measured by the GC-MS for blanks and RL18 samples.*

Sample ID	Pl	Pn	Vl	Vn	Pd	Sl	Sn	Vd	3,5-Bd	Sd	pCd	Fd
Blank 1	2059	665	271	98	3294	81	18	133	95	41	57	5
Blank 2	1365	60	84	1	822	9	0	116	64	4	2	4
Blank 3	806	44	98	0	737	11	1	91	43	8	0	3
Blank 4	1532	51	80	0	938	5	2	99	42	8	0	2
Blank 5	785	29	23	1	400	1	1	46	17	4	0	1
RL 18-1	5025	7502	8779	3902	43184	9447	4740	9101	1465	5376	790	343
RL 18-2	24261	30257	48199	21199	167804	55683	27500	43774	5881	20777	3148	1167
RL 18-3	21830	27018	38390	15999	120115	37267	18759	27649	4418	15044	3074	1143
RL 18-4	23790	29812	44467	19119	125748	46139	21457	28714	7909	18443	4326	2140
RL 18-5	19980	33521	73611	32516	188856	70827	35963	51040	13257	31682	4943	3091
RL 18-5b	21337	27074	38138	17346	109465	37196	19526	27482	5142	14944	3364	1758
RL 18-6	17585	25872	48886	18440	131130	41937	20210	32720	9532	13619	3493	1557
RL 18-7	24203	38675	88819	30938	205740	78763	33607	60101	13470	25783	4959	2620
RL 18-8	18391	28088	52110	22316	139670	56579	27086	40590	6560	22173	3547	1810
RL 18-9	6579	8890	19490	6943	54421	18927	7865	15921	3162	7465	829	555
RL 18-10	34143	30072	69012	25963	168097	68890	29615	45615	11836	20127	3837	1873
RL 18-11	16324	28800	61467	25052	151997	69039	28738	42136	9650	31348	3637	2628
RL 18-12	21977	32270	72433	28952	174349	78565	30381	42615	12135	35996	4147	3017
RL 18-13	11845	11516	22699	7922	62319	22423	7992	13441	3924	9773	1095	641
RL 18-14	17988	27028	67107	25546	145396	67497	25687	39636	7979	31081	3531	2421
RL 18-15	15443	19317	43216	16316	96892	44379	16792	28834	5934	21031	2117	1587
RL 18-16	17380	29197	92065	36038	182837	92479	35948	61807	12567	44083	4066	2982
RL 18-17	21882	27535	71340	29672	123976	72405	30806	44427	6533	32312	3443	2460
RL 18-18	16175	24357	71723	27020	124933	73359	29335	50343	6220	33107	3090	2169
RL 18-19	21764	41660	130242	56296	233531	146865	59682	86316	12723	63410	6901	6163
RL 18-20	25182	21118	47540	18195	106816	53775	21256	31372	6189	23685	2976	2037
RL 18-21	15259	28194	59810	25800	139299	67626	29582	41948	9668	32906	3741	2655
RL 18-22	8942	6869	29239	6539	41798	17134	6045	14386	2245	8239	774	507
RL 18-23	13942	13060	35556	14594	82381	38806	15250	25785	18287	19009	1619	1709
RL 18-24	9405	8482	17802	6830	44829	17631	6488	12169	10021	8470	949	715

Table A3. *Concentration of LOPs (in mg g-1) in the RL18 samples.*

Sample ID	Pl (mg g^{-1})	Pn (mg g^{-1})	Vl (mg g^{-1})	Vn (mg g^{-1})	Pd (mg g^{-1})	Sl (mg g^{-1})	Sn (mg g^{-1})	Vd (mg g^{-1})	3,5-Bd (mg g^{-1})	Sd (mg g^{-1})	pCd (mg g^{-1})	Fd (mg g^{-1})
RL 18-1	0.075 ± 0.005	0.10 ± 0.01	0.065 ± 0.007	0.038 ± 0.003	0.32 ± 0.03	0.088 ± 0.009	0.074 ± 0.006	0.101 ± 0.006	0.026 ± 0.003	0.103 ± 0.007	0.037 ± 0.005	0.027 ± 0.002
RL 18-2	0.095 ± 0.007	0.11 ± 0.01	0.09 ± 0.01	0.058 ± 0.005	0.35 ± 0.04	0.12 ± 0.01	0.106 ± 0.008	0.136 ± 0.008	0.029 ± 0.003	0.108 ± 0.008	0.036 ± 0.005	0.023 ± 0.002
RL 18-3	0.074 ± 0.005	0.086 ± 0.009	0.066 ± 0.007	0.040 ± 0.003	0.23 ± 0.02	0.08 ± 0.008	0.068 ± 0.005	0.082 ± 0.005	0.020 ± 0.002	0.073 ± 0.005	0.030 ± 0.004	0.019 ± 0.002
RL 18-4	0.077 ± 0.005	0.090 ± 0.009	0.072 ± 0.008	0.044 ± 0.004	0.24 ± 0.02	0.089 ± 0.009	0.073 ± 0.006	0.083 ± 0.005	0.029 ± 0.003	0.082 ± 0.006	0.035 ± 0.005	0.027 ± 0.002
RL 18-5	0.069 ± 0.005	0.10 ± 0.01	0.103 ± 0.01	0.066 ± 0.005	0.31 ± 0.03	0.12 ± 0.02	0.105 ± 0.008	0.126 ± 0.008	0.042 ± 0.005	0.117 ± 0.008	0.039 ± 0.005	0.034 ± 0.003
RL 18-5b	0.120 ± 0.004	0.14 ± 0.01	0.11 ± 0.01	0.069 ± 0.006	0.36 ± 0.04	0.13 ± 0.01	0.115 ± 0.009	0.134 ± 0.008	0.037 ± 0.004	0.119 ± 0.008	0.05 ± 0.007	0.040 ± 0.004
RL 18-6	0.087 ± 0.006	0.11 ± 0.01	0.11 ± 0.01	0.060 ± 0.005	0.34 ± 0.03	0.12 ± 0.01	0.098 ± 0.008	0.126 ± 0.008	0.046 ± 0.005	0.093 ± 0.007	0.043 ± 0.006	0.031 ± 0.003
RL 18-7	0.082 ± 0.006	0.11 ± 0.01	0.12 ± 0.01	0.066 ± 0.005	0.35 ± 0.03	0.13 ± 0.01	0.104 ± 0.008	0.147 ± 0.009	0.044 ± 0.005	0.106 ± 0.007	0.040 ± 0.005	0.032 ± 0.003
RL 18-8	0.110 ± 0.007	0.14 ± 0.01	0.14 ± 0.02	0.084 ± 0.007	0.43 ± 0.04	0.17 ± 0.02	0.14 ± 0.01	0.18 ± 0.01	0.044 ± 0.005	0.16 ± 0.01	0.053 ± 0.007	0.042 ± 0.004
RL 18-9	0.101 ± 0.007	0.12 ± 0.01	0.13 ± 0.01	0.065 ± 0.005	0.42 ± 0.04	0.15 ± 0.02	0.116 ± 0.009	0.17 ± 0.01	0.049 ± 0.005	0.14 ± 0.01	0.042 ± 0.006	0.039 ± 0.004
RL 18-10	0.16 ± 0.01	0.15 ± 0.01	0.16 ± 0.02	0.092 ± 0.007	0.48 ± 0.05	0.19 ± 0.02	0.15 ± 0.01	0.19 ± 0.01	0.064 ± 0.007	0.14 ± 0.01	0.055 ± 0.007	0.041 ± 0.004
RL 18-11	0.099 ± 0.007	0.15 ± 0.01	0.15 ± 0.02	0.089 ± 0.007	0.44 ± 0.04	0.19 ± 0.02	0.15 ± 0.01	0.18± 0.01	0.055 ± 0.006	0.19 ± 0.01	0.053 ± 0.007	0.050 ± 0.005
RL 18-12	0.110 ± 0.008	0.14 ± 0.01	0.15 ± 0.02	0.091 ± 0.007	0.45 ± 0.04	0.19 ± 0.02	0.14 ± 0.01	0.16 ± 0.01	0.059 ± 0.007	0.19 ± 0.01	0.052 ± 0.007	0.049 ± 0.004
RL 18-13	0.14 ± 0.01	0.14 ± 0.01	0.13 ± 0.01	0.067 ± 0.005	0.43 ± 0.04	0.16 ± 0.02	0.109 ± 0.009	0.140 ± 0.008	0.053 ± 0.006	0.16 ± 0.01	0.046 ± 0.006	0.040 ± 0.004
RL 18-14	0.123 ± 0.009	0.16 ± 0.02	0.18 ± 0.02	0.106 ± 0.009	0.50 ± 0.05	0.22 ± 0.02	0.16 ± 0.01	0.20 ± 0.01	0.057 ± 0.006	0.22 ± 0.02	0.060 ± 0.008	0.056 ± 0.005
RL 18-15	0.133 ± 0.009	0.15 ± 0.02	0.16 ± 0.02	0.091 ± 0.007	0.46 ± 0.05	0.20 ± 0.02	0.14 ± 0.01	0.19 ± 0.01	0.055 ± 0.006	0.20 ± 0.01	0.054 ± 0.007	0.052 ± 0.005
RL 18-16	0.102 ± 0.007	0.14 ± 0.01	0.20 ± 0.02	0.116 ± 0.009	0.50 ± 0.05	0.23 ± 0.02	0.17 ± 0.01	0.23 ± 0.01	0.065 ± 0.007	0.23 ± 0.02	0.056 ± 0.007	0.053 ± 0.005
RL 18-17	0.22 ± 0.02	0.25 ± 0.03	0.30 ± 0.03	0.18 ± 0.01	0.69 ± 0.07	0.35 ± 0.04	0.28 ± 0.02	0.33 ± 0.02	0.076 ± 0.008	0.35 ± 0.02	0.09 ± 0.01	0.086 ± 0.008
RL 18-18	0.17 ± 0.01	0.23 ± 0.02	0.29 ± 0.03	0.17 ± 0.01	0.68 ± 0.07	0.35 ± 0.03	0.26 ± 0.02	0.35 ± 0.02	0.072 ± 0.008	0.34 ± 0.02	0.08 ± 0.01	0.079 ± 0.007
RL 18-19	0.115 ± 0.008	0.18 ± 0.02	0.24 ± 0.03	0.16 ± 0.01	0.57 ± 0.06	0.30 ± 0.03	0.23 ± 0.02	0.29 ± 0.02	0.064 ± 0.007	0.29 ± 0.02	0.07 ± 0.01	0.078 ± 0.007
RL 18-20	0.17 ± 0.01	0.15 ± 0.02	0.16 ± 0.02	0.090 ± 0.007	0.45 ± 0.05	0.21 ± 0.02	0.15 ± 0.01	0.19 ± 0.01	0.052 ± 0.006	0.20 ± 0.01	0.060 ± 0.008	0.055 ± 0.005
RL 18-21	0.082 ± 0.006	0.12 ± 0.02	0.13 ± 0.01	0.079 ± 0.006	0.36 ± 0.04	0.16 ± 0.02	0.13 ± 0.01	0.155 ± 0.009	0.048 ± 0.005	0.17 ± 0.01	0.047 ± 0.006	0.044 ± 0.004
RL 18-22	0.180 ± 0.013	0.15 ± 0.02	0.24 ± 0.03	0.091 ± 0.007	0.51 ± 0.05	0.21 ± 0.02	0.14 ± 0.01	0.23 ± 0.01	0.056 ± 0.006	0.22 ± 0.02	0.06 ± 0.008	0.054 ± 0.005
RL 18-23	0.14 ± 0.01	0.13 ± 0.01	0.16 ± 0.02	0.095 ± 0.008	0.46 ± 0.05	0.21 ± 0.02	0.15 ± 0.01	0.20 ± 0.01	0.13 ± 0.01	0.22 ± 0.02	0.052 ± 0.007	0.062 ± 0.006
RL 18-24	0.19 ± 0.01	0.17 ± 0.02	0.18 ± 0.02	0.094 ± 0.008	0.54 ± 0.05	0.21 ± 0.02	0.15 ± 0.01	0.20 ± 0.01	0.16 ± 0.02	0.22 ± 0.02	0.066 ± 0.009	0.066 ± 0.006